HIGH RESOLUTION OBSERVATIONS AT 80 MHZ OF GALACTIC AND EXTRAGALACTIC RADIO SOURCES

IAN A. LOCKHART

1971

A THESIS SUBMITTED FOR THE DEGREE OF
DOCTOR OF PHILOSOPHY
THE AUSTRALIAN NATIONAL UNIVERSITY CANBERRA

Acknowledgements

I wish to thank my A.N.U. supervisor Professor O.J. Eggen for his continued support and advice during this project.

I am grateful for the guidance and understanding of my outside supervisor, Dr J.P. Wild.

The use of the C.S.I.R.O. radioheliograph and of other facilities was greatly appreciated.

Specially requested observations were kindly made by Dr J.V. Wall of the Division of Radiophysics and by Dr A. Turtle of the School of Physics Sydney University. I thank Professor B.Y. Mills for permitting the special observation with the Sydney University Mills Cross.

I acknowledge personal communications from Dr J.V. Wall, Dr J.B. Whiteoak and Dr F.F. Gardner, Mr V. Radhakrishnan, Dr J.L. Caswell, Mr D.K. Milne, Dr O.B. Slee, Mr R.G. Blesing, and Mr M.M. Komesaroff.

Computer programs were kindly provided by Dr D.J. McLean and Mr L.H. Heisler.

I thank Mr K.V. Sheridan who assisted with some of the observations and who has been responsible for the initial adjustment and continued maintenance of the radioheliograph.

For useful discussions and criticism of the manuscript I thank Dr J.P. Wild, Dr D.J. McLean, Mr V. Radhakrishnan, and, in particular, Dr J.A. Roberts.

The receipt of a Commonwealth Post Graduate Award at A.N.U. is acknowledged.

For many things I thank my wife.

The text of this thesis contains full acknowledgement of any part of this investigation which is not solely my own work

I.A. LOCKHART

Acknowledgements

I wish to thank my A.N.U. supervisor Professor O.J. Eggen for his continued support and advice during this project.

I am grateful for the guidance and understanding of my outside supervisor, Dr J.P. Wild.

The use of the C.S.I.R.O. radioheliograph and of other facilities was greatly appreciated.

Specially requested observations were kindly made by Dr J.V. Wall of the Division of Radiophysics and by Dr A. Turtle of the School of Physics Sydney University. I thank Professor B.Y. Mills for permitting the special observation with the Sydney University Mills Cross.

I acknowledge personal communications from Dr J.V. Wall, Dr J.B. Whiteoak and Dr F.F. Gardner, Mr V. Radhakrishnan, Dr J.L. Caswell, Mr D.K. Milne, Dr O.B. Slee, Mr R.G. Blesing, and Mr M.M. Komesaroff.

Computer programs were kindly provided by Dr D.J. McLean and Mr L.H. Heisler.

I thank Mr K.V. Sheridan who assisted with some of the observations and who has been responsible for the initial adjustment and continued maintenance of the radioheliograph.

For useful discussions and criticism of the manuscript I thank Dr J.P. Wild, Dr D.J. McLean, Mr V. Radhakrishnan, and, in particular, Dr J.A. Roberts.

The receipt of a Commonwealth Post Graduate Award at A.N.U. is acknowledged.

For many things I thank my wife.

TABLE OF CONTENTS

CHAPTER I PURPOSE OF OBSERVATIONS AND DISCUSSION OF INSTRUMENT

CHAPTER 2 OBSERVATIONAL METHOD, SOURCE SELECTION AND DATA REDUCTION

CHAPTER 3 ABSOLUTE FLUX DENSITY CALIBRATION AND THE MEASUREMENT OF BRIGHTNESS TEMPERATURES

CHAPTER 4 EXTRAGALACTIC SOURCES

CHAPTER 5 GALACTIC SOURCES

CHAPTER 1

PURPOSE OF OBSERVATIONS AND DISCUSSION OF INSTRUMENT

1.1 Purpose of observations

High resolution mapping of the structure of discrete radio sources has hitherto been confined to frequencies well above 100 MHz. There, adequate resolution has been obtained either by single paraboloids or by the use of multielement arrays of moderate physical dimensions. The completion of the C.S.I.R.O. 80 MHz radioheliograph in September 1967 presented the first opportunity of making pencil beam observations of comparable angular resolution at a frequency below 100 MHz.

For well resolved sources the comparison of maps made with similar beamwidths but at widely spaced frequencies discloses changes in structure with frequency. Such structural changes are of particular interest in those extragalactic sources whose integrated spectra deviate from a simple power-law relationship. It is then possible to determine from which regions these spectral deviations arise. Even for those sources which are not well resolved but where the existence of multiple components is discernible, any major changes in the spectrum of the components can be detected. Variations in spectral index across the source reveal optically thick regions within the source or variations in electron energy distribution for optically thin sources; whichever the cause it must be accounted for in any satisfactory evolutionary model.

Galactic sources are often a blend of thermal and non-thermal components which at high frequencies may both contribute significantly to the integrated spectrum. The predominance of the non-thermal contribution at low frequencies enables studies such as ours to distinguish between the two types and thereby separate the thermal and non-thermal regions.

1.2 Instrument

The C.S.I.R.O. radioheliograph was specifically designed to observe rapid changes in the two-dimensional radio emission from the Sun. Amongst the features that make it an attractive instrument for the study of discrete radio sources are its large collecting area and small beamwidth of 3'.75 arc.

Detailed accounts of the specifications, design, construction and operation of the radioheliograph, published in a special edition of The Proceedings of the Institution of Radio and Electronics Engineers Australia (Wild, 1967) will be referred to frequently in the succeeding chapters. In the following we give only a short description of the salient features.

The instrument consists of an array of 96 paraboloids, each of 13 m diameter arranged in a circle of diameter 3 km. Each paraboloid is equatorially mounted, permitting a declination coverage of ±42°. The hour-angle coverage is a function of declination with a maximum of $\pm 2^h 35^m$ in the declination range -17° to +22°. The signals from crossed dipoles on each of the 96 aerials are combined in a central processing unit to produce 48 independent beams in a north-south line. The separation between adjacent beams is (2'.148 x sec z)arc where z is the zenith angle of observation. For solar observations the 48 beams are swept in right ascension once per second to provide an array of sample points amply covering the radio diameter of the Sun. The present observations were made by either scanning the beams electronically as for solar observations, or by setting them to a predetermined position and allowing the Earth's rotation to scan the desired area of sky. In Table 1.1 we give all the relevant instrumental parameters.

A natural consequence of the unfilled and discrete nature of the array is the presence of both near annular sidelobes and far grating responses. An ingenious beam-shaping method developed by Wild (1965) and known as J^2 synthesis is employed to achieve almost total suppression of the near sidelobes. With optimum adjustment of the array, the near sidelobe level is everywhere <2% of the central response. The grating responses appear at intervals of 2° in radial distance from the central maximum. The peak amplitude of the first order response is approximately 5% of the central maximum and the amplitude of the higher order responses diminishes progressively. Whereas the solar observations are unaffected by these grating responses they are a potential source of error in the study of weak radio sources located in the vicinity of stronger ones. For the observations described in the succeeding chapters sources were selected to avoid undesirable responses from the grating lobes.

In Chapter 2 we describe the method of observations, source selection and data reduction. Chapter 3 deals with the absolute flux density calibration of the instrument and the measurement of brightness temperatures. Chapter 4 presents the results for extragalactic sources and in Chapter 5 we give results for the galactic sources. The conclusions to be drawn from the present observations are presented in Chapter 6.

TABLE 1.1

RADIOHELIOGRAPH INSTRUMENTAL PARAMETERS

Array diameter	3 km (800 wavelengths)
Number of aerials	96
Spacing between aerials	97.5 m
Total effective collecting area	$6.4 \times 10^3\ \mathrm{m}^2$
Aerial parameters	
Type	Equatorially-mounted paraboloidal reflector
Mean diameter	13 m
Primary beamwidth	Approximately 17° to half-power points
Sidelobe level	Everywhere $\lesssim$2.5% of the central response
Efficiency	42%
Declination coverage	±42°
Hour-angle coverage	Maximum $\pm 2^h 35^m$ in declination range -17° to 22°
R.F. system parameters	
Operating frequency	80.0 MHz
System bandwidth	1.0 MHz (rectangular profile)
Feed system	Orthogonal half-wavelength dipoles
Polarization modes	a) left-handed and right-handed circular components b) orthogonal linear components bisecting the angle between dipoles c) orthogonal linear components of each dipole
Stepped delay range	65° of zenith angle

TABLE 1.1 (contd)

Pencil beam parameters

Central response	Elliptical, 3'.75 x(3'.75 x sec z)arc, z the zenith angle of observation
Near sidelobe level	Everywhere ≤2% of central response (optimum phase and gain adjustment of the array)
Central response solid angle	1.193 x 10^{-6} steradians
Sample point spacing	2'.148 arc east-west and (2'.148 x sec z)arc north-south for meridian observations (the raster becomes non-rectangular away from the meridian - the sampling is always optimum for the projected aperture dimensions)
Number of sample points NS	48
Number of sample points EW	60
Field of view	2° x 2° sec z
Maximum amplitude of first order grating responses	5% of central response

Detector - Integrator System

Square law detector performance	Square law maintained to within ±1% over the upper 25 dB part of the range; an error of up to -3% is present at very low levels.
Integration time	a) 1/120 sec per picture point per polarization (rapid scanning) b) 2 sec (drift scans recorded on chart)
Proportion of total time in which aerials are connected in phase during beam formation	5/17

TABLE 1.1 (contd)

Recording system	
Magnetic tape	Complete picture once per second
Chart	8 Channels only - drift scans.

CHAPTER 2

OBSERVATIONAL METHOD, SOURCE SELECTION AND DATA REDUCTION

The mapping of sources at wavelengths of several metres with beamwidths as small as a few minutes of arc has not previously been attempted. The principal new problems encountered under these conditions all stem from the effects of ionospheric refraction. In this chapter we first outline these effects and discuss the choice of observational procedures to minimize them. We then give the criteria for the selection of sources, and describe the methods adopted for data reduction.

2.1 Ionospheric conditions

Source observations at long wavelengths, in particular those of high angular resolution, are susceptible to prevailing ionospheric conditions. Although ionospheric absorption at 80 MHz is unlikely to exceed 1%, difficulties are encountered with refraction effects produced by stationary and moving irregularities of electron density in the ionosphere. We now classify these refraction effects according to the manner in which they disturb point source observations. Much of the following data was obtained by Blesing (private communication) and by Slee (private communication) from point source observations made with the radioheliograph.

(a) Amplitude scintillations

Source observations made with the radioheliograph usually exhibit significant amplitude scintillations. Under typical conditions, amplitude variations of ~10% occur with time scales of ~15-30 sec: variations in amplitude over a period of 1 sec are typically ~1%. However, occasional severe ionospheric disturbances can produce amplitude variations of $\gtrsim 50\%$ during a 15 sec period.

(b) Wandering of the image

Wandering of the point source image is also frequently observed. The magnitude and time scale of this wandering depends upon the structure and movement of the electron density irregularities present. It is convenient to distinguish between the wandering which is typically encountered and extreme changes in position which are occasionally observed.

(i) Typical wandering

From many source observations covering a wide range of zenith angles it is estimated that, under typical conditions, irregular ionospheric refraction causes an r.m.s. fluctuation in position of ~1'.5 arc for observations of duration $\gtrsim 5$ min.

(ii) Extreme wandering

Observations under extreme conditions show that the movement of ionospheric irregularities can cause changes in position of $\gtrsim 8'$ arc during a 10 min period. Since conditions of severe ionospheric refraction are not readily predictable, the probability of such extreme wandering being observed increases with the duration of a given observation.

(c) Displacements in position

Large-scale electron density gradients in the ionosphere which remain stationary during the period of an observation produce a mean displacement of the source from its nominal position. Extreme displacements of ~14' arc have been recorded by both Blesing and Slee; similar extremes are evident in a few of the present observations. Observations by Slee (private communication) also suggest the existence of a small constant component ($\lesssim 1'$ arc) of refraction in the north-south direction which displaces the source towards the zenith by an amount which increases with the zenith angle of observation.

2.2 The choice of observational procedure

As described in Chapter 1, observational data may be recorded either as drift scans or as an image of a selected region of sky approximately 2° x 2° which is rapidly scanned, digital integration of many scans being used to form the final picture. With the latter procedure, a 2° interval in right ascension is scanned in 1 sec, whereas a drift-scan across the same interval takes approximately 480 sec. Thus to map a 2° x 2° field using the rapid scanning method, with the same sensitivity as would be obtained from drift scans, it is necessary to integrate about 480 1-sec scans.

In contrast to the drift-scan method however, rapid scanning allows the whole picture to be uniformly integrated throughout the 480 sec period.

The sources included in the present observations range in angular size from about 5' arc to 1°.5, corresponding to intervals in right ascension of between 20 sec and 360 sec. Contour maps of such objects obtained from drift scan observations can be seriously distorted by amplitude scintillations with time scales of 15-30 sec, while rapid scan observations are barely affected. Further, the image wandering typically encountered produces only uniform smearing of a contour map derived from integration of 1-sec scans, but can distort to a varying degree different parts of a map obtained from drift scan observations. Neither procedure is effective in dealing with the severe distortions which arise from extreme wandering of the image; several observations of a source are therefore needed to reject maps exhibiting such distortions. Finally, source displacements resulting from stationary electron-density gradients do not produce distortions but are more readily accommodated by the fast scanning technique since drift-scan observations with only 8 recording channels cover about one-sixth of the declination range recorded in fast scanning. In this context it is also apparent that the time required to map, at given sensitivity, a source of angular extent $\gtrsim 17'$ arc in declination is considerably less in a fast scanning observation than in a drift scan observation, since in the latter case observations at two or more declination settings are required to record the whole source. In such cases the probability of severe distortions is further increased with drift scan observations.

This comparison shows that the distortions described above are minimized with the fast scanning procedure which was therefore adopted for all mapping observations. Drift scans were used only in exploratory observations.

As mentioned above, irregular refraction of the source causes uniform smearing of maps made by fast scanning. To estimate the degree of broadening expected we assume that the effect of fluctuations in the position of a point source (§2.1, b(i)) is equivalent to convolving the undisturbed point source image with a Gaussian function of half-width equal to the r.m.s. fluctuation in position. Using the data obtained by Blesing and Slee, it is found that the image broadening is typically ~8%. For integrating times of more than about 5 min, this broadening is independent of the duration of observation. However, in order to minimize the occurrence of severe distortions (§2.1, b(ii)) and at the same time achieve a satisfactory signal-to-noise ratio when observing sources of low brightness temperature, a compromise upper limit to integration time of 15 min (900 s) was chosen.

This period had the added convenience that the data for each map could be stored on a single standard magnetic tape.

It should be mentioned that with direct integration of fast scans, a form of smearing arises in principle from the fact that the skewness of picture field varies with the hour-angle of observation (Beard et al. 1967). However, it may be shown that over a 15 min period the resulting increase in effective beamwidth amounts to not more than 5%. Direct integration was therefore adopted.

2.3 Criteria for selecting sources

2.3.1 Sensitivity limitations

The image recorded by the radioheliograph during fast scanning observations contains 48 x 60 sample points, spaced at the "optimum" interval i.e. the maximum interval for full retention of information (Bracewell and Roberts, 1954). In defining the "signal-to-noise" ratio of a point in this image, we assume the "signal" to be the mean output reading due to a source of arbitrary dimensions located within the image, and the "noise" to be the r.m.s. fluctuation in the output reading in the presence of receiver and galactic background noise in addition to the source itself. The "peak signal-to-noise" ratio is defined as the ratio of the maximum signal to the average r.m.s. noise level. These definitions also apply to drift-scan observations provided the analogue data is divided into and averaged over time intervals equal in length to the "optimum" interval.

The accurate mapping of an extended source requires a reasonably high peak signal-to-noise ratio. For instance, if it is desired to map a circular Gaussian source of arbitrary size such that random errors in the radius of those contours close to the half-power contour are to have an r.m.s. deviation of less than 5%, it may be shown that a peak signal-to-noise ratio of ~30 is required. We now estimate the minimum source strength capable of yielding a peak signal-to-noise ratio of 30 with the radioheliograph employed in its fast scanning mode, assuming an integrating time of 900 sec. Under these conditions, we therefore require a peak signal-to-noise ratio of $30/\sqrt{900} = 1$ for each 1-sec scan. For one polarized component of an unpolarized source the required value is then $\frac{1}{\sqrt{2}} \simeq 0.7$.

It may be shown (Wild, 1967a) that the peak signal-to-noise ratio, η for one polarized component of a circular source of angular radius R radians, radiating with uniform brightness temperature T_B in the presence of receiver noise and uniform galactic noise of equivalent temperatures T_R and T_G respectively, is given by

$$\eta \gtrsim \frac{(\beta A\Omega/\lambda^2)\ T_B(\tau\Delta f)^{1/2}}{(AR/\pi a\lambda)\ T_B + (T_R+T_G)} , \qquad 2.1$$

where A is the effective collecting area of the array, a the radius of the annulus, λ the wavelength, Ω the effective solid angle of the corrected beam, and β the proportion of the total time in which the aerials of the array are connected in phase during the beam correcting process. Both the integration time τ, and the bandwidth Δf are defined for rectangular profiles. This expression is valid when the angular size of the source is large compared with that of the beam ($R >> \lambda/2\pi a$). Alternatively we may specify the source defined above in terms of its flux density S, which when specified for one polarized component is given by

$$S = \frac{kT_B}{\lambda^2}(\pi R^2) \qquad 2.2$$

where k is Boltzmann's constant.

Using equation 2.2, equation 2.1 reduces to

$$\eta \simeq \frac{\beta A\Omega S.(\tau\Delta f)^{1/2}}{(SAR\lambda/\pi a) + \pi R^2 kT_N} \qquad 2.3$$

where $T_N = (T_R + T_G)$.

When the source is unresolved by the array ($R << \lambda/2\pi a$) the expression for η takes the form

$$\eta = \frac{\beta^{1/2}\ AS(\tau\Delta f)^{1/2}}{\{(AS + kT_N)^2 + (\beta^{-1} - 1)(kT_N)^2\}^{1/2}} \qquad 2.4$$

For the polar diagram used in the present observations we have $\beta = 5/17$ and $\Omega = 2.4/4\pi a^2$. With τ set to the normal integration time for fast scanning ($\tau = 1/120$ sec) and with $\Delta f = 1$ MHz, $A = 6.4 \times 10^3 m^2$, $a = 1.5 \times 10^3$ m, $\lambda = 3.75$ m, we obtain the set of curves shown in Figures 2.1 and 2.2.

In Figure 2.1, η is plotted as a function of the flux density S (in units of 10^{-26} W m^{-2} Hz^{-1}) for one polarized component of an unresolved source according to equation 2.4, with various background temperatures T_G ranging from 1000°K to 10,000°K. We have adopted T_R = 300°K (Sheridan and Sparks, 1967). In regions well away from the galactic plane the 80 MHz values of T_G lie between 1000°K and 2000°K, whilst values of between 5000°K and 8000°K occur along the plane (Yates, 1968). It can be seen from Figure 2.1 that under the most favourable conditions, i.e. where the background temperature $T_G \simeq$ 1000°K, a peak signal-to-noise ratio of 0.7 is registered in a 1-sec scan by an unresolved source whose flux density for one polarized component is approximately

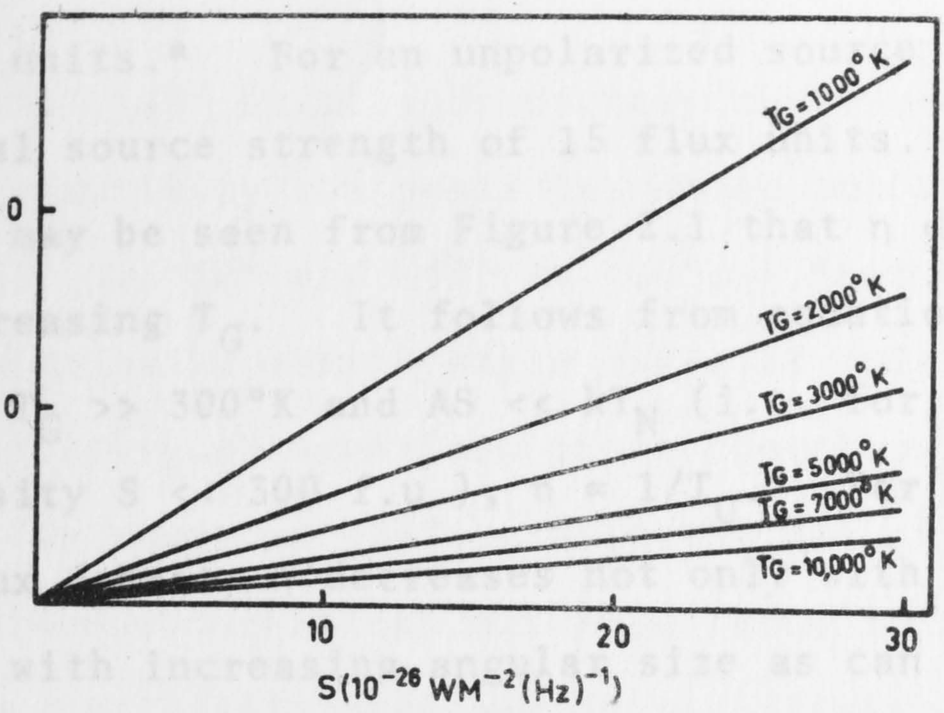

Fig. 2.1 - The peak signal-to-noise ratio, η, registered in a single 1-sec scan by one polarized component of a point source whose flux density for that polarization is S. Dependence of η on background temperature T_G is shown.

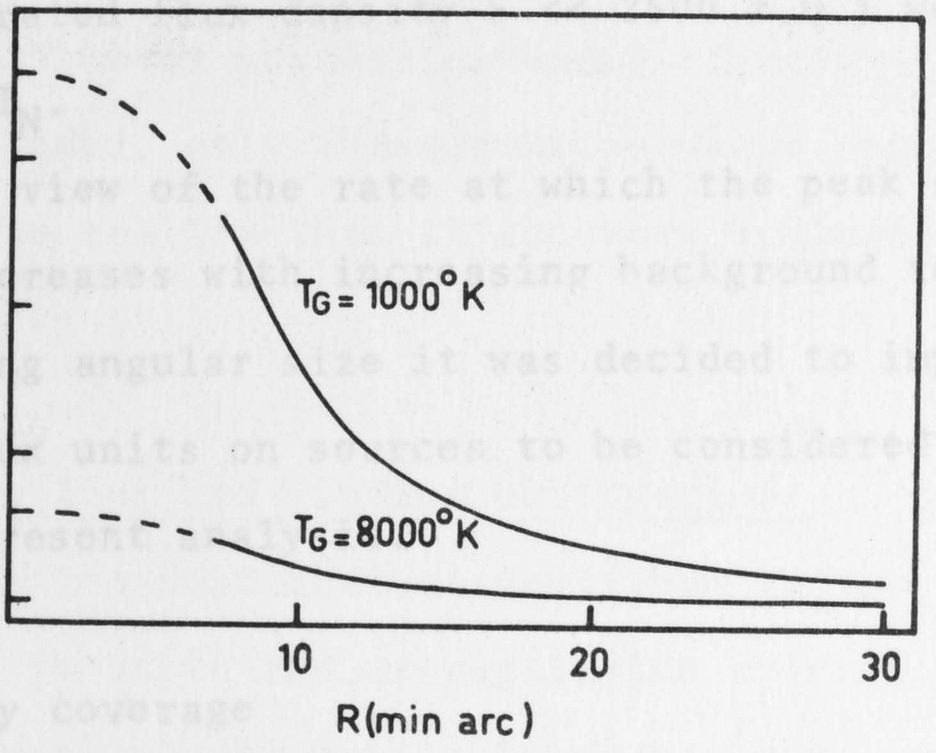

Fig. 2.2 - The peak signal-to-noise ratio, η, registered in a single 1-sec scan by one polarized component of a uniform circular source of angular radius R, having a flux density for that polarization of 7.5 f.u. The dependence of η on background temperature T_G is shown.

7.5 flux units.* For an unpolarized source this corresponds to a total source strength of 15 flux units.

It may be seen from Figure 2.1 that η decreases rapidly with increasing T_G. It follows from equation 2.4 that, provided $T_G >> 300°K$ and $AS << kT_N$ (i.e. for sources of flux density $S << 300$ f.u.), $\eta \propto 1/T_G$. For a source of given flux density η decreases not only with increasing T_G but also with increasing angular size as can be seen from Figure 2.2 in which η is plotted as a function of the angular radius R (in minutes of arc) according to equation 2.3, for an unpolarized source of integrated flux density 15 flux units. In this figure we have also adopted $T_R = 300°K$, the two curves corresponding to background temperatures of 1000°K and 8000°K as shown. For values of $R > 8'$ arc (for which equation 2.3 is valid) and provided $SAR\lambda/\pi a << \pi R^2 kT_N$ (i.e. for sources of integrated flux density $S << 2500$ f.u.) we obtain $\eta \propto 1/R^2 T_N$.

In view of the rate at which the peak signal-to-noise ratio decreases with increasing background temperature and increasing angular size it was decided to impose a lower limit of 15 flux units on sources to be considered for inclusion in the present analysis.

2.3.2 Sky coverage

The selection of sources is further restricted by the sky coverage of the radioheliograph. The aerial system has declination limits at ±42° and a primary beamwidth to half-power points of approximately 17°. In principle, therefore, observations at full sensitivity may be made between

---

*1 flux unit (f.u.) = 10^{-26} W m^{-2} $(Hz)^{-1}$.

declinations ±42°, while satisfactory observations at slightly reduced sensitivity are possible within the declination ranges +42° to +50° and -42° to -50°. However the stepped delay system has a zenith angle range of only 65°, restricting full sensitivity observations of the northern hemisphere to declinations south of +35°. Nevertheless it may be shown that provided observations are made close to the meridian, there is a negligible decrease in sensitivity due to loss of coherence in the extreme north and south aerial channels for observations taken as far north as +45°. The declination limits imposed by the instrument are therefore -50° to +45°.

2.3.3 Angular size criteria

Angular size data is in general only available from high frequency observations. To allow for the possibility that some sources possess extended structure with a steep spectral index, only those sources whose angular size was known to be smaller than 1' arc were excluded from the initial list.

2.4 Source list and finding observations

With the restrictions described in the previous section, a list of galactic and extragalactic objects was compiled from a search of the available survey catalogues and interferometer or single dish results. In general, those sources which were described as "extended" or "possibly extended" in the survey literature were included provided they satisfied the other criteria of section 2.3.

In order to select from this list those sources warranting detailed investigation, each source was examined in a number of drift scan observations. Data was recorded on chart, several scans of each source being used to allow for ionospheric effects. A source was eliminated if either its peak brightness temperature was too low for adequate detection in these observations or if it was insufficiently resolved. The elimination in these drift-scan observations was such that the satisfactory detection of those sources selected was assured in the fast scanning observations employed in subsequent detailed investigations.

2.5 Observational procedure and data reduction

2.5.1 Observational procedure

As described above, the fast scanning procedure was adopted for detailed mapping of the selected sources. For each observation the array was phased to the nominal declination of the source and the appropriate right ascension selected to ensure complete inclusion of the source in the field of view. The source was then automatically followed. Observations, each of 15 min duration, were centred about the mean transit time of the source. When observing sources of limited angular extent the integration time was doubled by recording half the normal 2° x 2° field twice per second. Instrumental effects described below precluded the use of quarter scans.

2.5.2 Data reduction

Each 15 min observation was digitally integrated by direct addition of corresponding sample points by computer. After offsets were subtracted and channel gains equalized the integrated record was printed in separate and combined polarizations and also written as a single record on magnetic tape.

Subsequent reduction was complicated by an instrumental effect in the form of curved baselines generated by imperfect circuitry in the detector-integrators. (This effect is only significant with weak sources requiring a large number of integrations and does not hamper the reduction of the solar observations for which the instrument was designed.) The shape of each baseline was that of an exponential decay curve with decay constants that varied from channel to channel and with the sky background temperature. It was necessary, therefore, to plot either by hand or by computer all channels in the source region and then to match each baseline to one of a set of exponential curves.

After baseline correction the data from each observation was tabulated and punched on computer cards in order to produce a contour map in a versatile computer program devised by D.J. McLean of the Division of Radiophysics. The principal function of this program is to produce smooth contour diagrams by interpolating the original data and by smoothing noise fluctuations.

This interpolation and smoothing is achieved by an exact method in which:

1) the Fourier transform is generated.

2) the high frequency components beyond the resolution limit of the array are removed to reduce noise fluctuations.

3) - in the case of "noisy" records only - the accepted high frequency components are damped relative to the low frequencies by multiplying the Fourier transform by a cosine-bell function.

4) the domain of the Fourier transform is extended by including frequencies beyond the resolution limit of the array with zero amplitude (a procedure necessary for exact interpolation).

5) the inverse transform is generated in the form of a fine-raster matrix.

6) the coordinate system is transformed to the true sky system.

7) a contour diagram is produced by the use of an x-y plotter.

The smoothing procedure is shown schematically in Figure 2.3 while in Figure 2.4 examples are shown of maps drawn by computer before and after interpolation. Where a number of observations of a source appeared to be relatively unaffected by the ionosphere (except for displacements from the nominal position), this program was used to average these observations, thereby improving the signal-to-noise ratio of the final map.

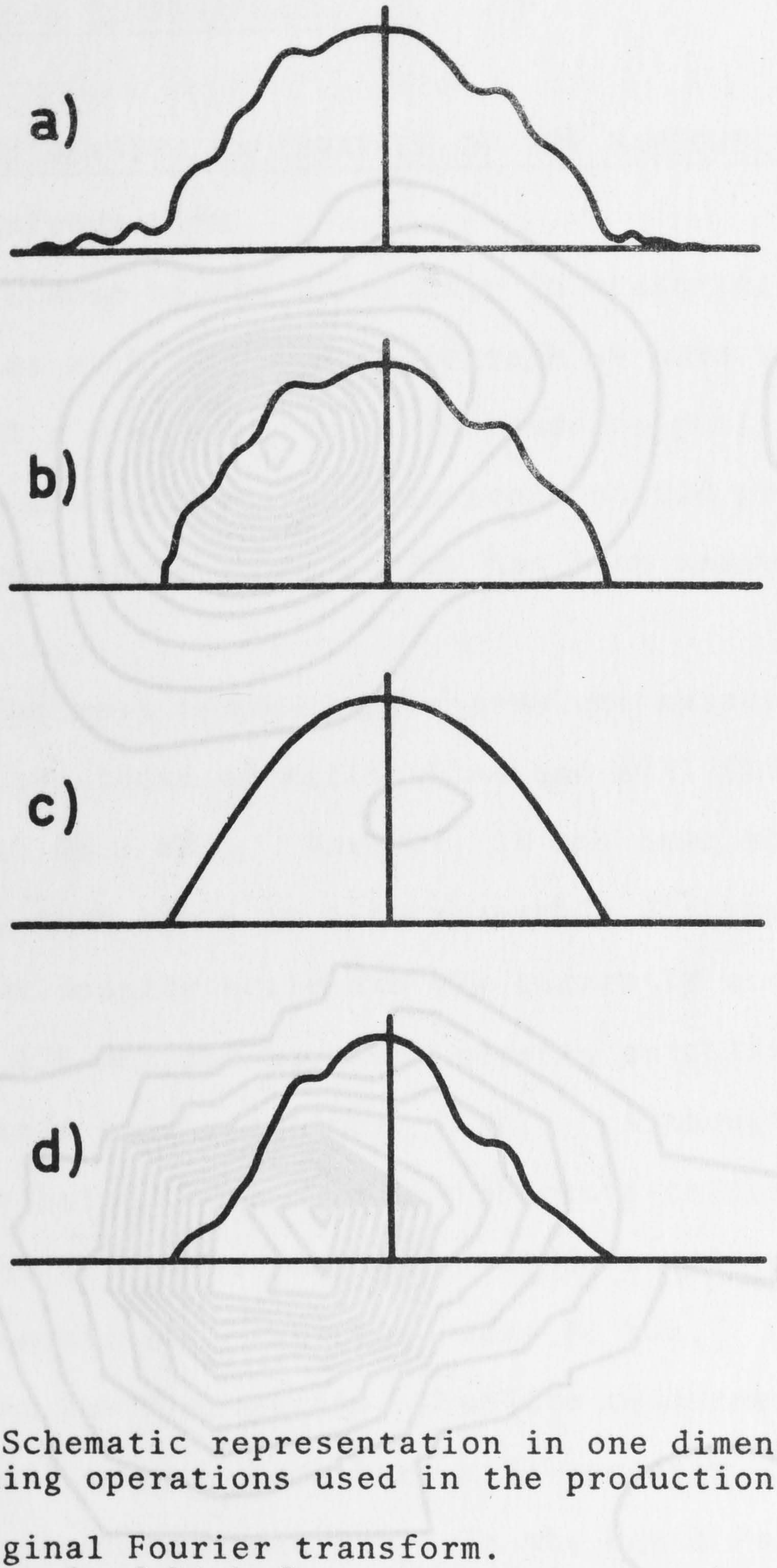

Fig. 2.3 - Schematic representation in one dimension of smoothing operations used in the production of contour maps.

a) Original Fourier transform.

b) Removal of high-frequency components beyond the resolution limit of the array. Since the weightings of the accepted spatial frequencies are unaltered the beamwidth remains constant.

c) Profile of the multiplying cosine-bell function used to smooth "noisy" records.

d) Reweighting of the accepted spatial frequencies achieved by multiplying b) by c). This reweighting increases the effective beamwidth by approximately 20%.

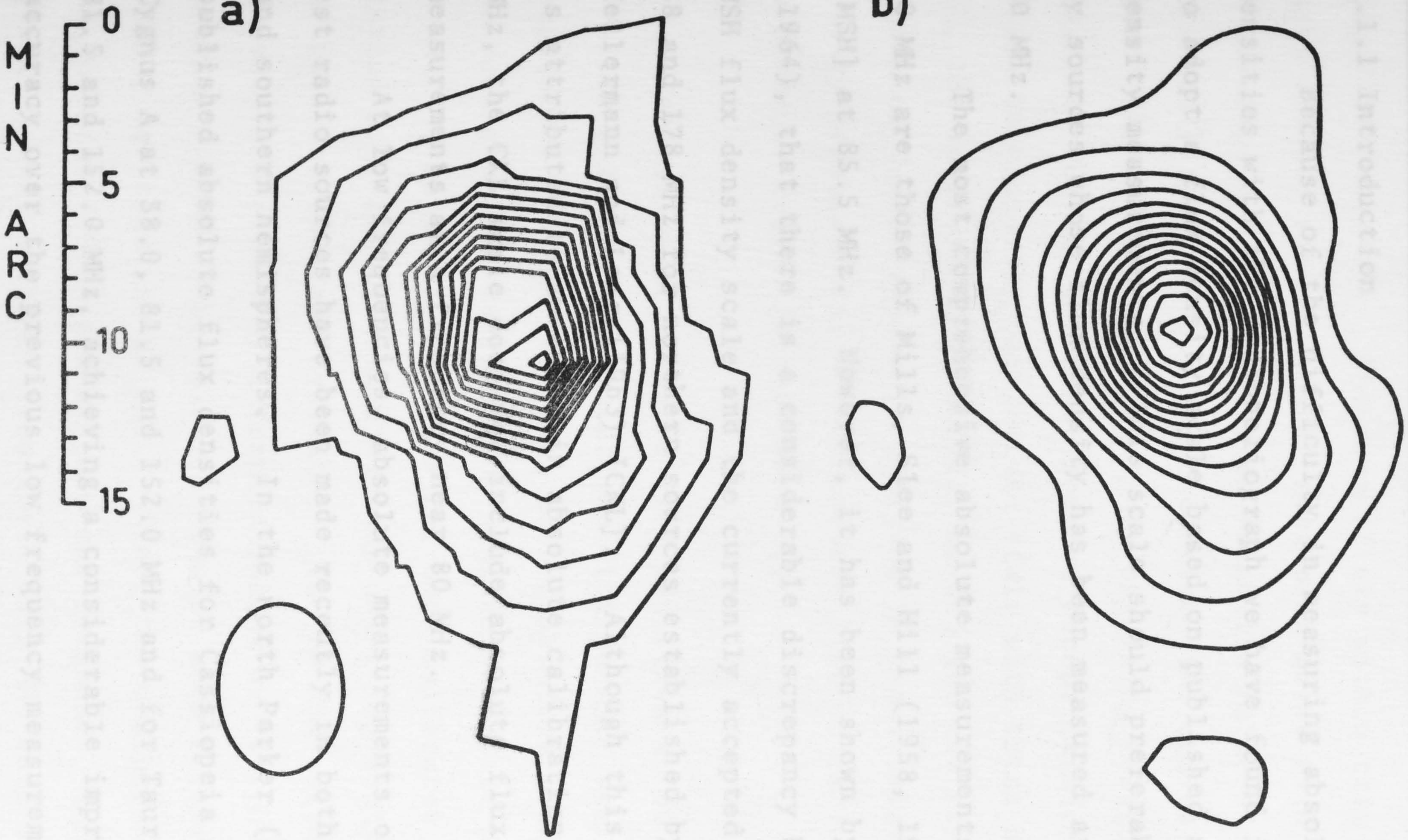

Fig. 2.4 - Examples of contour diagrams plotted by computer a) before interpolation b) after interpolation. The beamwidth is indicated by the ellipse in the lower left-hand corner.

CHAPTER 3

ABSOLUTE FLUX DENSITY CALIBRATION AND THE MEASUREMENT OF BRIGHTNESS TEMPERATURES

3.1 FLUX DENSITY CALIBRATION OF THE RADIOHELIOGRAPH

3.1.1 Introduction

Because of the difficulty in measuring absolute flux densities with the radioheliograph we have found it is necessary to adopt a flux density scale based on published absolute flux density measurements. This scale should preferably be defined by sources whose flux density has been measured at or near 80 MHz.

The most comprehensive absolute measurements near 80 MHz are those of Mills, Slee and Hill (1958, 1960, 1961) [MSH] at 85.5 MHz. However, it has been shown by Kellermann (1964), that there is a considerable discrepancy between the MSH flux density scale and the currently accepted scales at 38 and 178 MHz for northern sources established by Conway, Kellermann and Long (1963) [CKL]. Although this discrepancy is attributed to an error in absolute calibration at 85.5 MHz, the CKL scale does not include absolute flux density measurements at a frequency near 80 MHz.

At low frequencies, absolute measurements of the strongest radio sources have been made recently in both the northern and southern hemispheres. In the north Parker (1968) has published absolute flux densities for Cassiopeia A and Cygnus A at 38.0, 81.5 and 152.0 MHz and for Taurus A at 81.5 and 152.0 MHz, achieving a considerable improvement in accuracy over the previous low frequency measurements of these sources. In the south, absolute flux densities at 85 and 150 MHz for the sources Virgo A, Fornax A, Pictor A, Hydra A and Hercules A are available from a series of Parkes measurements based on carefully determined absolute flux density scales [Landecker (private communication); Yates, Wielebinski and Landecker (1967)].

With the radioheliograph it is possible to measure the relative flux densities of sources within the declination range -50° to +45°. The area of sky within this range contains all the strong sources mentioned above with the exception of Cassiopeia A. In order to establish an absolute flux density scale at 80 MHz, we have compared the scales of Parker (1968) and Yates et al. (1967) by obtaining relative flux densities for all the above sources except Cassiopeia A. To assist in comparing our derived scale with those of MSH and CKL, the sources 3C 33, 3C 123, 3C 273 and the strong central region of Centaurus A were included in these relative flux density measurements. The complete list of calibrator sources is given in column (1) of Table 3.1.

3.1.2 Derivation of absolute flux densities at 80 MHz

To allow comparison of the flux density scales it was necessary to obtain from each set of absolute measurements the best possible estimates of flux densities at precisely 80 MHz. The absolute values for each calibrator source were plotted as a function of frequency using logarithmic scales for both abscissa and ordinate. The 80 MHz estimate was then obtained either by interpolation or by "slight" extrapolation - i.e. using values at two or more frequencies including one close to 80 MHz. Since the measurements of MSH and Sheridan (1958) are at only one frequency, the 80 MHz estimates were obtained from their 85.5 MHz data with the aid of the Parkes 150 MHz results or of other published data at frequencies above 85.5 MHz.

TABLE 3.1

(1)	(2)		(3)		(4)		(5)		(6)	
	80 MHz Absolute Flux Density (10^{-26} W m^{-2} (Hz)$^{-1}$)									
Source	Parker or Landecker	±p.e.	MSH & Sheridan	±p.e.	CKL	±p.e.	Measured Relative Flux Density (80 MHz)	±p.e.	Adopted Flux Density (80 MHz)	±p.e.
Cygnus A	16500	500	-	-	15800	1600	9.43	0.08	16500	500
Taurus A	1900	190	-	-	1900	190	1.11	0.02	1900	150
Virgo A	1730	130	-	-	1850	180	1.06	0.06	1850	130
Centaurus A (central components)	-	-	2290	350	-	-	1.01	0.05	1750	170
Fornax A	950	140	1020	160	-	-	0.50	0.02	880	80
Hercules A	660	130	980	100	730	140	0.43	0.02	750	70
Hydra A	570	110	740	75	-	-	0.30	0.03	530	40
Pictor A	610	60	610	60	-	-	0.29	0.03	515	55
3C 123	-	-	-	-	380	40	0.23	0.03	390	30
3C 273	-	-	180	20	115	15	0.07	0.02	130	15
3C 33	-	-	-	-	96	13	0.05	0.01	91	10

The 80 MHz flux densities, with probable errors, obtained from the measurements of Parker (1968) and Yates et al. (1967) are given in column (2) of Table 3.1. Those obtained from the measurements of MSH or Sheridan (1958) and CKL are given in columns (3) and (4) respectively of Table 3.1.

3.1.3 Observational Procedure

To obtain accurate relative flux density measurements with the radioheliograph a three-day observing period was set aside for daily transit observations of the sources listed in Table 3.1. The rapid scanning method of observation described earlier was used throughout. With the exception of Fornax A it was possible to record two images per second using half the normal 2° x 2° picture field of the radioheliograph, thereby yielding 1800 half images in each 15 min observation.

Integration of 1800 successive images ensured a satisfactory signal-to-noise ratio for all sources. In the case of Fornax A, which has the lowest surface brightness of all the sources in Table 3.1 and for which only 900 1-sec scans were integrated, the peak signal-to-noise ratio was about 25. In all other cases the final peak signal-to-noise ratio was >100.

To check the linearity of the square-law detectors in the presence of strong sources, the three most intense sources Cygnus A, Taurus A and Virgo A were recorded first without attenuation and then with a 7 db attenuator inserted in the intermediate frequency system. There was no evidence, within the errors of measurement, of non-linearity in the relative flux densities thus obtained.

3.1.4 Data reduction

Relative flux densities for each source were obtained directly from the integrated record by summation of readings at those picture points containing the source. The validity of this procedure is demonstrated in Appendix I.

All source observations for the 3 days were processed in this manner, yielding three sets of relative flux density measurements. These 3 sets were then combined using scaling factors chosen to give more weight to the strongest sources since the measurements of these sources are most accurate. The scaling factors were, in fact, found to be equal within a few percent. As a check, these relative flux densities were compared, where possible, with measurements made on other days when two or more of the sources listed in Table 3.1 were observed. No significant variations were found.

3.1.5 Results

The relative flux densities thus obtained are listed in Table 3.1, column (5), and plotted in Figure 3.1 against the corresponding absolute values given in columns (2), (3) and (4). To avoid confusion in this diagram the absolute flux densities in column (4) (CKL) for Cygnus A, Taurus A, Virgo A and Hercules A have been omitted. Probable errors in absolute and relative flux density are indicated by vertical and horizontal bars respectively. The scale of both abscissa and ordinate is logarithmic.

A straight line of best fit (labelled "line A") has been drawn at 45° through the points corresponding to the absolute flux density measurements of Parker (1968) and Yates et al. (1967) (column (2) of Table 3.1). In fitting this line, more weight was given to the most accurate measurements.

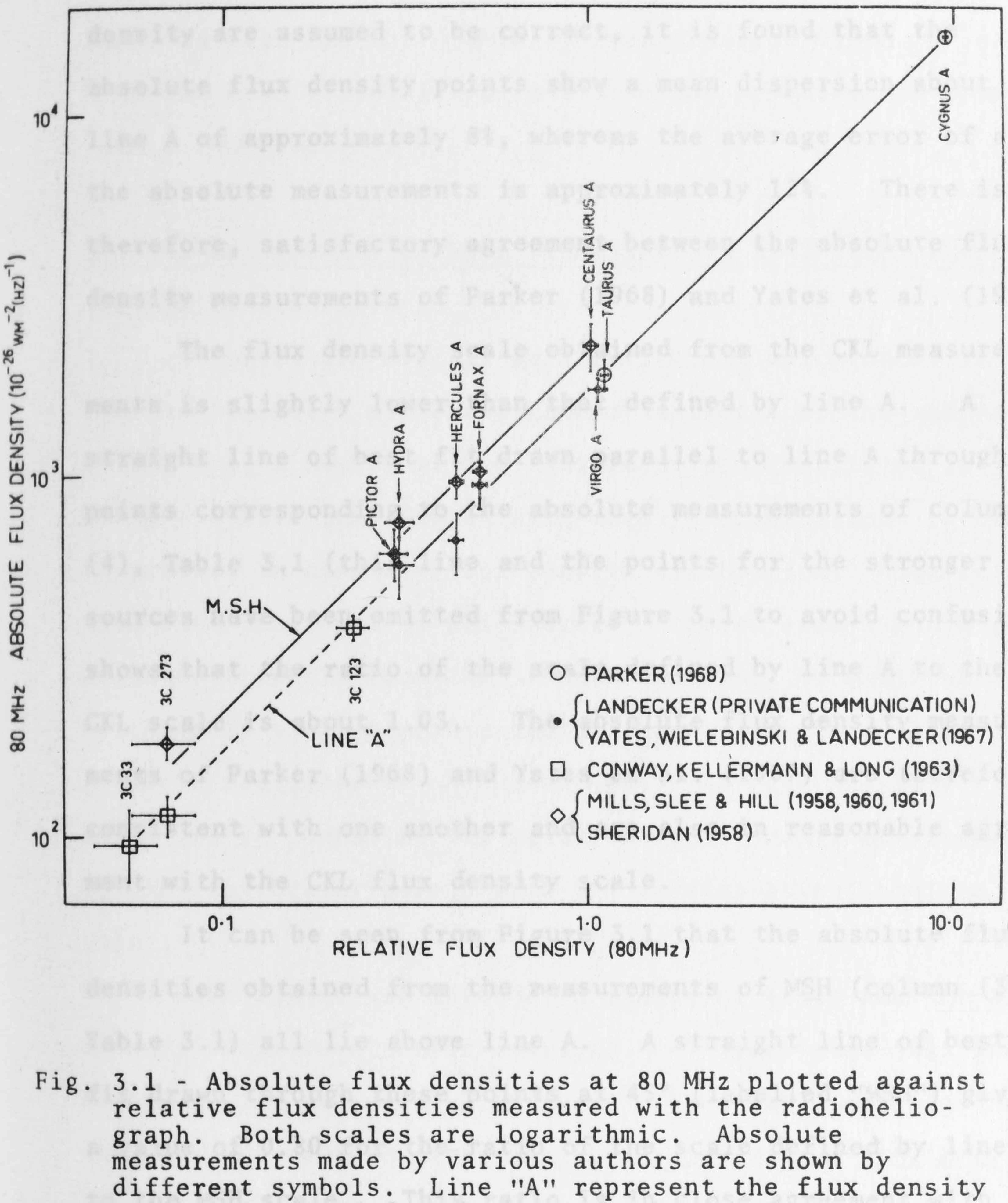

Fig. 3.1 - Absolute flux densities at 80 MHz plotted against relative flux densities measured with the radioheliograph. Both scales are logarithmic. Absolute measurements made by various authors are shown by different symbols. Line "A" represent the flux density calibration used for the present observations.

If the radioheliograph measurements of relative flux density are assumed to be correct, it is found that the absolute flux density points show a mean dispersion about line A of approximately 8%, whereas the average error of all the absolute measurements is approximately 12%. There is, therefore, satisfactory agreement between the absolute flux density measurements of Parker (1968) and Yates et al. (1967).

The flux density scale obtained from the CKL measurements is slightly lower than that defined by line A. A straight line of best fit drawn parallel to line A through points corresponding to the absolute measurements of column (4), Table 3.1 (this line and the points for the stronger sources have been omitted from Figure 3.1 to avoid confusion) shows that the ratio of the scale defined by line A to the CKL scale is about 1.03. The absolute flux density measurements of Parker (1968) and Yates et al. (1967) are therefore consistent with one another and are also in reasonable agreement with the CKL flux density scale.

It can be seen from Figure 3.1 that the absolute flux densities obtained from the measurements of MSH (column (3), Table 3.1) all lie above line A. A straight line of best fit drawn through these points at 45° (labelled "MSH") gives a value of 0.80 for the ratio of the scale defined by line A to the MSH scale. This ratio is in close agreement with the scaling factor of 0.82 which Kellermann (1964) has suggested should be applied to the MSH flux density measurements.

The 80 MHz flux density scale which has been adopted for the present measurements is that defined by line A. The absolute flux densities thus obtained are listed in column (6) of Table 3.1. In view of the close agreement between these values and the corresponding absolute flux densities obtained from the CKL measurements, it is felt that the flux density scale adopted has a probable systematic error which is less than the mean dispersion of the absolute measurements from line A i.e. <8%.

3.2 THE MEASUREMENT OF FLUX DENSITIES AND BRIGHTNESS TEMPERATURES

3.2.1 Flux densities

To allow for overall gain variations which occur from time to time with phase and gain adjustments of the radioheliograph, a number of the calibrator sources listed in Table 3.1 were included in each night's observations in order to provide an absolute flux density calibration. The relative flux densities of all sources observed each night were obtained directly from the integrated record by addition of readings at picture points containing the source. These relative measurements were then converted into absolute flux densities by comparing the relative flux density measurement of each calibrator source with its corresponding absolute value.

Each source was recorded a number of times and the flux density measurements were averaged. It was found that the errors in the averaged values were in general less than the estimated systematic error of ±8% in the adopted flux density scale. The final error in the flux density of each source was estimated by combining the error in measurement with the systematic error in the scale.

3.2.2 Brightness temperatures

The distribution of brightness temperatures over each source could be calculated directly from the digital record once the constant, α, relating relative flux density S_R and absolute flux density S_A was known.

Since S_R is just the summation of the readings S_{Ri} at picture points containing the source, S_A represents the summation of flux density contributions S_{Ai} from these points, where $S_{Ai} = \alpha S_{Ri}$.

Each picture point can be regarded as subtending a solid angle $\Delta\Omega$ in the shape of a rectangle (for meridian observations) whose sides are defined by the picture point spacings. For observations in the meridian at zenith angle z the east-west picture point spacing is 2'.148 arc and the north-south spacing is (2'.148sec z)arc so that

$$\Delta\Omega = \frac{(2.148)^2 \sec z}{3600\ (180/\pi)^2} \qquad 3.1$$

where $\Delta\Omega$ is in steradians. The brightness temperature T_{Bi} of each point is then derived from the relation

$$S_{Ai} = \frac{2k}{\lambda^2}\ (T_{Bi}\Delta\Omega) \qquad 3.2$$

where k is Boltzmann's constant and λ the wavelength.

Brightness temperatures measured in this way only have their true significance when the angular size of the source is very much greater than that of the beam. In cases where the source is not well resolved by the beam the present measurements give only a lower limit to the true brightness temperatures.

CHAPTER 4

EXTRAGALACTIC SOURCES

4.1 Introduction

Results are presented in this chapter for 21 radio sources which are known or believed to be extragalactic. An 80 MHz contour map and flux density has been obtained for each source. All the sources are sufficiently removed from strong sources or are themselves strong enough to ensure negligible interference from grating responses.

Maps of Fornax A and Pictor A, obtained during preliminary observations with the radioheliograph, have been published already (Morimoto and Lockhart, 1968). The results presented here for these and all other sources were obtained at later times with better sensitivity and reduced sidelobe levels. Observations of Centaurus A have also been published (Lockhart and Sheridan, 1970) and are included here for completeness; the flux density given in Table 3.1 is of greater accuracy than the published value.

Where possible the structure at 80 MHz has been compared with that observed at higher frequencies. In Table 4.1 we give references to the high frequency observations used in these comparisons together with the operating frequencies and observing beamwidths or range of aerial spacings. Beamwidths of the Parkes 210 ft telescope operated at 5000 MHz, the 408 MHz Mills Cross and the 80 MHz radioheliograph are similar, allowing direct comparison of maps at these three frequencies.

TABLE 4.1

Frequency (MHz)	Instrument	Beamwidth or range of aerial spacings	Ref. in text	Ref. No.
408	Sydney University Mills Cross	Elliptical: 2'.86 x 2'.86sec z arc	SMa	1
"	"	"	SMb	2
"	"	"		3
408	Cambridge 1.5 km aperture synthesis	Elliptical: 80" x 80" cosec δ arc	MNR	4
"	"	"	MKN	5
468	Parkes variable baseline interferometer	Baselines 191-652λ		6
960	Caltec variable baseline interferometer (EW)	Baselines 195-1557λ		7
"	" (NS)	"		8
"	"	Baselines 195-1557λ (EW and NS)		9
1403	Parkes variable baseline interferometer	Baselines 574-1950λ		6
1407	Cambridge 1.5 km aperture synthesis	Elliptical: 23" x 23" cosec δ arc	MNR	4
"	"	"	MKN	5
1420	Nancay variable baseline interferometer	400-7000λ EW; 400-1800λNS		10
1425	Caltec variable baseline interferometer (EW)	144-2626λ		11
2695	NRAO aperture synthesis	Elliptical approx. 8" arc		12
4995	Cambridge 1.5 km aperture synthesis	6".5 x 6".5 cosec δ arc		13
5000	Parkes 210-ft paraboloid	Circular 4'.0 arc	WG	14
"	"	"	W	15
5009	"	"		16

References for Table 4.1

1. Schilizzi, R.T. and McAdam, W.B. (1969) Proc. A.S.A., 1, 228.
2. Schilizzi, R.T. and McAdam, W.B. (1970) Proc. A.S.A., 1, 337.
3. Cameron, M.J. (1969) Proc. A.S.A., 1, 229.
4. Macdonald, G.H., Neville, A.C., and Ryle, M. (1966) Nature, Lond., 211, 1241.
5. Macdonald, G.H., Kenderdine, S., and Neville, A.C. (1968) Mon. Not. R. ast. Soc., 138, 259.
6. Ekers, R.D. (1969) Aust. J. Phys., Astrophys. Suppl. No. 6.
7. Moffet, A.T., (1962) Astrophys. J. Suppl. Ser. 67, 93.
8. Maltby, P., (1962) Astrophys. J. Suppl. Ser. 67, 124.
9. Maltby, P., and Moffet, A.T., (1962) Astrophys. J. Suppl. Ser. 67, 141.
10. Lequeux, J., (1962) Ann. d'Astrophys. 25, 221.
11. Fomalont, E.B., (1968) Astrophys. J. Suppl. Ser. 15, 203.
12. Hogg, D.E., Macdonald, G.H., Conway, R.G., and Wade, C.M. (1969) Astron. J. 74, 1206.
13. Komesaroff, M.M., private communication.
14. Whiteoak, J.B., and Gardner, F.F., private communications.
15. Wall, J.V., private communications.
16. Shimmins, A.J., Manchester, R.N., Harris, B.J. (1969) Aust. J. Phys., Astrophys. Suppl. No. 8.

4.2 Presentation of results

4.2.1 Contour maps

All maps are drawn on Cartesian coordinates with equal angular scales for δ and $\alpha \cos \delta$. The maps are at 80 MHz unless otherwise noted. The half-power beam is indicated in each case by an ellipse of appropriate eccentricity drawn in the lower left- or right-hand corner of the diagram. Since all observations were made at transit, the major axis of the beam is parallel to the ordinate of the diagram. Where the map has been smoothed by computer as described in §2.5.2(3), the half-power beam indicated in the diagram has been increased accordingly.

The contour interval is determined in the computer plotting routine by dividing the range from the zero-level to the maximum brightness into a specified number of equal steps. The number of steps depends on the flux density and complexity of the individual source and was chosen so that as much information as possible may be given without the maps becoming obscure. The contours plotted are at the half, one-and-a-half, two-and-a-half etc. levels with the top contour one-half contour interval below the maximum. The lowest contour drawn on most of the maps presented below is one-half the contour interval above the zero level. A minus sign has been placed within those contours representing a depression in the observed structure. Table 4.2 gives the peak brightness temperature and contour interval for each source.

Generally, the limitation to the accuracy of the zero-level determination is distant sidelobe structure, giving deflections of about ±3% of the maximum brightness. In a few cases the zero-level determination is limited by noise, giving deflections of about ±10% of the maximum brightness.

TABLE 4.2
SOURCE LIST

(1)	(2)	(3)		(4)		(5)	(6)	(7)	(8)	(9)	(10)
Parkes Number	3C or other name	S_{80}*	±p.e.	Peak T_B $(10^{4}\,^{\circ}K)$	±p.e.	Contour Interval $(10^{3}\,^{\circ}K)$	Error in RA (sec)	Error in Dec('arc)	α_{80}	$\alpha_{1400-5000}$	Θ $(^{\circ})$
PKS 0106+13	33	91	10	19	2	11.9	-5.5	-2.5	0.72	0.68	20
PKS 0123-01	40	58	7	4.0	0.5	2.67	-4.7	1.2	0.86	0.84	
PKS 0131-36		45	5	7.1	0.6	5.46	-3.5	0.7	0.64	0.70	92
0220+42	66	49	5	2.3	0.3	1.77	-13.9	-3.4	0.43	0.75	
0254+06		13	2						0.77	0.77	
PKS 0255+05	75	48	4	7.1	0.7	5.91	-6.8	1.1	0.74	0.74	
0316+41	84,Perseus A	159	14	13	1	10.0	-14.8	2.5			
PKS 0320-37	Fornax A	880	80	12	1	8.57	0.0	1.5	0.94	0.57	105
PKS 0349-27		44	5	12	2	8.00	1.1	0.7	0.49	0.80	66
PKS 0511-30		37	4	4.3	0.4	4.30	-3.0	-0.3	0.80	1.00	20
PKS 0518-45	Pictor A	515	55	81	9	54.0	0.5	0.0	0.75	0.71	103
PKS 0634-20		74	6	9.6	1.6	8.00	-2.6	0.1	0.61	0.88	178
PKS 0800-09		31	5	3.1	0.7	2.82	0.2	1.4	1.00	0.40	
PKS 0819-30		30	3	5.9	0.5	4.54	-4.0	0.2	0.82	1.03	126
PKS 1228+12	274,Virgo A	1850	130	250	20	167	-9.0	-0.1	0.78	0.88	
PKS 1322-42	Centaurus A	1750	170	270	24	220	-5.5	1.0	0.64	0.64	44
PKS 1559+02		90	10	21	3	17.5	-6.6	0.4	0.89	0.80	97
PKS 1648+05	348,Hercules A	750	70	170	20	100	-5.0	-0.4			
PKS 2058-28		55	5	6.2	0.6	4.77	4.2	1.5	0.77	0.85	0
PKS 2104-25		92	17	15	1	12.50	-3.8	4.3?	0.60	0.82	

TABLE 4.2 (contd)

(1)	(2)	(3)	(4)	(5)	(6)	(7)	(8)	(9)	(10)
PKS 2221-02	445	45 10	4.8 0.6	4.00	-6.6	2.2	0.78	0.78	167
PKS 2335+26	465	68 10	5.0 0.6	3.33	-7.3	0.3	0.78	0.78	

---

* In units of $10^{-26} Wm^{-2} (Hz)^{-1}$

The overall accuracy of each map is a function of source size, sidelobe structure, noise fluctuations and ionospheric distortion effects. For most maps the limitation to the accuracy is sidelobe structure near the central response giving deflections of about half a contour. A few sources of low surface brightness are limited by noise, giving deflections of about one contour. The lowest contour in particular is subject to error and is shown as a broken line on each map merely to indicate the overall extent of the source.

The coordinates shown on each map were measured directly with the radioheliograph and precessed to 1950.0. No attempt has been made to correct for displacements in position caused by ionospheric refraction. Comparisons with high frequency observations have, in most cases, allowed the probable errors in position to be estimated. These are given in Table 4.2. It was found, after the maps had been drawn, that a slight error in the computer plotting routine had displaced each map 0'.72 arc to the west of the measured right ascension. No correction has been made for this error so that all the right ascensions given on the maps are too small by 0'.72 arc. After allowing for this error, it is estimated that the measured positions are accurate to about ±1' arc in both coordinates. As the measured positions do not improve on previous accuracy, new optical identifications were not attempted.

4.2.2 Source list

The sources observed are listed in Table 4.2, whose successive columns give:

(1) The Parkes number of the source or the number of the source in the Parkes system.

(2) The number of the source in the revised 3C catalogue

or any alternative source name.

(3) The measured 80 MHz flux density with probable error.

(4) The 80 MHz peak brightness temperature with probable error.

(5) The contour interval used in plotting the contour diagram.

(6) Estimated error in the measured right ascension.

(7) Estimated error in the measured declination.

(8) The approximate spectral index, α, for the whole source at 80 MHz, where α is defined in the sense $S \propto \nu^{-\alpha}$.

(9) The approximate spectral index, α, for the whole source between 1400 and 5000 MHz.

(10) The position angle on the sky, θ, of the main radio axis. No value is given for sources with complex structure or for barely resolved sources.

4.2.3 Spectral index diagrams

The same format has been used for all spectral index diagrams. The frequency (in MHz) is plotted along the abscissa and the flux density (in units 10^{-26} W m^{-2} $(Hz)^{-1}$) along the ordinate. Both scales are logarithmic. The present measurements of integrated flux density are indicated by an open circle and all other measurements by filled circles.

Criteria were established in order to select the most reliable flux density measurements from the large volume of material available. In Table 4.3 we give references to the material used together with a reliability rating for each source of data. Measurements with a rating (1) were used wherever possible. A rating (2) indicates that the flux densities included in the reference were used only when measurements at that frequency or in that frequency range with a rating (1) were not available. Below 38 MHz all

TABLE 4.3

References to flux density measurements used in plotting spectral index diagrams

(1) Frequency (MHz)	(2) Author and Publication	(3) Rating
4.7	Ellis, G.R.A., and Hamilton, P.A.,(1966) Astrophys. J.,143 (1), 227.	1
10.03	Bridle, A.H., and Purton, C.R., (1968), Astron. J., 73, 717	1
12.6 to 25	Braude, S.Ya., Zhuk, I.N., et al.,(1968), Soviet Phys. Doklady,13, 512	1
12.6 to 25	Braude, S.Ya., Lebedeva, O.M. et al.,(1969), Astrophys. Letters, 5, 129	1
12.6 to 25	Braude, S.Ya., Lebedeva, O.M., et al.,(1969), Mon. Not. R. astr. Soc., 143, 289	1
13.1	Andrew, B.H., (1967), Astrophys. J., 147, 423	1
19.7	Shain, C.A., (1958), Aust. J. Phys., 11, 517	1
22.25	Roger, R.S., Costain, C.H., and Lacey, J.D., (1969), Astron. J., 74, 366	1
26.3	Erickson, W.C., and Cronyn, W.M.,(1965), Astrophys. J.,142, 1156	1
38, 178, 750, 1400, 2695, 5000	Kellermann, K.I., Pauliny-Toth, I.I.K., and Williams, P.J.S.,(1969), Astrophys. J., 157, 1	1
38, 178, 240, 408, 412, 710, 958, 1420, 3200	Conway, R.G., Kellermann, K.I., and Long, R.J.,(1963), Mon. Not. R. astr. Soc., 125, 261	2

TABLE 4.3 (contd)

38, 178, 617, 1417	Long, R.J., Smith, M.A., Stewart, P., and Williams, P.J.S., (1966), Mon. Not. R. astr. Soc. 134, 371	2
38, 178, 610.5 1417	Williams, P.J.S., and Stewart, P., (1967), Mon. Not. R. astr. Soc. 135, 319	2
38, 178, 408, 1410, 2650	Williams, P.J.S., Collins, R.A., Caswell, J.L., and Holden, D.J., (1968), Mon. Not. R. astr. Soc. 139, 289	2
38, 81.5, 152	Parker, E.A., (1968), Mon. Not. R. astr. Soc. 138, 407	1
85	Yates, K.W., Wielebinski, R., and Landecker, T.L., (1967), Aust. J. Phys. 20, 595	1
85, 150	Landecker, T.L., private communication	1
408, 1410, 2650	Day, G.A., Shimmins, A.J., Ekers, R.D., and Cole, D.J., (1966), Aust. J. Phys. 19, 35	2
408, 1410, 2650	Shimmins, A.J., Day, G.A., Ekers, R.D., and Cole, D.J., (1966), Aust. J. Phys. 19, 837	2
408, 1410, 2650	Bolton, J.G., Gardner, F.F., and Mackay, M.B., (1964), Aust. J. Phys. 17, 340	2
408, 1407	Macdonald, G.H., Neville, A.C., and Ryle, M., (1966), Nature, 211, 1241	2
408, 1407	Macdonald, G.H., Kenderdine, S., and Neville, A.C., (1968), Mon. Not. R. astr Soc. 138, 259	2
408, 1407	Mackay, C.D., (1969), Mon. Not. R. astr. Soc. 145, 31	2
408, 1407	Ryle, M., and Windram, M.D., (1968), Mon. Not. R. astr. Soc. 138, 1	2
468, 1403	Ekers, R.D., (1969), Aust. J. Phys. Astrophys. Suppl. No.6	1
475 to 2841	Kellermann, K.I., (1964a), Astron. J., 69, 205.	1
635,1410,2650	Shimmins, A.J., and Day, G.A., (1968), Aust. J. Phys., 21, 377	2

TABLE 4.3 (contd).

750 to 15000	Kellermann, K.I., and Pauliny-Toth, I.I.K., (1968), Astrophys. J.,152,(2Pt1),639	1
960	Harris, D.E., and Roberts, J.A., (1960) P.A.S.P., 72, 237	1
960	Moffet, A.T., (1962), Astrophys. J. Suppl. Ser., 67, 93	1
1425	Fomalont, E.B., (1967), Publ. Owens Valley Radio Observatory, 1, No. 3	1
2695	Hogg, D.E., Macdonald, G.H., Conway, R.G., and Wade, C.M., (1969), Astron. J., 74, 1206	1
2695, 4995	Horton, P.W., Conway, R.G., and Daintree, E.J., (1969), Mon. Not R. astr. Soc., 143, 245	1
5009	Shimmins, A.J., Manchester, R.N. and Harris, B.J., (1969), Aust. J. Phys. Astrophys. Suppl. No. 8	1
8000	Dent, W.A., and Haddock, F.T., (1966) Astrophys. J. 144, 568	1

measurements were plotted irrespective of probable errors in absolute calibration or in the relative flux density measurements.

4.3 Results

0106+13 (3C 33)

At 408 and 1407 MHz, 3C 33 consists of three components of small angular size and unequal intensity (MKN). All three components are <25" arc in diameter. The two outer and most intense components are separated by 4'.07 arc in PA = 20°; the much weaker third component lies between them on the major axis and is separated from the southern component by 1'.53 arc.

The components are not resolved at 80 MHz, but the contours (Fig. 4.1(a)) are elongated in PA = 15°. The convolution of the asymmetrical source structure with the elliptical 80 MHz beam accounts for the apparent discrepancy in position angle between these observations and those of MKN.

Although the components are not resolved at 80 MHz, their intensities have been estimated from the contour diagram with the aid of the position and angular size measurements at 1407 MHz. It was assumed that the relative positions and angular sizes of the components do not change significantly between 80 MHz and 1407 MHz. All three components are then of sufficiently small angular size to be treated as point sources at 80 MHz.

The profile in PA = 20° obtained from the 80 MHz map is shown as a full line in Figure 4.1(b). After numerous attempts it was found that this profile could not be reproduced by two point sources separated by 4'.07 arc: a third source situated between them was required. Using the known

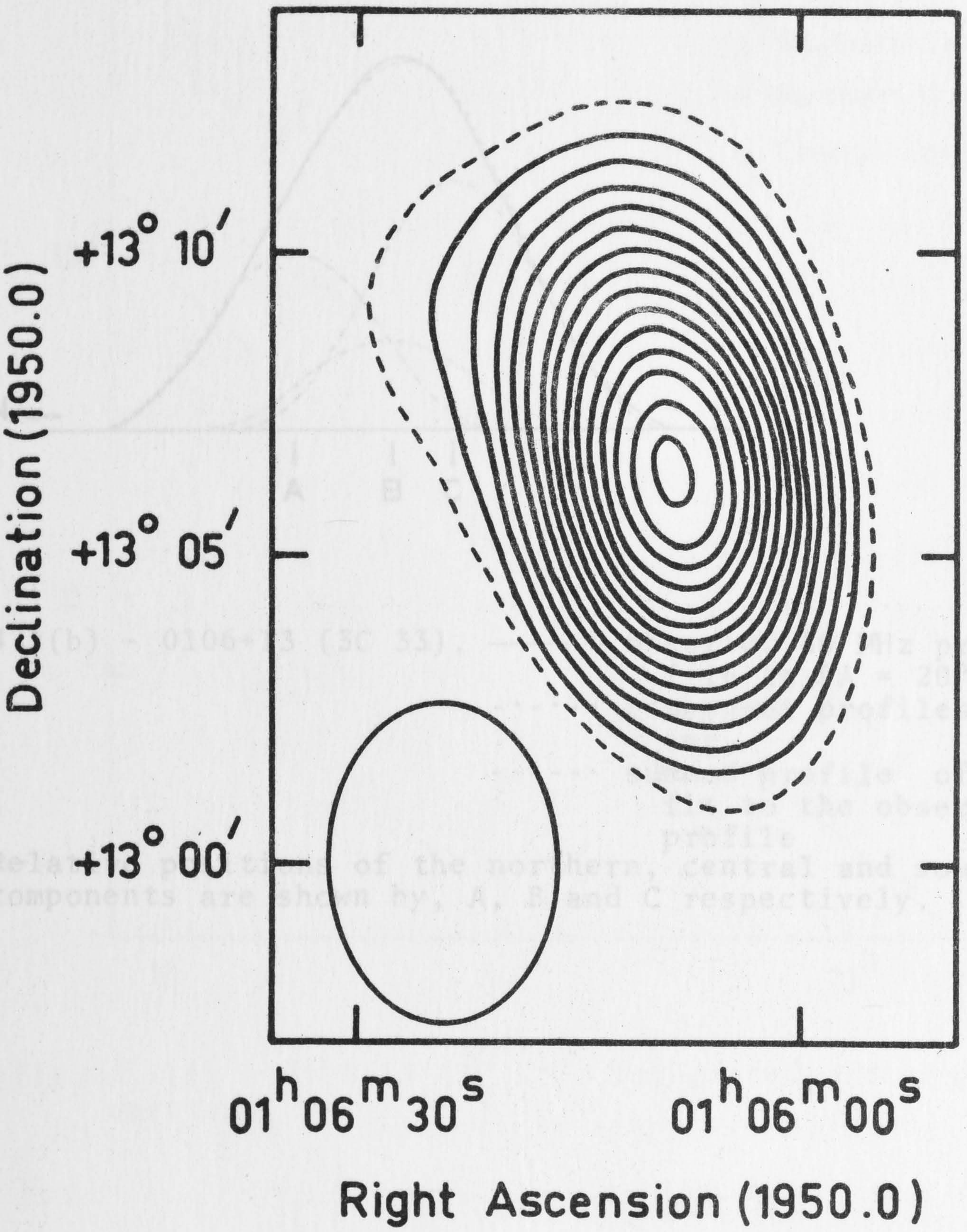

Fig. 4.1(a) - 0106+13 (3C 33).

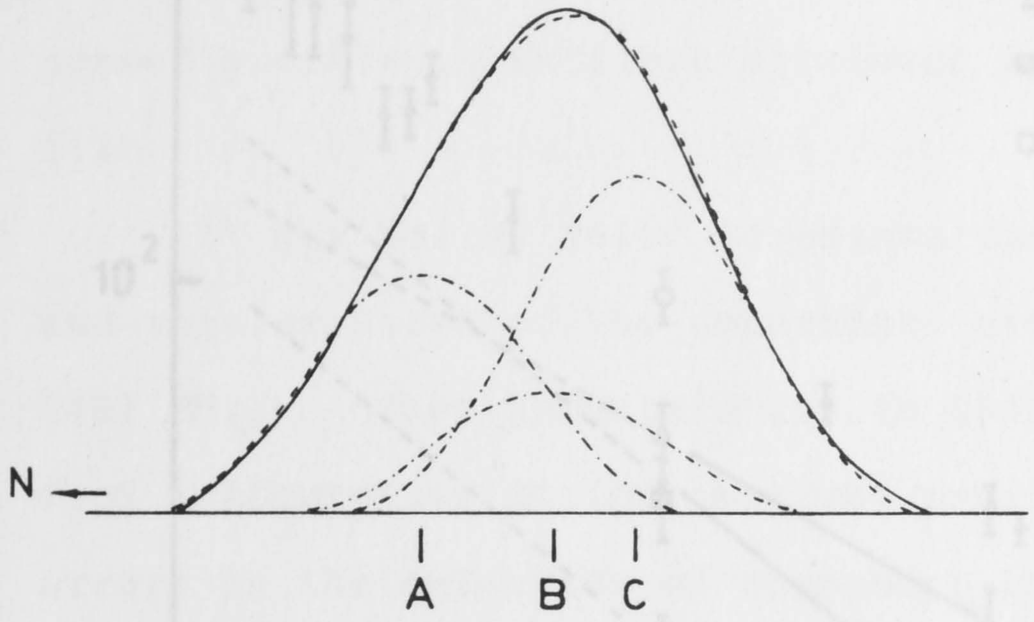

Fig. 4.1(b) - 0106+13 (3C 33). ——— observed 80 MHz profile in PA = 20°
-·-·-· component profiles giving,
------ summed profile of best fit to the observed profile

Relative positions of the northern, central and southern components are shown by, A, B and C respectively.

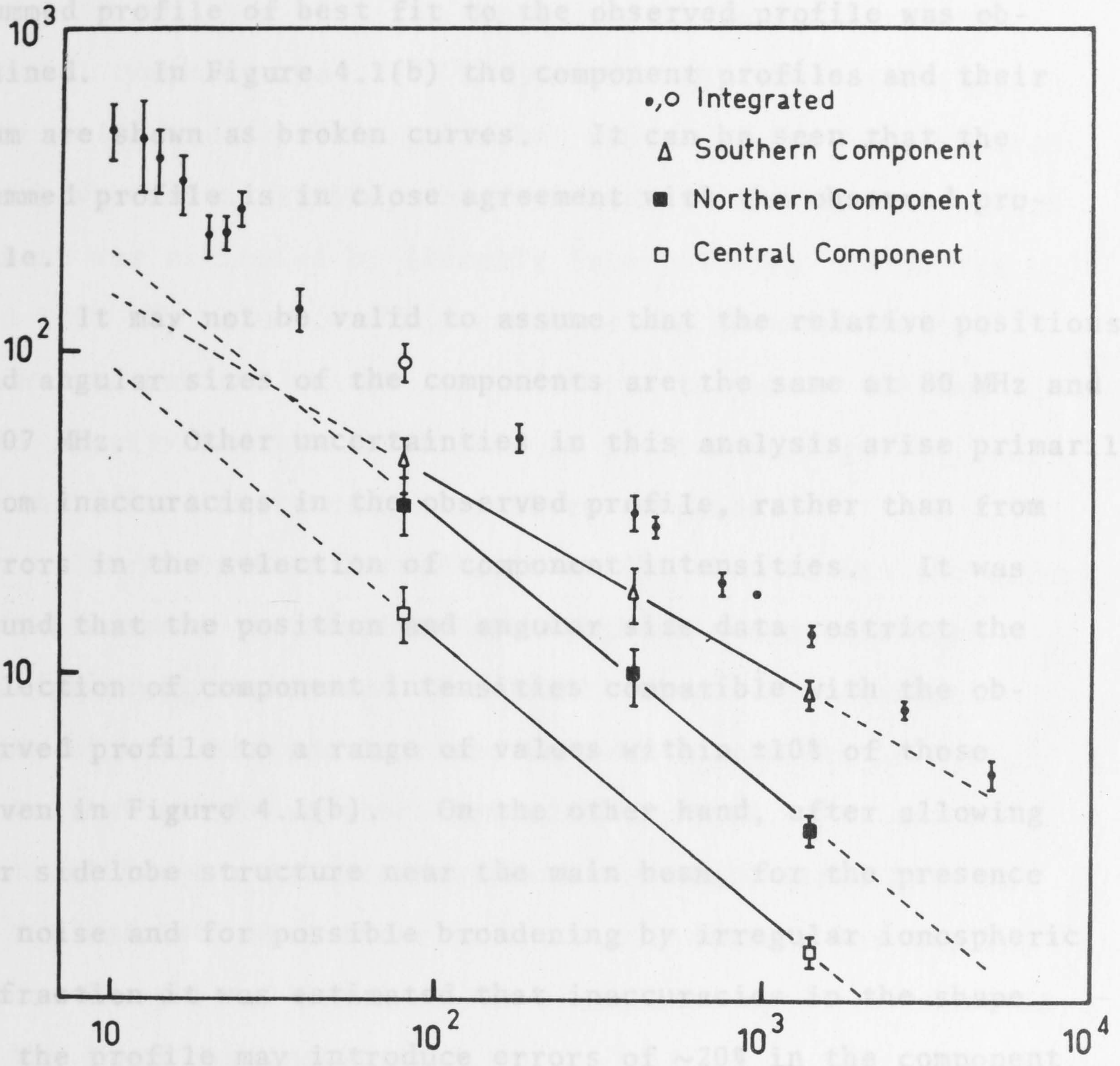

Fig. 4.1(c) - 0106+13 (3C 33). Integrated and component spectra.

position of the third component detected at 1407 MHz, the intensities of the three components were adjusted until a summed profile of best fit to the observed profile was obtained. In Figure 4.1(b) the component profiles and their sum are shown as broken curves. It can be seen that the summed profile is in close agreement with the observed profile.

It may not be valid to assume that the relative positions and angular sizes of the components are the same at 80 MHz and 1407 MHz. Other uncertainties in this analysis arise primarily from inaccuracies in the observed profile, rather than from errors in the selection of component intensities. It was found that the position and angular size data restrict the selection of component intensities compatible with the observed profile to a range of values within ±10% of those given in Figure 4.1(b). On the other hand, after allowing for sidelobe structure near the main beam, for the presence of noise and for possible broadening by irregular ionospheric refraction it was estimated that inaccuracies in the shape of the profile may introduce errors of ~20% in the component intensities.

The relative intensities of the components have been combined with the integrated flux density measurement at 80 MHz to give the flux density of each component. In Figure 4.1(c) the spectrum of each component is shown together with measurements of the integrated spectrum between 10 MHz and 5000 MHz.

The component flux density measurements at 408 MHz given by MKN have been scaled up by 36% so that their sum agrees with the integrated value given by Conway, Kellermann and Long (1963). The flux densities published by MKN at both 408 and 1407 MHz are for the northern component alone and for the southern and central components combined. In order to separate the flux densities of the southern and central components at 1407 MHz, their relative intensities were estimated from the published map. At 408 MHz, where a map was not available, the flux density of the central component was estimated by linearly interpolating the 80 MHz and 1407 MHz values. This estimate was then subtracted from the combined central and southern component 408 MHz flux density and the difference is plotted in Figure 4.1(c) as the flux density of the southern component.

It can be seen from Figure 4.1(c) that within the errors of measurement the northern and southern components have straight spectra between 80 and 1407 MHz. The spectral index of both the northern and central components is 0.83, while that of the southern component is 0.58. If these spectral indices are constant over the whole range between 10 MHz and 1407 MHz, their values would account for the increase in spectral index of the integrated spectrum observed at the lower frequencies.

The spectra of the outer components are consistent with the evolutionary model proposed by Ryle and Longair (1967) in that the southern component, which lies nearer the parent galaxy, has a much flatter spectrum than the northern component. The model assumes that two identical components are ejected from the parent galaxy with equal and opposite relativistic velocities along a straight line making an angle ϕ with the line of sight. Unless the axis of the system is perpendicular to the line of sight, the two components will subsequently be observed at significantly different ages, with the receding component nearer the parent galaxy and apparently younger than the approaching component. The southern and northern components of 3C 33 are separated from the optical position by 109" arc and 135" arc respectively. The model thus implies that the southern component is younger than the northern component, giving ages of 1.536×10^6 years and 1.9×10^6 years with an assumed value of $\phi = 60^o$ (Ryle and Longair, 1967).

On the other hand, it is believed (Kellermann, 1966) that initially the spectra of radio sources are relatively flat ($\alpha \sim 0.25$) and that a gradual steepening results from the combined effects of synchrotron radiation losses and repeated particle injection. If it is assumed that initially the outer components of 3C 33 had similar spectra with $\alpha \sim 0.25$, the observed difference in their spectra at the present time implies that the southern component is younger than the northern component, in agreement with the results of Ryle and Longair.

Depending on their stage of evolution, sources in which repeated particle injection is not occurring are expected to either have spectral indices of ~0.25 or ~1.33 over the entire observed frequency range, or to exhibit a sharp transition from $\alpha \sim 0.25$ at low frequencies to $\alpha \sim 1.33$ at high frequencies. Since the components of 3C 33 do not show these spectral characteristics, it seems probable that repeated particle injection is occurring. It is unlikely that the parent galaxy constitutes the source of relativistic particles since the radio emitting regions are far removed and are very compact. Apparently, particle acceleration is occurring within the components themselves.

The spectrum of the central component appears to contradict the evolutionary model of Ryle and Longair (1967).

This component is closest to the parent galaxy and yet it has a spectral index similar to that of the most distant component. A possible explanation is that this region is made up of material originally in the southern component which has been separated during expansion and is now evolving more rapidly than the outer components.

0123-01 (3C 40)

This source has very complex structure. The 80 MHz map in Figure 4.2(a) shows that in addition to the two main components there is an arc-like component to the south-west of the southern peak and an extended plateau whose shape indicates the presence of another component to the north of the secondary peak. There is additional structure to the west of the northern peak.

The source is associated with NGC 545-547, a pair of closely spaced, 13^m elliptical galaxies which are classified as cD4 by Matthews, Morgan and Schmidt (1964). A third 13^m elliptical, NGC 541, lies 4'.6 arc to the south-west of the double galaxy. The positions of these galaxies are indicated by crosses in Figure 4.2(a). According to Zwicky (1961), there is a luminous bridge connecting NGC 545-547 to NGC 541, with a fainter extension toward a spiral situated directly in line with the ellipticals and 8'.9 arc to the south-west of NGC 545-574. The three 13^m elliptical galaxies are the brightest members of cluster Abell 194 and are distant approximately 53 Mpc (Matthews, Morgan and Schmidt, 1964). Accurate positions for all three galaxies have been measured by Griffin (1963).

A previously unpublished 5000 MHz map is available from Parkes (W). This map has been reproduced to the same scale

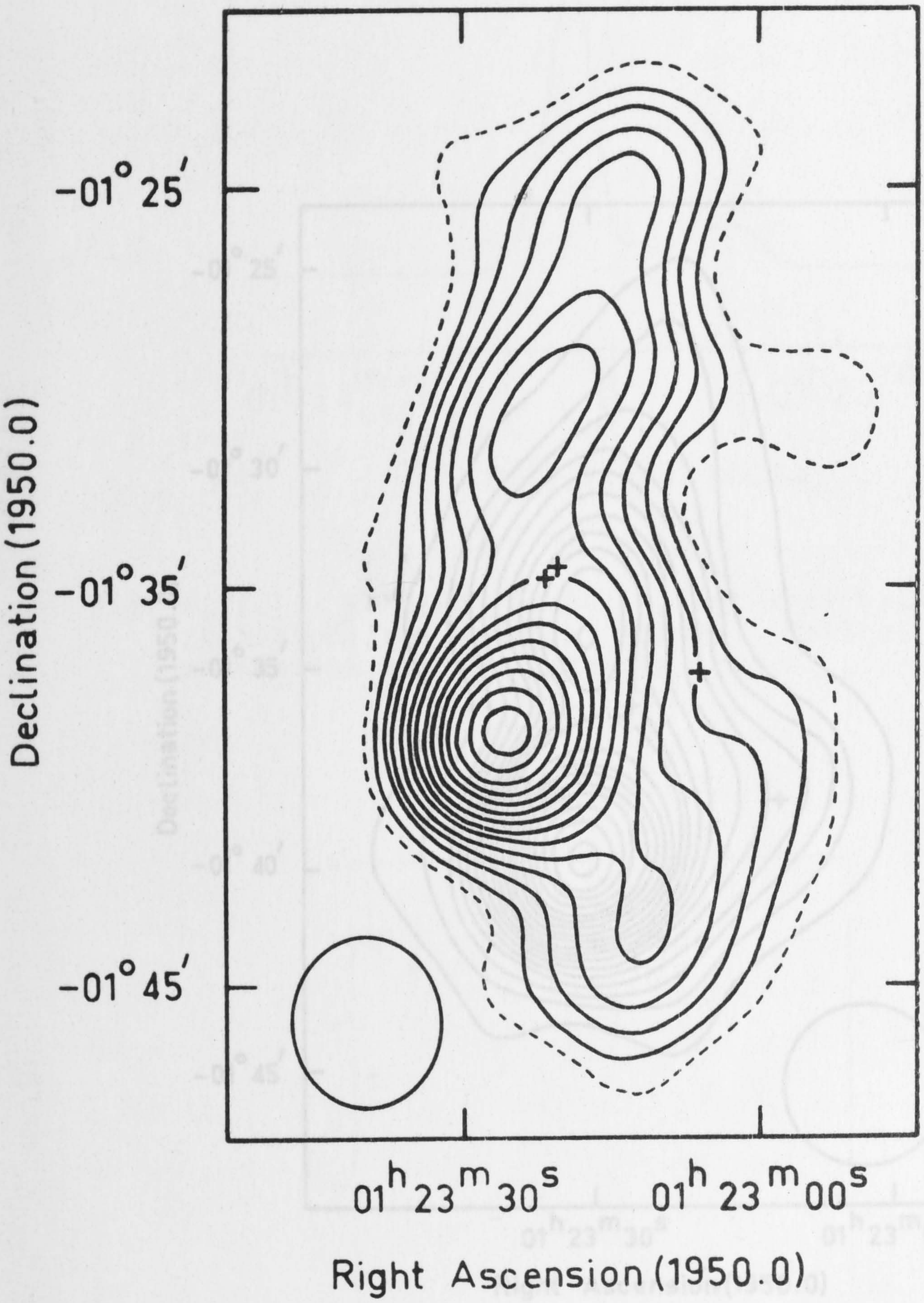

Fig. 4.2(a) - 0123-01 (3C 40). Approximate positions of NGC 545-547 are shown by two closely spaced crosses. The position of NGC 541 is shown by the cross to the south-west of NGC 545-547.

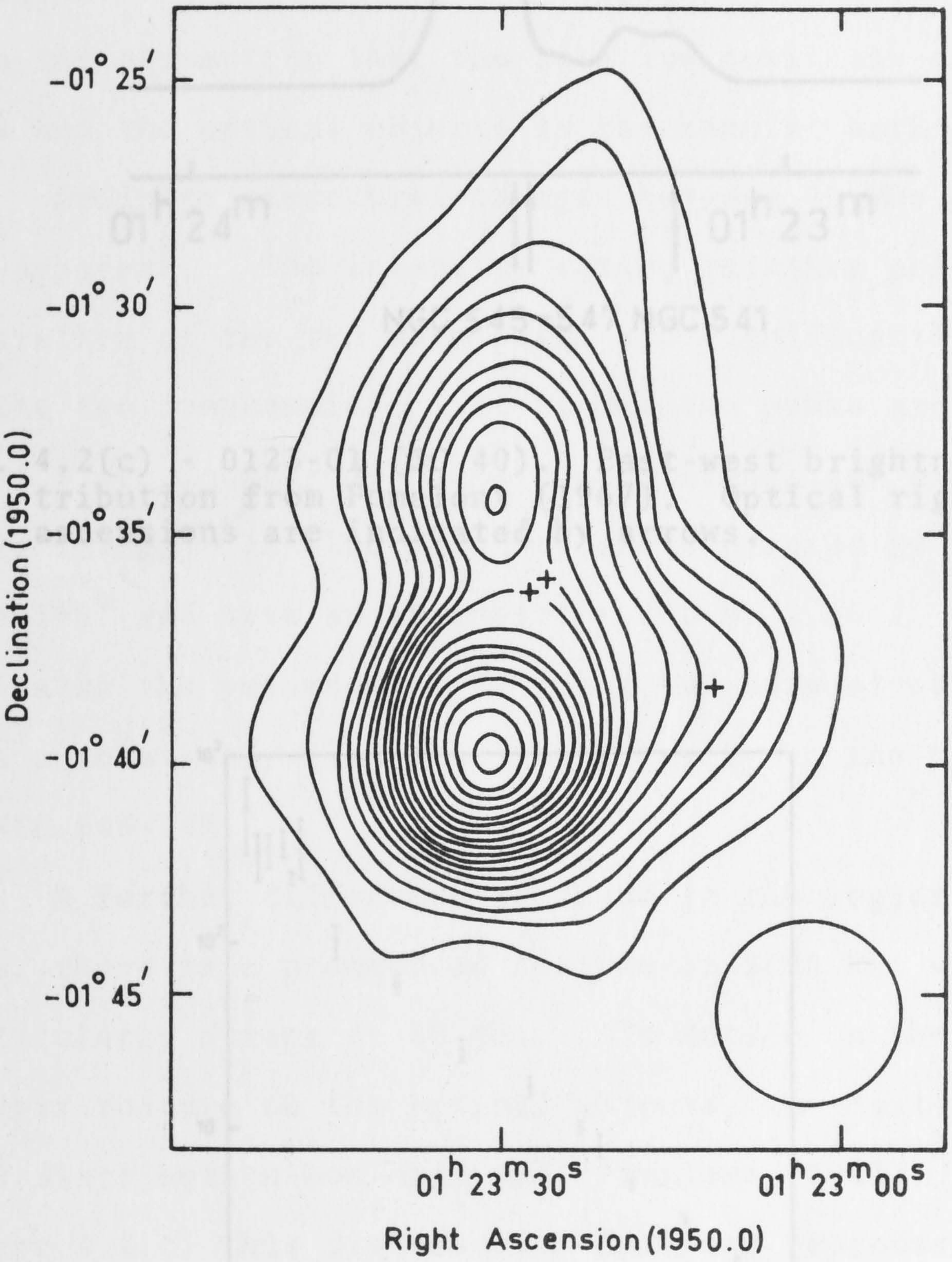

Fig. 4.2(b) - 0123-01 (3C 40). 5000 MHz map reproduced to the same scale as Fig. 4.2(a). The positions of NGC 545-547 and NGC 541 are shown by the double and single crosses respectively. The lowest contour and the contour interval is 0.05 f.u.

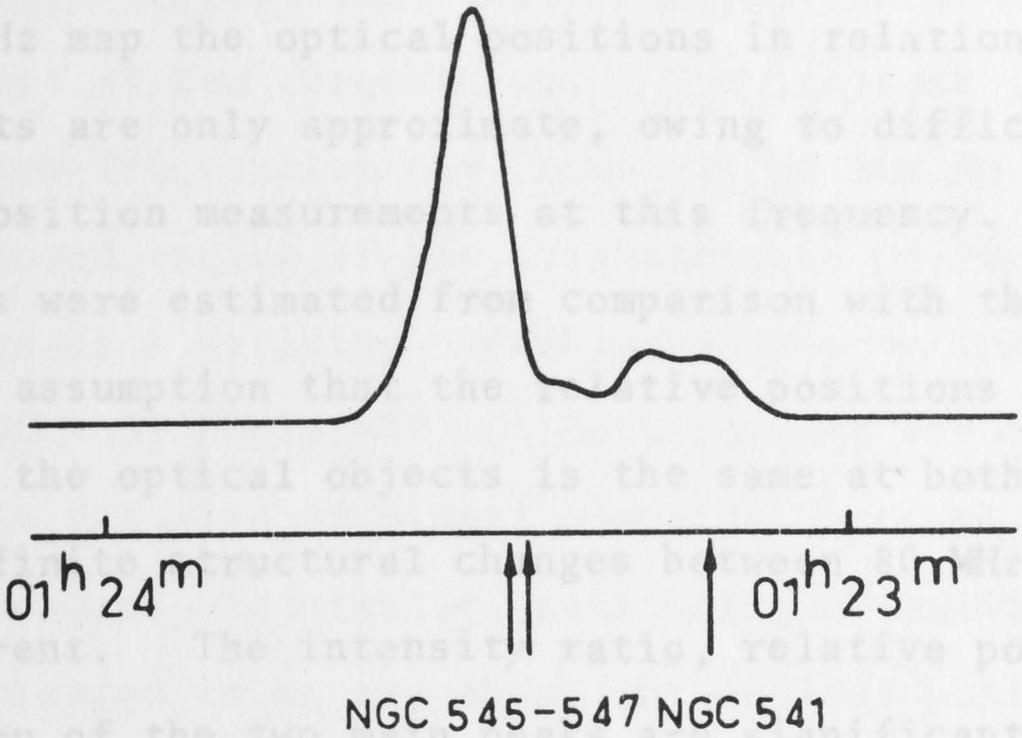

Fig. 4.2(c) 0123-01 (3C 40). East-west brightness distribution from Fomalont (1967). Optical right ascensions are indicated by arrows.

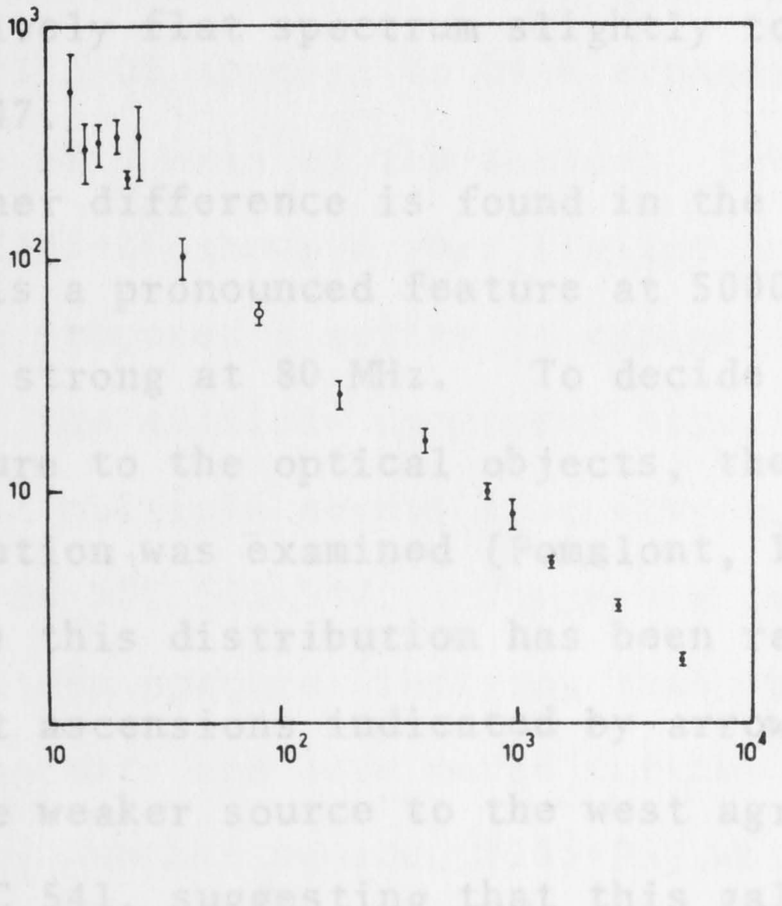

Fig. 4.2(d) - 0123-01 (3C 40). Integrated spectrum.

as the 80 MHz map and is shown in Figure 4.2(b); the positions of the galaxies are again indicated by crosses. On the 80 MHz map the optical positions in relation to the radio components are only approximate, owing to difficulties in accurate position measurements at this frequency. The relative positions were estimated from comparison with the 5000 MHz map with the assumption that the relative positions of the southern peak and the optical objects is the same at both frequencies.

Definite structural changes between 80 MHz and 5000 MHz are apparent. The intensity ratio, relative position and separation of the two main peaks are significantly different at the two frequencies. At 80 MHz the peaks are separated by 7'.8 arc in PA = 174^{o} and their intensities are in the ratio 1.9:1. At 5000 MHz they are separated by 5'.5 arc in PA = 189^{o} and have an intensity ratio of 1.65:1. This change indicates the presence of at least one unresolved component with a relatively flat spectrum slightly to the north-east of NGC 545-547.

A further difference is found in the region of NGC 541. Here, there is a pronounced feature at 5000 MHz which is not particularly strong at 80 MHz. To decide on the relation of this feature to the optical objects, the east-west brightness distribution was examined (Fomalont, 1967). In Figure 4.2(c) this distribution has been reproduced with the optical right ascensions indicated by arrows. It can be seen that the weaker source to the west agrees well in position with NGC 541, suggesting that this galaxy is also a radio source. Its spectrum must be relatively flat.

In contrast the outer components of 0123-01 to the north and south-west must have rather steep spectra, since they are much more prominent at 80 MHz than at 5000 MHz.

The south-western component, in particular, is barely in evidence at 5000 MHz. The integrated flux density measurements (Fig. 4.2(d)) suggest that these steeper spectrum components are dominant at low frequencies. The increase in spectral index at low frequencies may, however, be due to the inclusion of an extended region of low brightness as is found with 3C 66.

There is a striking resemblance between this source and 2335+26 (3C 465) (MNR, MKN). Both sources are identified with double galaxies of almost identical optical type. Their radio structures are similar, consisting of multiple components arranged in an arc about the optical position. In 2335+26 there is a very compact component coincident with the optical position; this may also be the case with 0123-01. Furthermore an outer component with a very steep spectrum is present in 2335+26; both the outer components of 0123-01 have spectra which are considerably steeper than the integrated spectrum of the source. The outer south-western component of 0123-01 appears to have expanded almost orthogonally to the main axis of the source; the south-western component of 2335+26 shows a very similar expansion.

MNR have proposed a series of explosions in the galaxy to account for the multiple component structure of 2335+26. It appears that multiple events have also occurred at different epochs in NGC 545-547. The outer components of 0123-01 have steep spectra, implying that they are older than the inner components and have moved further away from the parent galaxy. Another source, 0255+05, which also resembles 2335+26 is discussed below.

The luminous bridge connecting NGC 545-547 to NGC 541 suggests an interaction between these systems. It is possible that the radio emission from NGC 541 has been generated by relativistic particles incident from NGC 545-547, in analogy with the interaction between NGC 1275 and NGC 1265 (Ryle and Windram, 1968).

0131-36

At 80 MHz this source is resolved into two components (Fig. 4.3(a)) with a peak intensity ratio of 1.7:1 and an integrated flux density ratio of about 1.2:1. The eastern component is more intense than the western component. The peaks are separated by 8'.4 arc in PA = 92°. Both components are resolved along and perpendicular to the major axis and there is evidence of additional structure to the north-east of the eastern peak and to the south of the western peak.

Observations of this source have been made at 5000 MHz with the Parkes 210 ft. telescope (WG). Comparison with these results shows that the structure of the source is similar at 80 MHz and 5000 MHz. The ratio of the peak intensities and the integrated flux density ratio are in close agreement at the two frequencies, implying that the structure of the source does not change significantly with frequency. The integrated spectrum is shown in Figure 4.3(b). The 2650 MHz flux density may be underestimated, owing to partial resolution of the source. The spectrum appears to be straight between 80 MHz and 2650 MHz with a spectral index of 0.64.

Interferometer observations by Ekers (1969) at 468 and 1403 MHz indicate considerable complexity especially in PA = 177° with at least 5% of the total intensity arising from a region (or regions) of <0'.5 arc. The east-west interferometer observations of Fomalont (1967) at 1425 MHz

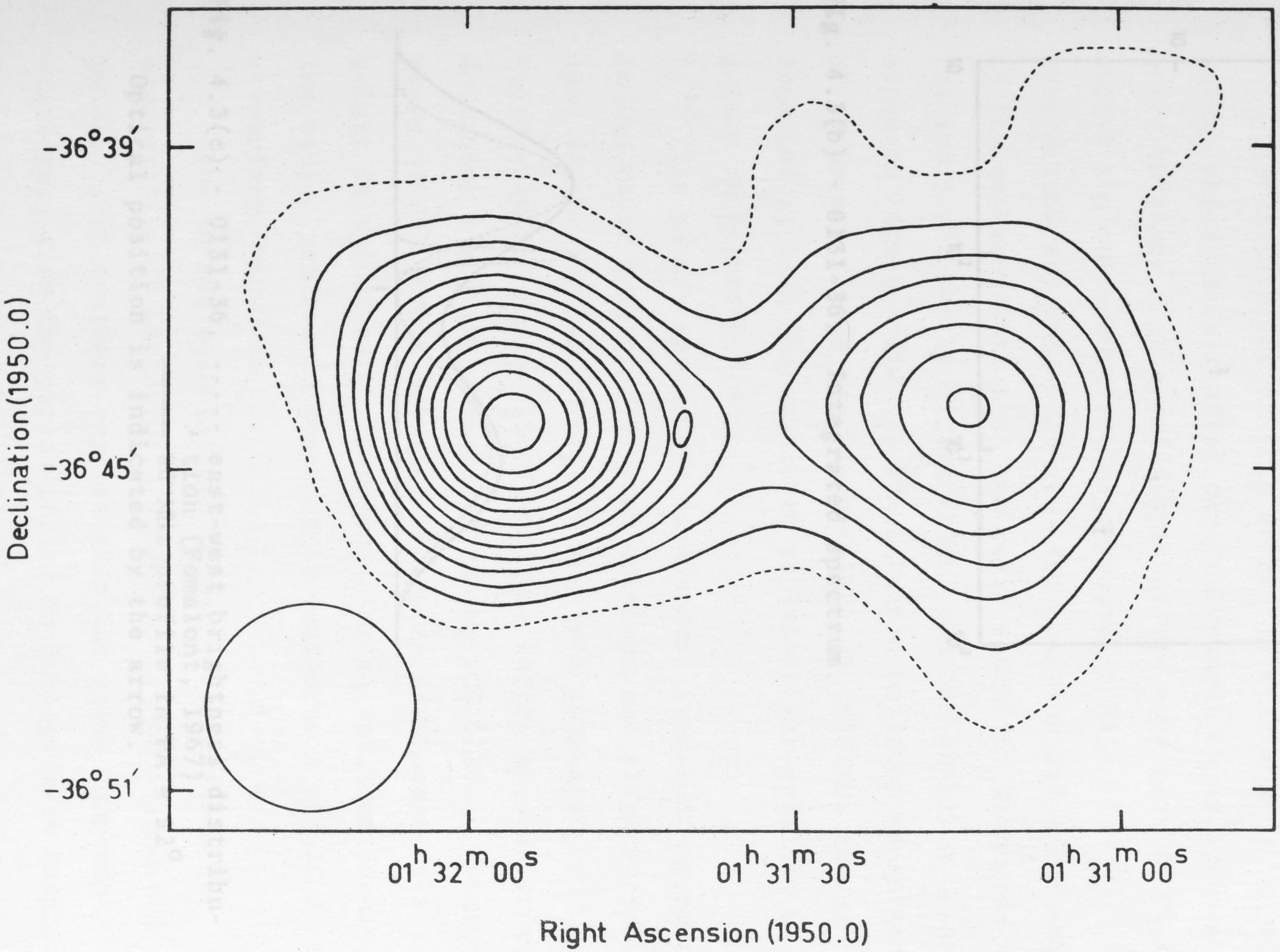

Fig. 4.3(a) - 0131-36. Position, orientation and size of the optical identification is shown by the small ellipse near the radio centroid.

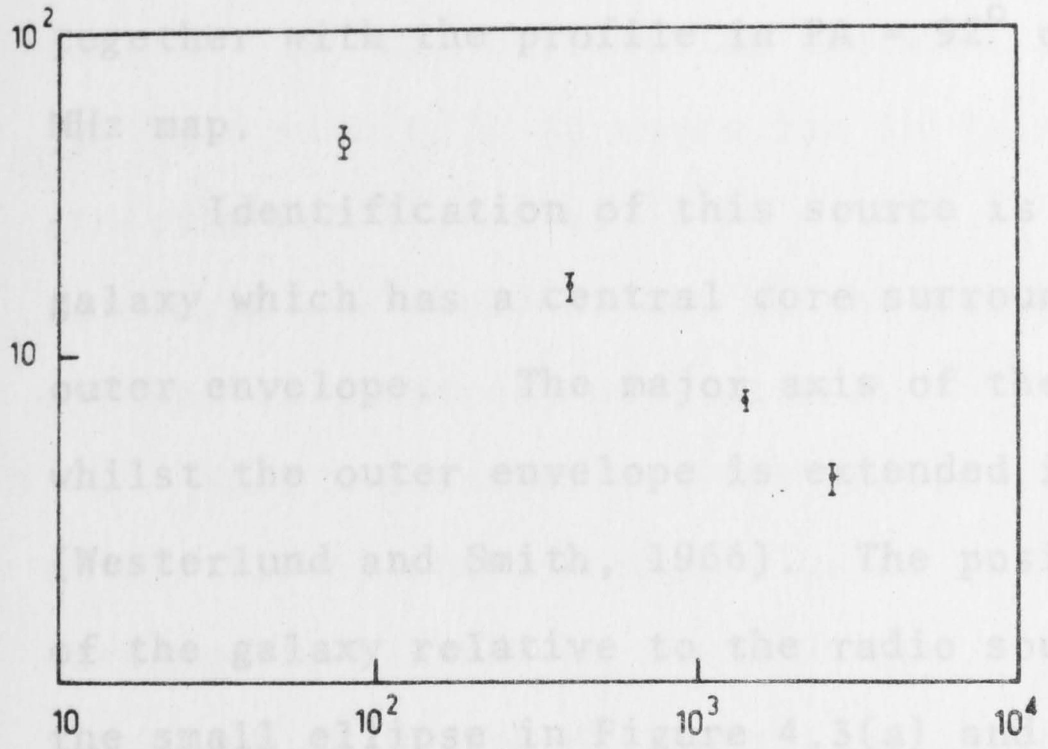

Fig. 4.3(b) - 0131-36. Integrated spectrum.

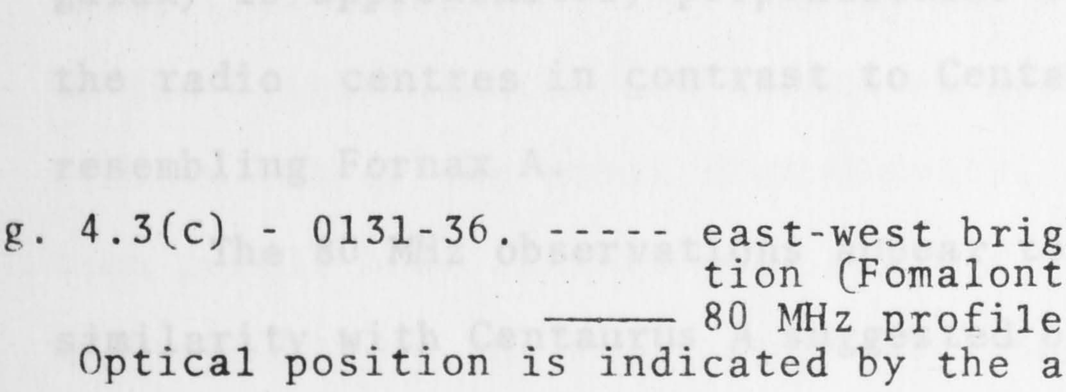

Fig. 4.3(c) - 0131-36. ----- east-west brightness distribution (Fomalont, 1967)
——— 80 MHz profile in PA = 92°

Optical position is indicated by the arrow.

also reveal fine structure. The east-west brightness distribution obtained by Fomalont is shown in Figure 4.3(c), together with the profile in PA = 92° obtained from the 80 MHz map.

Identification of this source is with a peculiar SO-Sa galaxy which has a central core surrounded by an elliptical outer envelope. The major axis of the core lies in PA = 5° whilst the outer envelope is extended in PA = 170° (Westerlund and Smith, 1966). The position and orientation of the galaxy relative to the radio source is indicated by the small ellipse in Figure 4.3(a) and its position by an arrow in Figure 4.3(c). The accurate position measurements of Shimmins, Clarke and Ekers (1966) at 2650 MHz and of Fomalont at 1425 MHz were used to locate the position of the galaxy in Figure 4.3(a).

The galaxy appears to have a dust lane running parallel to the major axis of the outer envelope and slightly to the east of the central core. It has been suggested by Westerlund and Smith (1966) that the source is similar to Centaurus A and its associated galaxy NGC 5128. However, Ekers (1969) points out that the outer envelope of the galaxy is approximately perpendicular to the line joining the radio centres in contrast to Centaurus A and 3C 33 but resembling Fornax A.

The 80 MHz observations appear to strengthen the similarity with Centaurus A suggested by Westerlund and Smith. The contours suggest that the radio components curve away from the parent galaxy in analogy with Centaurus A. (Cooper, Price and Cole, 1965.)

The similarity between the two systems may be seen by rotating the map of 0131-36 through a position angle of -65°.

The positions relative to the parent galaxy, intensities and shape of the components in the two systems are then remarkably alike. In this orientation the dust lane of the galaxy associated with 0131-36 would lie in PA = 105^{o}; the dust lane crossing NGC 5128 lies in PA = 120^{o}. This discrepancy is not large and could be due to the effect of viewing the two systems in different projections.

With a redshift of 9008 km/sec determined by Westerlund et al. (1966) and assuming a value of H = 100 km/sec/Mpc, the distance to 0131-36 is about 90 Mpc. If it were situated at 4 Mpc, which is the distance to Centaurus A (Sersic, 1961), the separation of the peaks would be about 3^{o}.2, whereas the outer peaks of Centaurus A are separated by about 2^{o}.7. On the other hand the integrated flux density of 0131-36 at 408 MHz would be approximately 8200 f.u. making it 3 times more powerful than Centaurus A at this frequency. Thus, although the dimensions of the two systems are similar, 0131-36 may be intrinsically more powerful than Centaurus A.

It is of interest that Fomalont's east-west distribution contains a bright region of small angular size located near the optical object and contributing about 10% of the total flux density. This region may be somewhat analogous to the bright central components of Centaurus A which contribute 22% of the total flux density. Very high resolution pencil beam observations of this radio source and measurements of the rotation of the associated galaxy would be of considerable interest.

0220+42 (3C 66)

Aperture synthesis mapping (MNR, MKN) at 408 MHz and 1407 MHz with beamwidths of 80" arc and 23" arc respectively

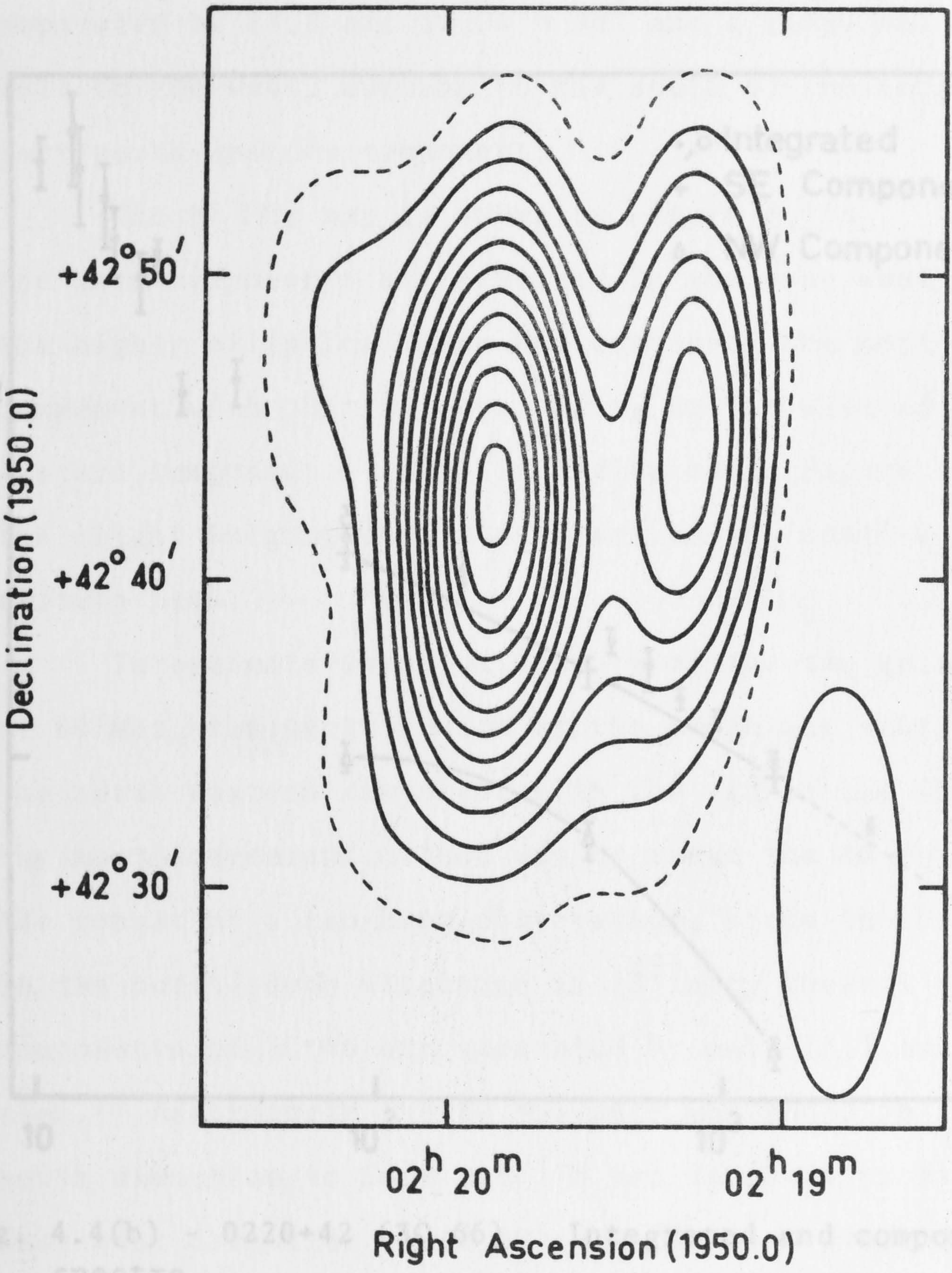

Fig. 4.4(a) - 0220+42 (3C 66).

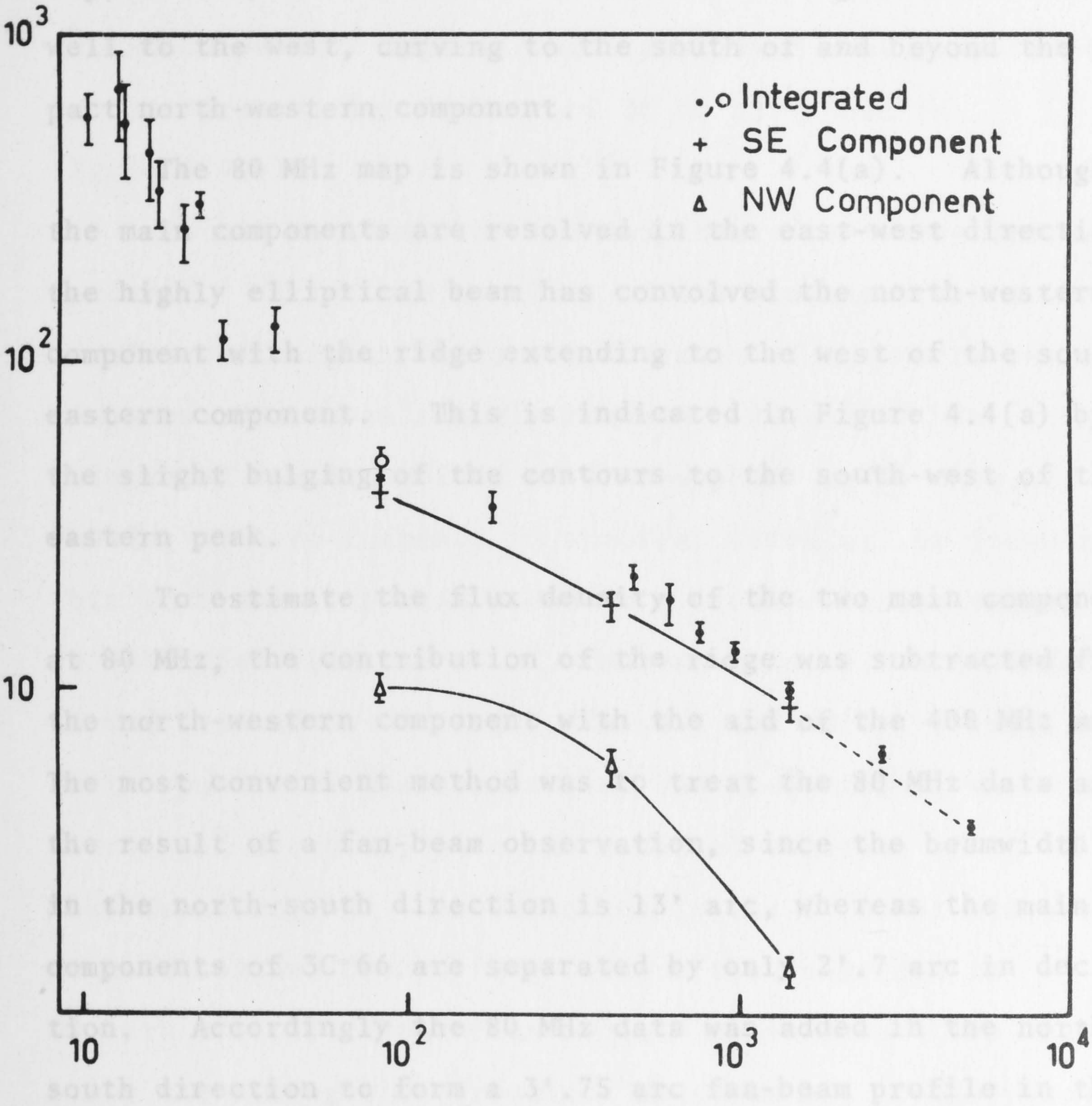

Fig. 4.4(b) - 0220+42 (3C 66). Integrated and component spectra.

show that 3C 66 has two main components. The north-western component is unresolved at both frequencies and therefore has an angular diameter <10" arc. On the other hand the south-eastern component shows complex structure, with two peaks separated by 1'.8 arc in PA = 90^o and a ridge which extends well to the west, curving to the south of and beyond the compact north-western component.

The 80 MHz map is shown in Figure 4.4(a). Although the main components are resolved in the east-west direction, the highly elliptical beam has convolved the north-western component with the ridge extending to the west of the south-eastern component. This is indicated in Figure 4.4(a) by the slight bulging of the contours to the south-west of the eastern peak.

To estimate the flux density of the two main components at 80 MHz, the contribution of the ridge was subtracted from the north-western component with the aid of the 408 MHz map. The most convenient method was to treat the 80 MHz data as the result of a fan-beam observation, since the beamwidth in the north-south direction is 13' arc, whereas the main components of 3C 66 are separated by only 2'.7 arc in declination. Accordingly the 80 MHz data was added in the north-south direction to form a 3'.75 arc fan-beam profile in the east-west direction. An 80" arc fan-beam profile of the south-eastern component, obtained from the 408 MHz map was then numerically smoothed to a beamwidth 3'.75 arc. Since the 3'.75 arc beam ensures that the eastern peak of the 80 MHz profile is not affected by the north-western component, the smoothed 408 MHz profile could be fitted to this peak. After separating the components in this way, their relative flux densities were measured. The method was checked by ensuring that the north-eastern component was unresolved and that the separation of the peaks in right ascension was in agreement with their separation at 408 MHz.

The 80 MHz flux densities of the components have been combined with measurements at 408 and 1407 MHz. The spectrum of the components together with published measurements of the integrated flux density of 3C 66 are shown in Figure 4.4(b).

It can be seen that the components have very different spectra. Whilst the spectrum of the south-eastern component is almost straight, the spectral index of the north-western component decreases sharply between 1407 and 80 MHz. The integrated spectrum of 3C 66 also appears to be unusual, showing a sharp increase in spectral index at low frequencies. This increase is probably due to a broad emission region with an estimated diameter of 1°, centred about 0.8 min of RA to the west of 3C 66 (Roger, Costain and Lacey, 1969). Most of the published measurements at low frequencies, where beamwidths $\gtrsim 1^{\circ}$ are used, give the combined emission of 3C 66 and this broad region. An exception is the 26.3 MHz measurement of Erickson and Cronyn (1965) where the beamwidth is 14' arc x $1^{\circ}.5$; their flux density measurement lies well below the average low-frequency spectrum and probably contains only a partial contribution from the extended region. Extrapolation of the spectra of the components of 3C 66 to low frequencies implies that the extended region has a very steep spectrum.

The dimensions and spectra of the components of 3C 66 are so strikingly different that it seems improbable that they are the result of the same generating event. They may not even be related to the same optical object. The south-eastern component is extended with complex structure and has a straight spectrum. In contrast the north-western component is of small angular size and has a spectrum which is steep at high frequencies and shows a low frequency cutoff. Such spectra are always associated with sources of extremely high brightness temperature (Kellermann et al. 1969) and it is probable that the cutoff is due to synchrotron self-absorption (Slish, 1963; Williams, 1963).

The possible optical identifications have been discussed by MNR. An elliptical (ED2) galaxy of M_{pg} = 14.2 coincides precisely with the western peak of the south-eastern component. There are no optical objects which can be associated with the eastern peak of the south-eastern component or with the compact north-western component, but a second elliptical galaxy of M_{pg} = 15.0 lies almost exactly midway between the compact component and the western peak of the south-eastern component. If this galaxy is assumed to be the correct identification for both components of 3C 66 the difference in their spectrum implies that we are viewing the two regions at very different stages of evolution. The possibility that the components originated in the same event in the galaxy but are observed at significantly different epochs owing to relativistic effects (Ryle and Longair, 1967) seems to be ruled out by their marked difference in size. On the other hand the spectrum of the north-eastern component is not compatible with its distance from the parent galaxy, in that radio sources exhibiting a low frequency cut-off in the spectrum are not found at large distances from the optical position. This excludes the possibility suggested by MNR that the components are the result of multiple explosions in the galaxy. An alternative explanation is that the two components are unrelated. This suggests that the south-eastern component is associated with the $14^m.2$ EP2 galaxy whilst the optical object associated with the compact north-western component is optically faint.

0255+05 (3C 75)

The 80 MHz contours (Fig. 4.5(a)) are elongated to the north-west and to the east of the central peak, suggesting an arc-like structure for this source. In Figure 4.5(b) the map has been combined with the east-west distribution obtained by Fomalont (1967) to allow an estimate of the relative positions of the components. These are shown as open circles in the diagram at the top of Figure 4.5(b) whilst the approximate position of the optical identification is indicated by two crosses. The map and the east-west distribution suggest additional structure to the north-west of the western component. This is indicated by a dotted line in Figure 4.5(b).

Optical identification is with a pair of closely spaced, 15^m galaxies, classified as DB by Matthews, Morgan and Schmidt (1964). Their position in relation to the radio components was estimated from the accurate position measurements of Fomalont (1967) and of Shimmins, Clarke and Ekers (1966).

The radio structure resembles that of 2335+26 (3C 465) (MNR, MKN). For 2335+26 the suggested identification is also a double galaxy, NGC 7720, which is coincident with a weak radio component of small angular size. The similarity between 0123-01 and 2335+26 has already been described. It is possible that the rather unusual radio structure of these three systems is caused by some interaction between their

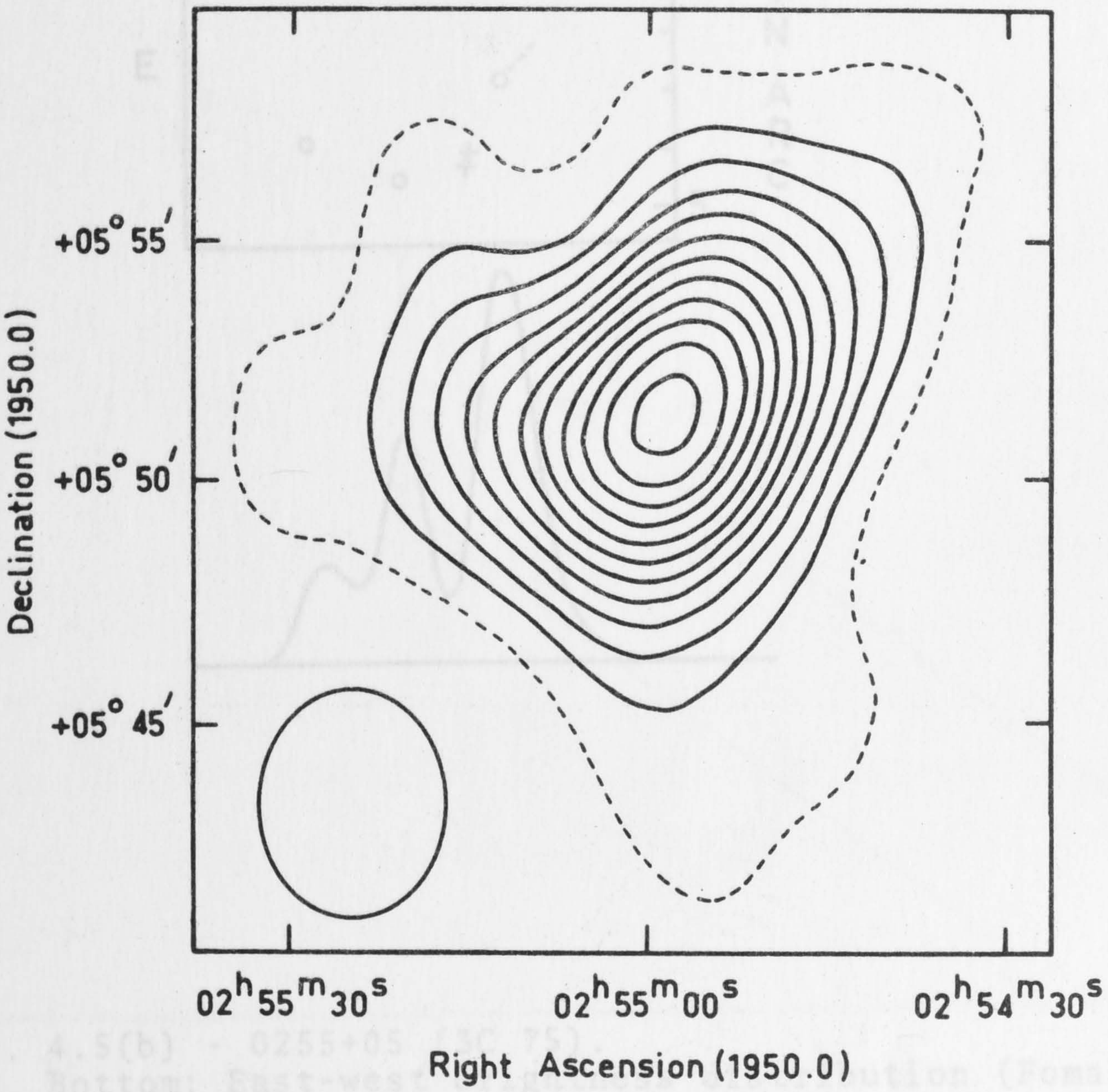

Fig. 4.5(a) - 0255+05 (3C 75).

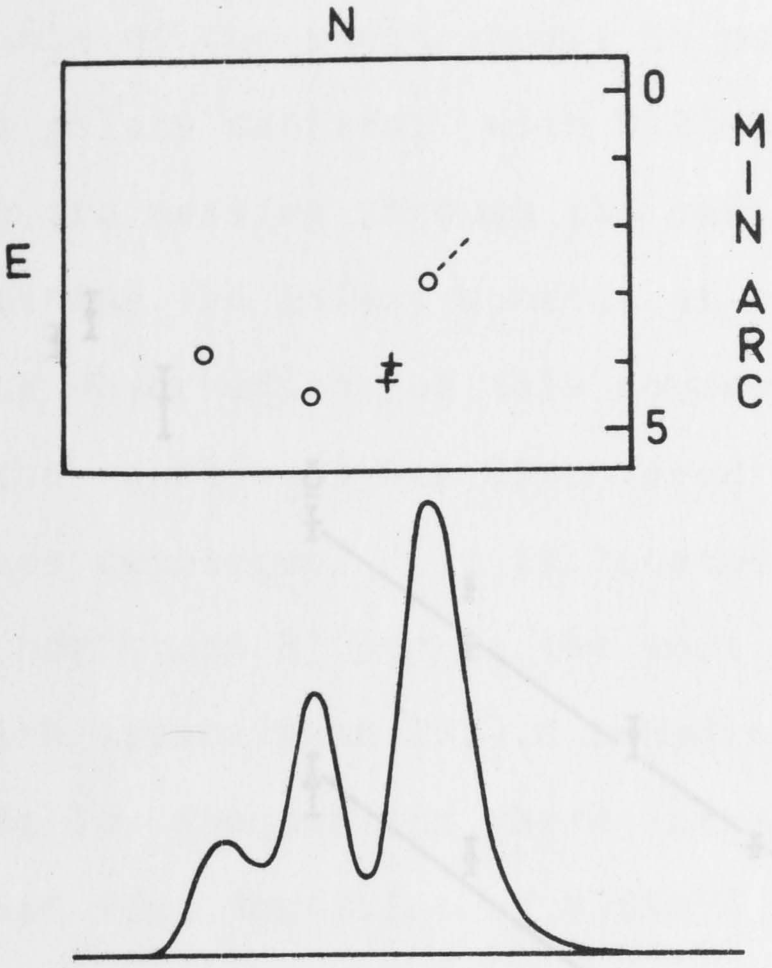

Fig. 4.5(b) - 0255+05 (3C 75).
Bottom: East-west brightness distribution (Fomalont, 1967).
Top: Approximate positions of the radio components (open circles) relative to the optical position (double cross).

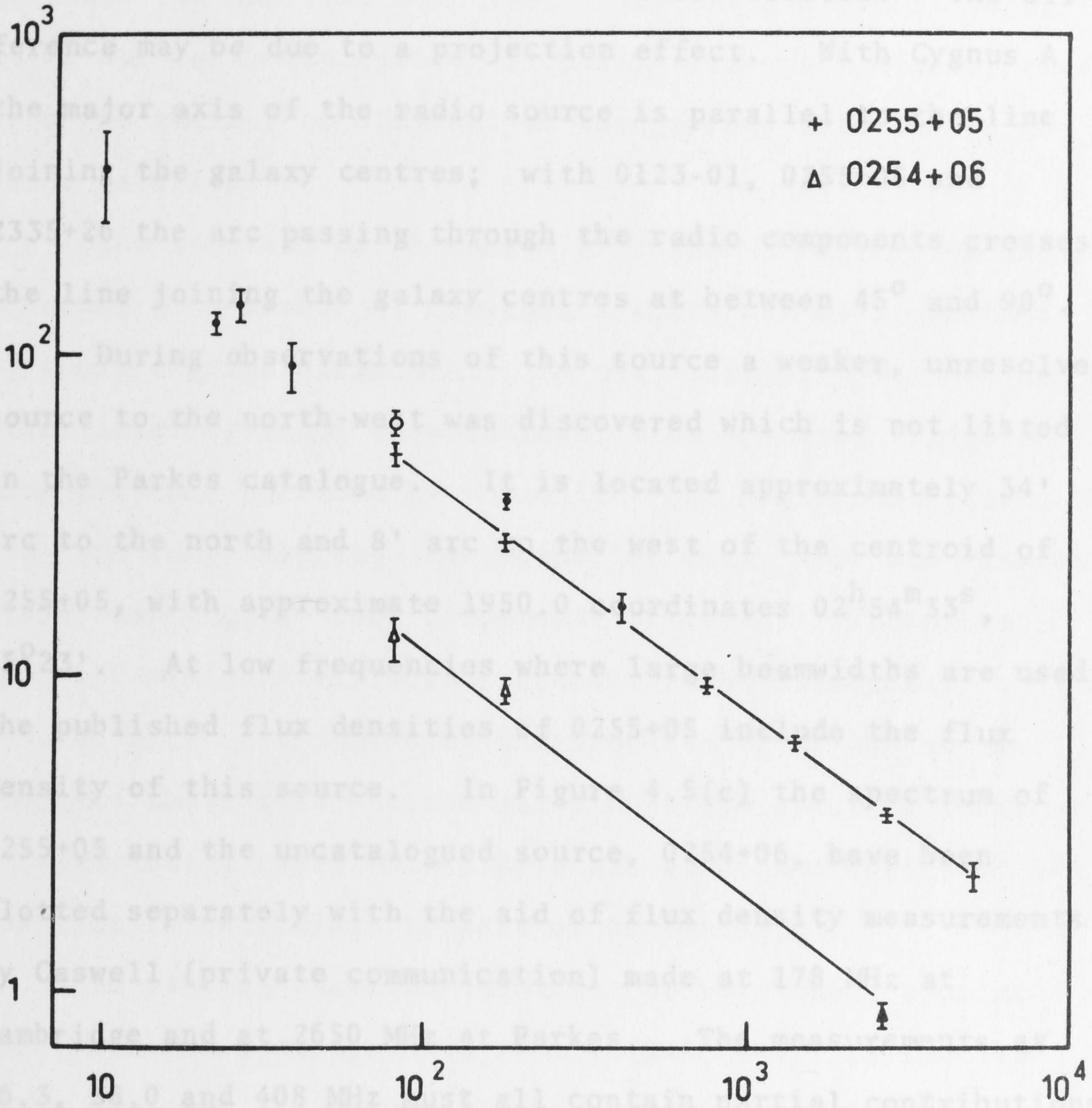

Fig. 4.5(c) - 0255+05 (3C 75). Spectrum of 0255+05 and 0254+06.

associated double galaxies. However the radio structure of Cygnus A, which is also identified with a double galaxy, does not resemble the structure of these sources. The difference may be due to a projection effect. With Cygnus A the major axis of the radio source is parallel to the line joining the galaxy centres; with 0123-01, 0255+05 and 2335+26 the arc passing through the radio components crosses the line joining the galaxy centres at between 45^o and 90^o.

During observations of this source a weaker, unresolved source to the north-west was discovered which is not listed in the Parkes catalogue. It is located approximately 34' arc to the north and 8' arc to the west of the centroid of 0255+05, with approximate 1950.0 coordinates $02^h54^m33^s$, $05^o23'$. At low frequencies where large beamwidths are used, the published flux densities of 0255+05 include the flux density of this source. In Figure 4.5(c) the spectrum of 0255+05 and the uncatalogued source, 0254+06, have been plotted separately with the aid of flux density measurements by Caswell (private communication) made at 178 MHz at Cambridge and at 2650 MHz at Parkes. The measurements at 26.3, 38.0 and 408 MHz must all contain partial contributions from the uncatalogued source. The primary beam used by Fomalont has a half-power width of about 33' arc, which ensures that his east-west distribution of 0255+05 is barely affected by the nearby source.

0316+41 (3C 84, Perseus A)

Probably the most extensively observed radio source is Perseus A, which is associated with the Seyfert galaxy NGC 1275. Observations of the Perseus cluster and in particular of Perseus A by Ryle and Windram (1968) have revealed a remarkable interaction between NGC 1275 and two other galaxies, NGC 1265 and IC 310, which lie at distances of about 600 kpc from NGC 1275. The interaction is thought to be due to the incidence of relativistic particles ejected from the nucleus of NGC 1275 on the gaseous material in these galaxies.

The spectrum of Perseus A is complex, indicating the presence of a number of components which are distinguished by their angular structure. On the basis of their own and other interferometer observations, from spectral evidence, from evidence provided by variability at high frequencies and from long baseline interferometer data, Ryle and Windram (1968) distinguish four components of 3C 84. These are:

3C 84A(i). A variable component whose diameter is 0".001 arc. It dominates the spectrum of 3C 84A at frequencies above 8000 MHz and has a negative spectral index. Observations at 4995 MHz by Ryle and Windram showed that its position is very close to that of 3C 84A(ii).

3C 84A(ii). A second component of very small angular size which is distinguished from 3C 84A(i) by its spectrum. It is dominant at frequencies between 300 and 1400 MHz and shows a low frequency cut-off.

From interferometer observations by Palmer et al. (1967) at 2695 MHz it was concluded that 3C 84A(i) and (ii) must both have an angular size <0".05 arc and that they must be situated within 0".05 arc of each other. Both regions are coincident with the Seyfert nucleus of NGC 1275.

3C 84A(iii). This third component is described as having an angular extent of approximately 5' arc in both coordinates and having a position and size in agreement with the outer envelope of the filaments of NGC 1275. It has a very steep spectrum and is the major contributor to the total flux density of 3C 84A at low frequencies.

3C 84B. Low resolution pencil-beam observations showed the presence of a source of very large extent and low surface brightness. It shows a marked elongation towards NGC 1265.

It would be concluded from this analysis that at 80 MHz the 5' arc source 3C 84A(iii) should completely dominate the spectrum of 3C 84A. Contrary to this conclusion, the present observations show two distinct, superimposed components of different angular size which we shall designate 3C 84A(iii)(a) and (b). The 80 MHz map shown in Figure 4.6(a) does not indicate these components clearly, since the more extended region 3C 84A(iii)(b) is of relatively low brightness and has been overshadowed in places by the sidelobe structure of the apparently unresolved central component. They are more clearly discernible in Figure 4.6(c), which is an east-west scan through the peak of the source, corrected for sidelobes from the compact component.

Separation of the components was achieved by the method adopted for Virgo A (§4.14), in which a record of the unresolved source 3C 123 was aligned with the centre of the compact component of 3C 84A and then subtracted with the appropriate weighting. Flux densities for each component were thus obtained and a contour diagram of the extended region was produced. In Figure 4.6(b) we give the 80 MHz contour map of the extended region, which has an east-west half-power width of about 8'.5 arc and is clearly elongated in the same direction as the outer envelope of the filaments of NGC 1275. The position of the compact component 3C 84A(iii)(a) is indicated by the cross.

The previous observations at higher frequencies have

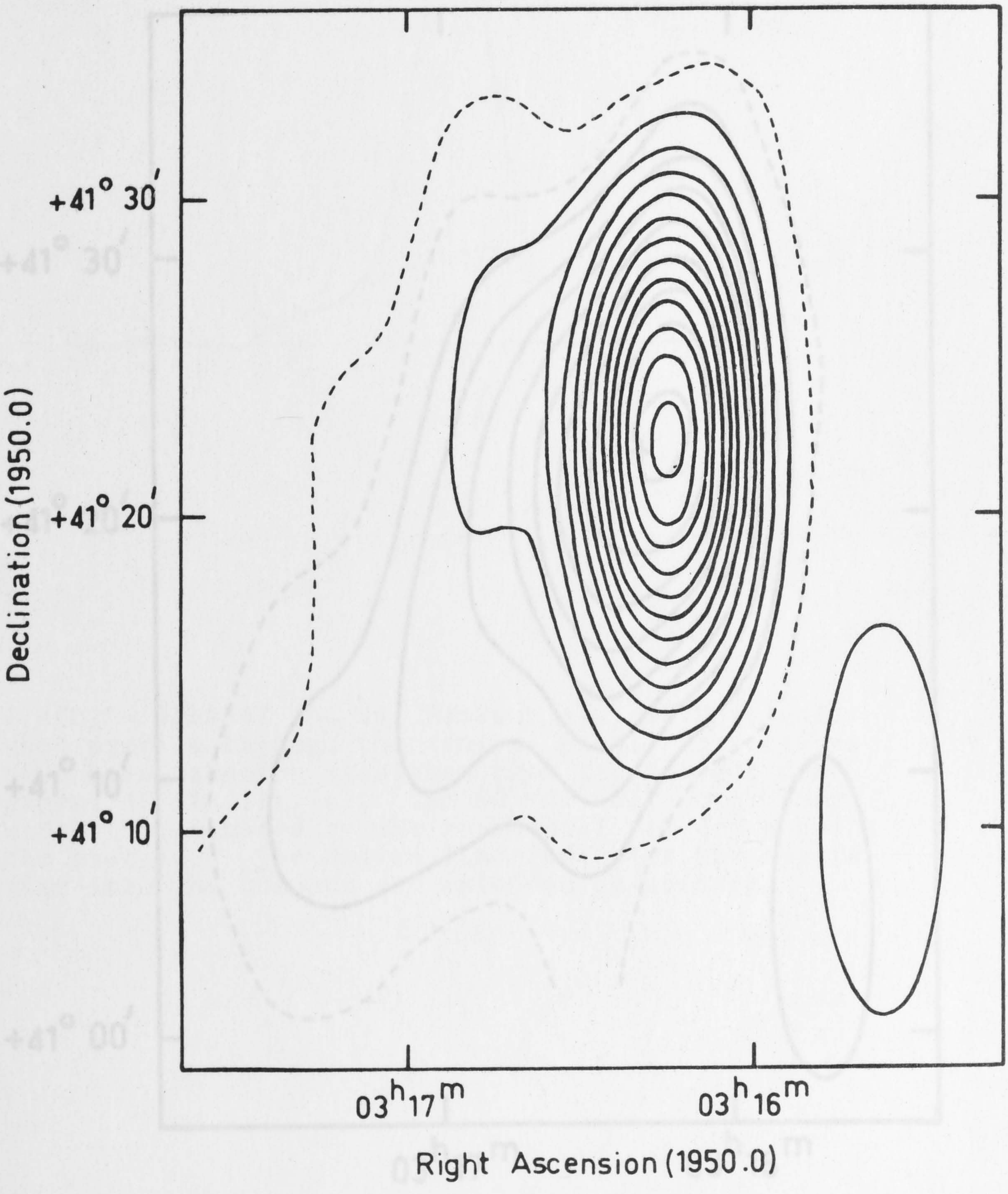

Fig. 4.6(a) - 0316+41 (3C 84, Perseus A).

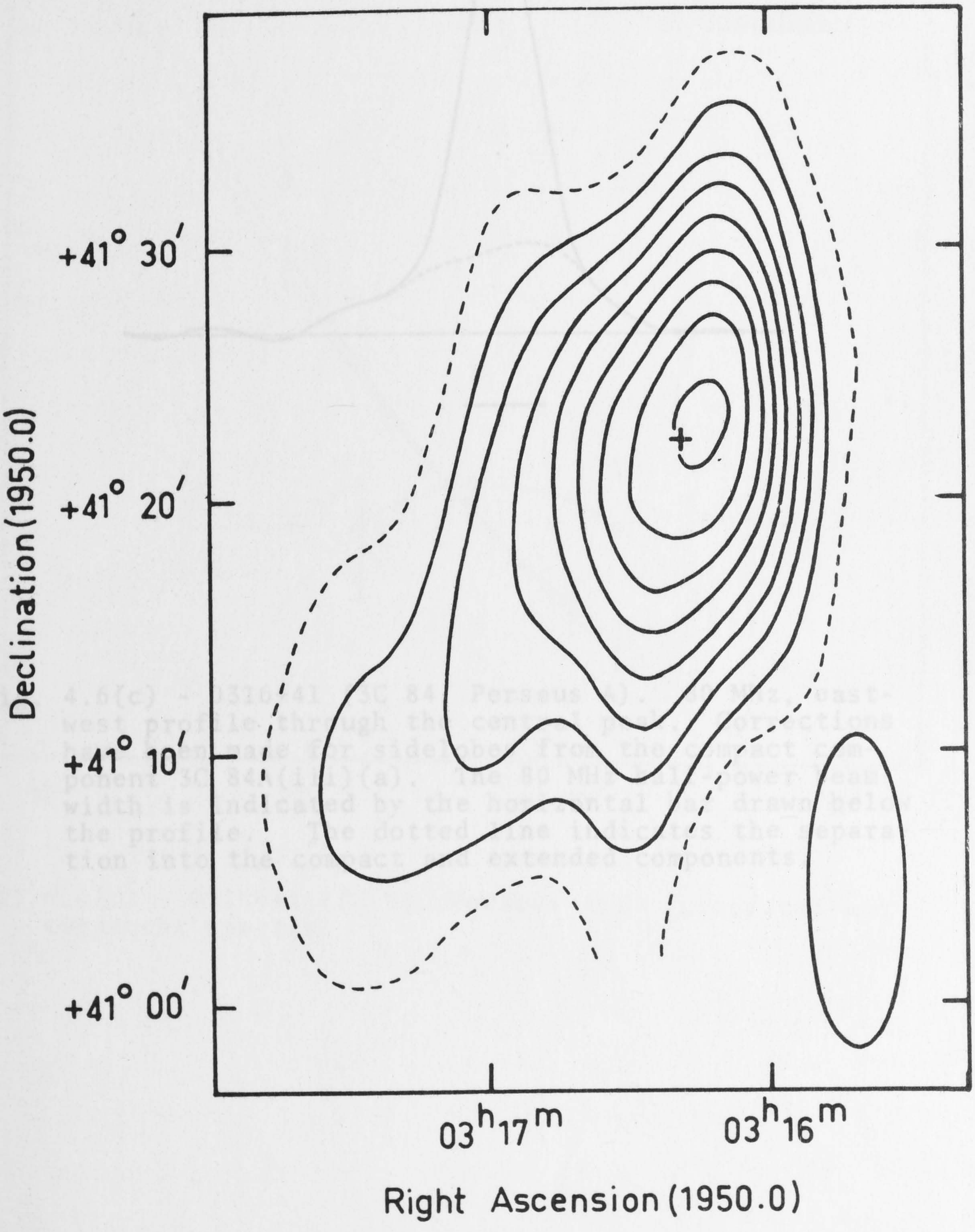

Fig. 4.6(b) - 0316+41 (3C 84, Perseus A). 80 MHz map of the extended component 3C 84A(iii)(b). The position of the compact component 3C 84A(iii)(a) is shown by a cross.

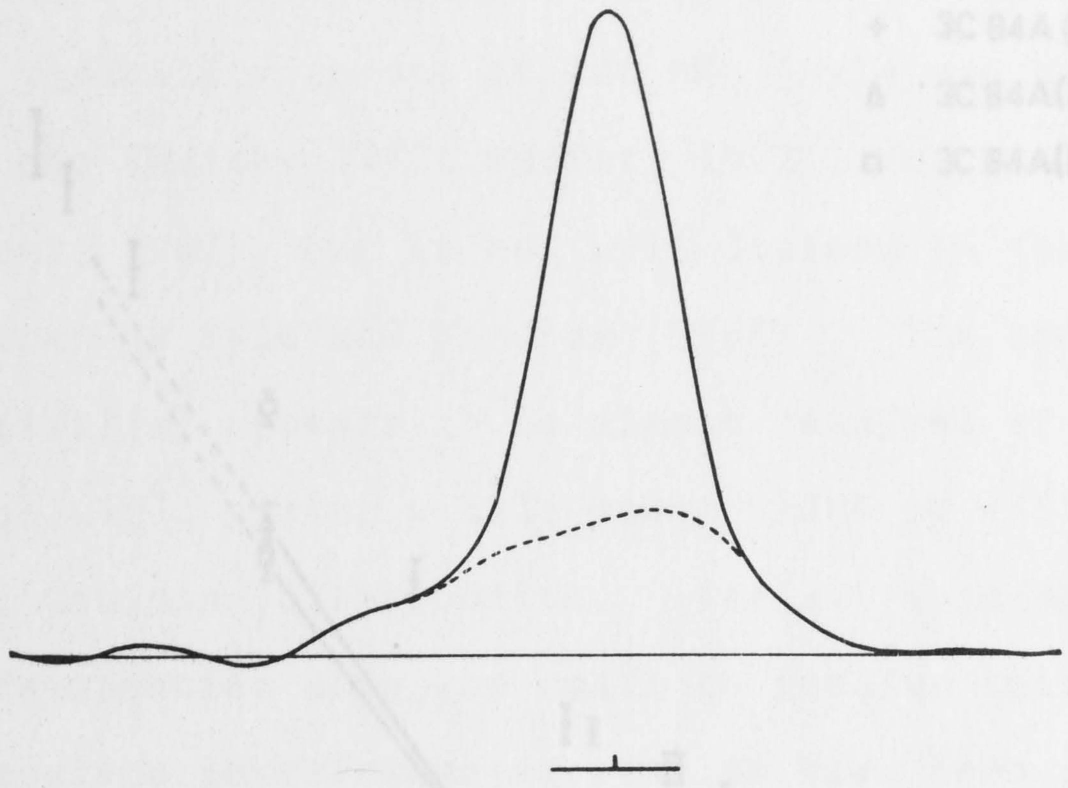

Fig. 4.6(c) - 0316+41 (3C 84, Perseus A). 80 MHz, east-west profile through the central peak. Corrections have been made for sidelobes from the compact component 3C 84A(iii)(a). The 80 MHz half-power beamwidth is indicated by the horizontal bar drawn below the profile. The dotted line indicates the separation into the compact and extended components.

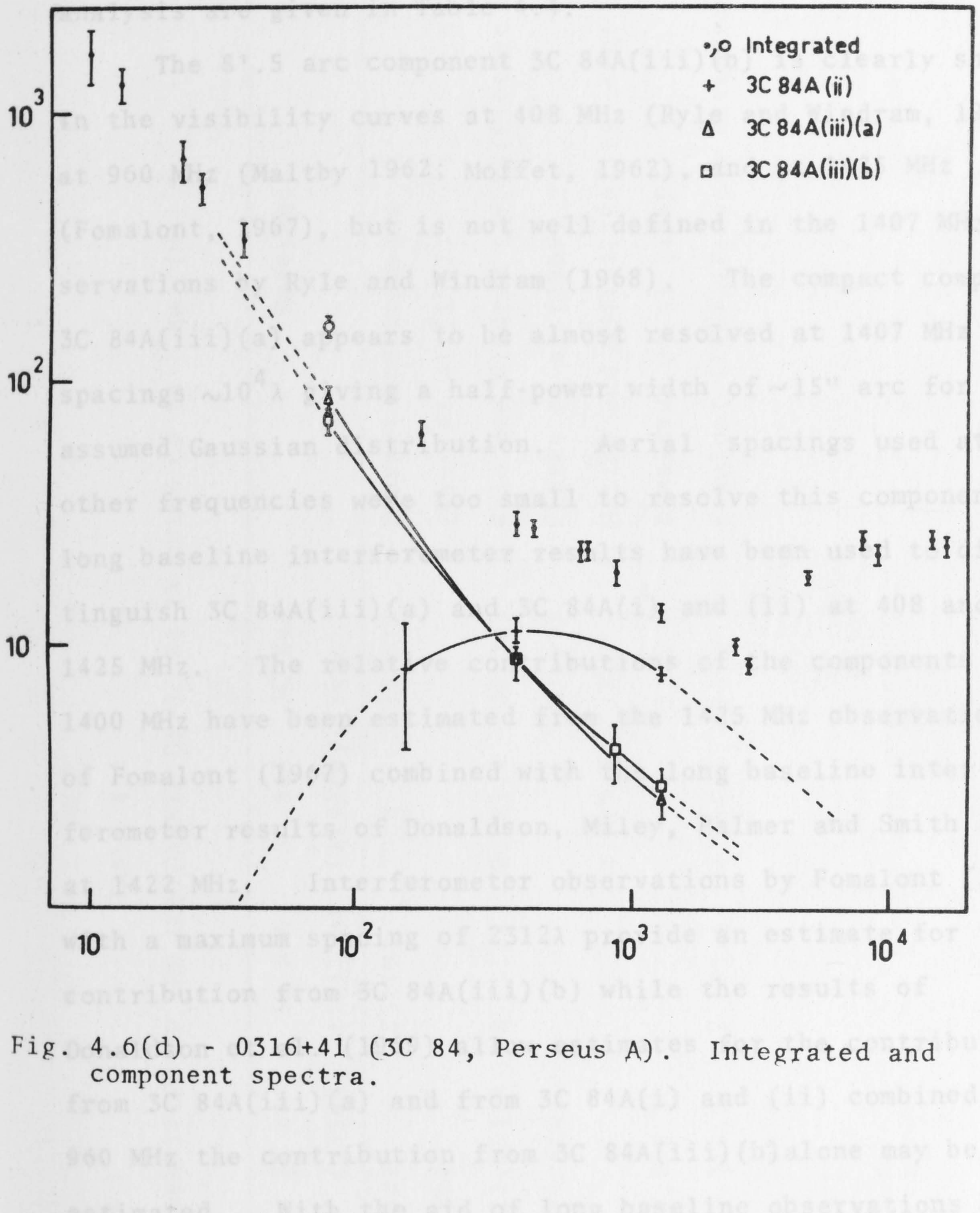

Fig. 4.6(d) - 0316+41 (3C 84, Perseus A). Integrated and component spectra.

been re-examined in order to relate the structure observed at 80 MHz to the high frequency structure. The results of this analysis are given in Table 4.4.

The 8'.5 arc component 3C 84A(iii)(b) is clearly shown in the visibility curves at 408 MHz (Ryle and Windram, 1968), at 960 MHz (Maltby 1962; Moffet, 1962), and at 1425 MHz (Fomalont, 1967), but is not well defined in the 1407 MHz observations by Ryle and Windram (1968). The compact component 3C 84A(iii)(a) appears to be almost resolved at 1407 MHz at spacings $\sim 10^4\lambda$ giving a half-power width of ~15" arc for an assumed Gaussian distribution. Aerial spacings used at the other frequencies were too small to resolve this component; long baseline interferometer results have been used to distinguish 3C 84A(iii)(a) and 3C 84A(i) and (ii) at 408 and 1425 MHz. The relative contributions of the components near 1400 MHz have been estimated from the 1425 MHz observations of Fomalont (1967) combined with the long baseline interferometer results of Donaldson, Miley, Palmer and Smith (1969) at 1422 MHz. Interferometer observations by Fomalont (1967) with a maximum spacing of 2312λ provide an estimate for the contribution from 3C 84A(iii)(b) while the results of Donaldson et al. (1969) allow estimates for the contributions from 3C 84A(iii)(a) and from 3C 84A(i) and (ii) combined. At 960 MHz the contribution from 3C 84A(iii)(b) alone may be estimated. With the aid of long baseline observations by Clarke, Broten et al. (1969) the observations of Ryle and Windram (1968) provide estimates at 408 MHz for 3C 84A(iii)(a), 3C 84A(iii)(b), and for 3C 84A(ii). Since the interferometer data at 158 MHz (Allen et al., 1962) indicates a turnover in the spectrum of 3C 84A(ii) at low frequencies, the contribution from this component at 80 MHz is probably about 4 f.u. This contribution has been allowed for in calculating the

TABLE 4.4

FLUX DENSITIES OF THE COMPONENTS OF 3C 84 IN UNITS OF $10^{-26}\mathrm{Wm}^{-2}(\mathrm{Hz})^{-1}$

Frequency (MHz)	3C 84A (i+ii)	3C 84A (iii)(a)	3C 84A (iii)(b)	3C 84A Total	Reference
80	4±2	85±10	70±8	159±15	Present measurements
158	8±4				Allen et al (1962)
408	11.2±1.4	8.7±1.4	8.8±1.4	28.7±3	Ryle and Windram (1968)(Present estimates)
448	10.8±4			27.9±3	Clarke et al (1969)
960			4.0±0.5	18.5	Maltby and Moffet(1962)(Present estimates)
1422	7.8±0.3			13.2	Donaldson et al (1969)
1425	7.8±0.3	2.6±0.4	2.9±0.5	13.3	Fomalont (1967)(Present estimates)

flux density of 3C 84A(iii)(a) at 80 MHz. The integrated flux density measurement at 80 MHz is in excellent agreement with the 81.5 MHz value obtained by Collins (Ryle and Windram, 1968).

The component spectra are plotted in Figure 4.6(d), together with measurements of the integrated flux density of 3C 84A. The integrated flux density values were obtained from the data compiled by Ryle and Windram (1968) and from the observations of Kellermann et al. (1969).

Figure 4.6(d) shows that the spectra and flux densities of 3C 84A(iii)(a) and (b) are very similar between 80 and 1425 MHz. The spectral index of both components increases from about 0.75 near 1425 MHz to about 1.48 at 80 MHz, suggesting the presence in each component of at least two distinct regions with differing power-law spectra. Indeed, the 80 MHz map of the 8'.5 arc component, 3C 84A(iii)(b), suggests the presence of at least two regions.

It is of interest that the model for 3C 84A(ii) proposed by Clarke et al. (1969) also consists of two components of equal intensity, diameters of 0".0008 ± 0".0002 arc and separated by 0".037 ± 0".002 arc in PA = $175^{\circ} \pm 10^{\circ}$. There is clearly a preferred direction of expansion in NGC 1275 since the very extended source, 3C 84B, the 8'.5 component, 3C 84A(iii)(b) and 3C 84A(ii) are all elongated in approximately the same direction.

The similarity between the spectra of 3C 84A(iii)(a) and (b) would infer that these regions were produced at the same epoch. However, their linear dimensions differ by a factor of ~40, suggesting that 3C 84A(iii)(b) is considerably older than 3C 84A(iii)(a). If we suppose that these regions did originate at different times in NGC 1275 it would appear that in addition to the recent event leading to the variable component 3C 84A(i) at least four earlier periods of intense activity have occurred. The source 3C 84B is presumably the oldest and most evolved region. 3C 84A(iii)(b) is somewhat younger and has expanded apparently in the same directions as 3C 84B but by a lesser amount. The component 3C 84A(iii)(a) was produced at an even later time and has expanded to dimensions much larger than 3C 84A(ii) but much smaller than 3C 84A(iii)(a). The component 3C 84A(ii) presumably originated more recently than 3C 84A(iii)(a) and is at a very early stage of evolution.

<u>0320-37 (Fornax A)</u>

Fornax A is associated with the peculiar SO galaxy NGC 1316 and has been the subject of a number of investigations at higher frequencies. Preliminary drift-scan observations with the radioheliograph (Morimoto and Lockhart, 1968) showed both components of Fornax A to have an arc-like structure. The present observations (Fig. 4.7(a)) confirm these initial results and reveal in more detail the fine structure at 80 MHz. Both regions have multiple components and appear to contain ridge-like structures running from the centres almost radially outward to the extremities of each region. The components are very similar in shape and size; in fact there is a remarkable degree of radial symmetry with respect to the optical position if one allows for the difference in the intensities of the components.

A comparison has been made with maps obtained with the Mills Cross at 408 MHz (Cameron, 1969) and with the Parkes 210-ft telescope at 5000 MHz (WG). The general structure of both components is very similar at all three frequencies

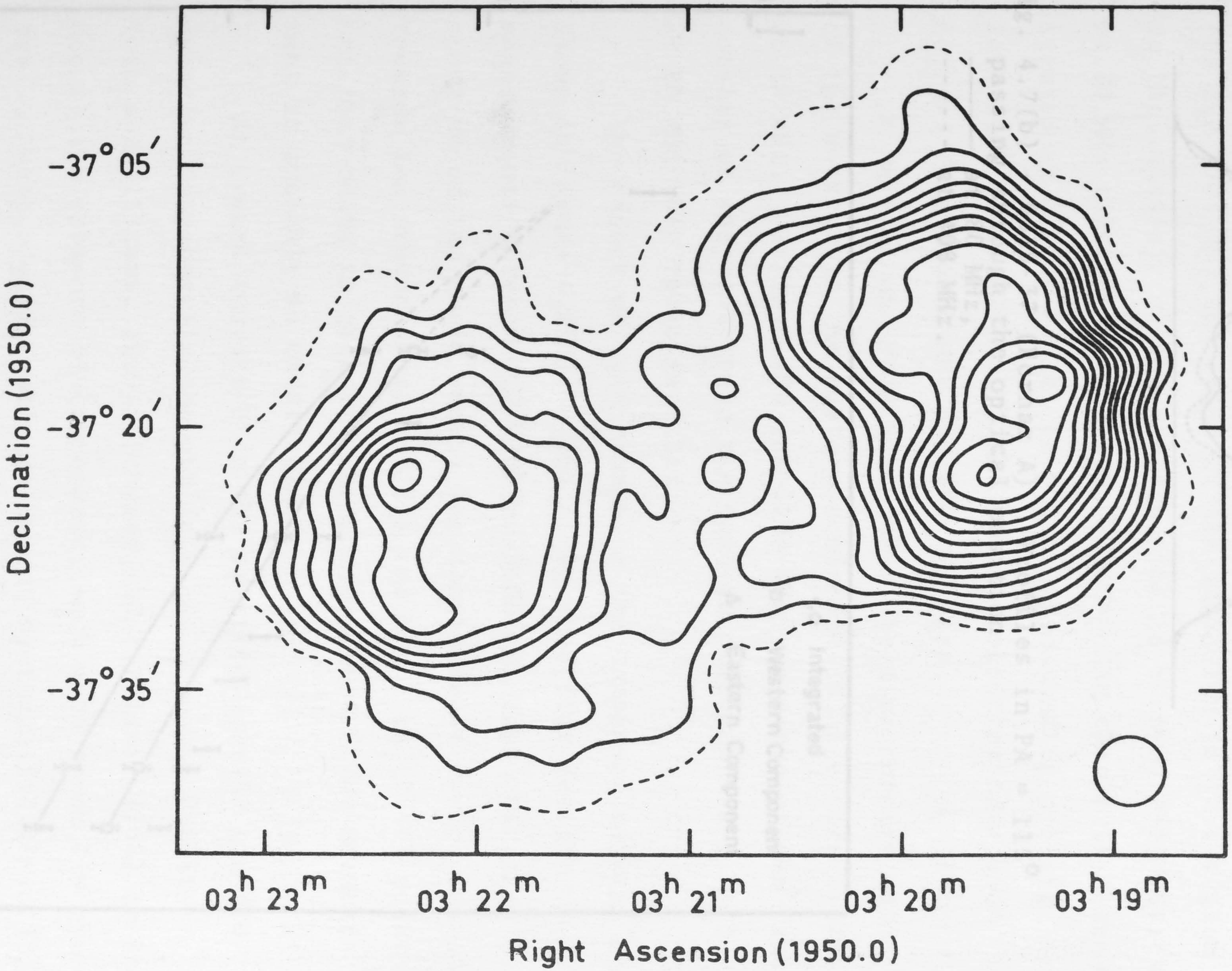

Fig. 4.7(a) - 0320-37 (Fornax A).

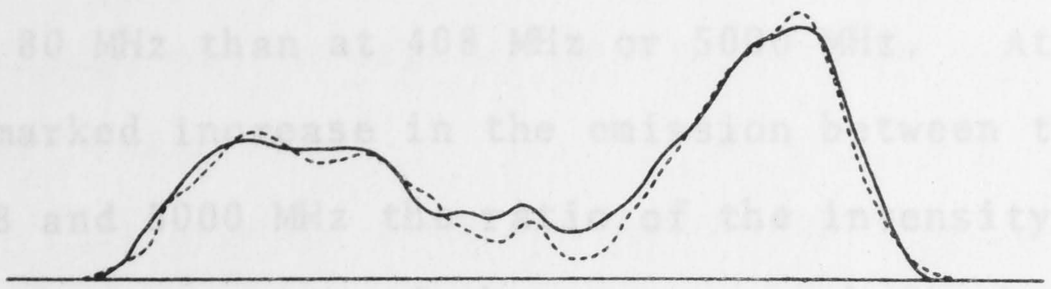

Fig. 4.7(b) - 0320-37 (Fornax A). Profiles in PA = 115°
passing through the optical position
——— at 80 MHz,
- - - - at 408 MHz.

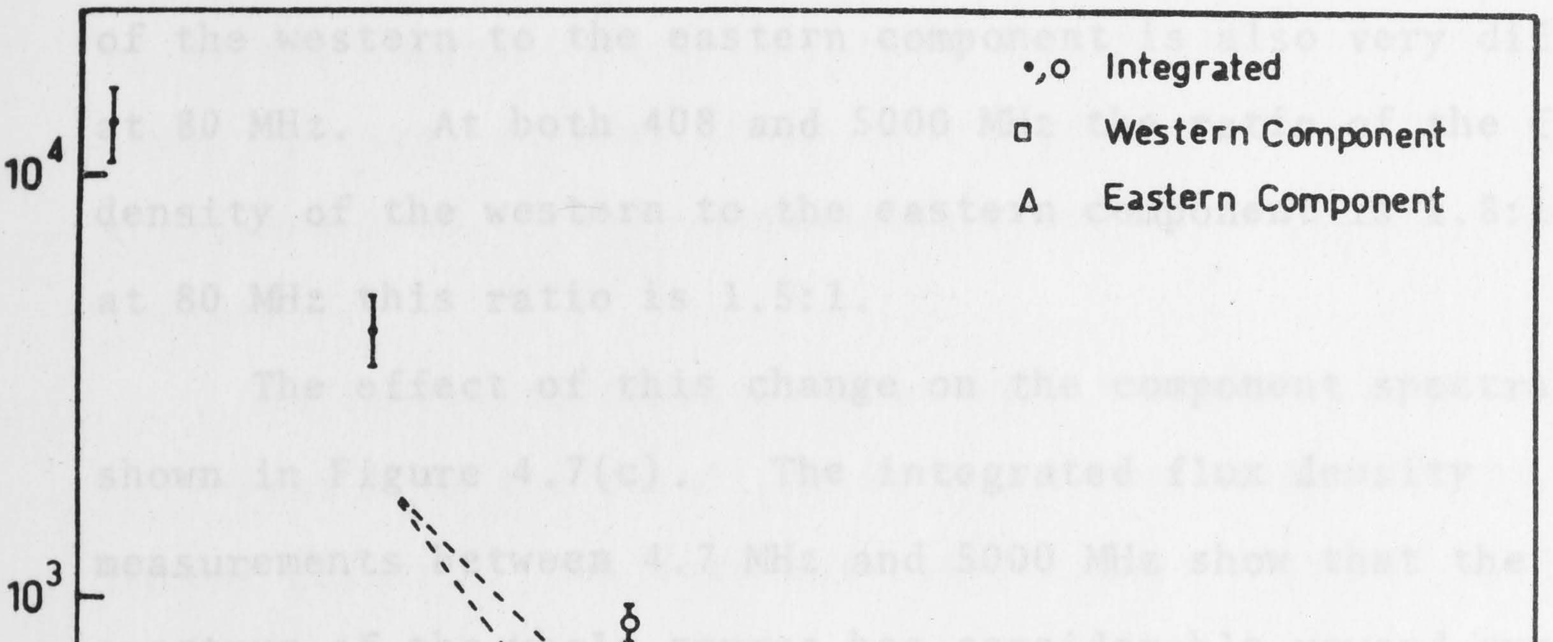

Fig. 4.7(c) - 0320-37 (Fornax A). Integrated and component spectra.

although the ridge-like structure is much more pronounced at 80 MHz than at 408 MHz or 5000 MHz. At 80 MHz there is a marked increase in the emission between the components. At 408 and 5000 MHz the ratio of the intensity in this region to the intensity of the western peak is about 0.1:1, whereas at 80 MHz this ratio is about 0.2:1. The change is demonstrated in Figure 4.7(b) in which corresponding profiles in PA = 115^o passing through the optical position have been derived from the 80 MHz and 408 MHz maps.

A careful analysis shows that the flux density ratio of the western to the eastern component is also very different at 80 MHz. At both 408 and 5000 MHz the ratio of the flux density of the western to the eastern component is 1.8:1; at 80 MHz this ratio is 1.5:1.

The effect of this change on the component spectra is shown in Figure 4.7(c). The integrated flux density measurements between 4.7 MHz and 5000 MHz show that the spectrum of the whole source has considerable upward curvature towards low frequencies. Ellis and Hamilton (1966) point out that owing to galactic absorption the 4.7 MHz measurement is probably an underestimate.

An upward curvature in the spectrum towards low frequencies is generally thought (e.g. Kellermann, Pauliny-Toth and Williams, 1969; Scheuer and Williams, 1968) to be due to the presence of components, each with power law spectra but with significantly different spectral indices. This interpretation does not seem to be directly applicable to Fornax A, since both components have curved spectra. The increase in spectral index towards low frequencies is more rapid for the eastern component; an extrapolation, making allowance for the spectral curvature, implies that at 19.7 MHz the components should be of comparable intensity. The contour map produced by Shain (1958) at this frequency, although of low angular resolution, is not inconsistent with this prediction.

It appears from the nature of their spectra that both components contain regions with significantly different spectral indices. The similarity between the maps at 80, 408 and 5000 MHz implies that these regions are not highly localized, but are rather uniformly distributed across each component. The ridge-like structures observed at 80 MHz may provide an explanation. Their more prominent character at 80 MHz suggests that they are regions with relatively steep spectra, whereas their rather general distribution would not lead to any outstanding structural changes with frequency.

An immediate conclusion is that the observed structure of Fornax A is the result of at least two events in the parent galaxy. The somewhat steeper low-frequency spectrum of the eastern component suggests that the regions of this component which are strong at low frequencies are at a more advanced evolutionary stage than are the regions of the western component. This apparent difference in age could be explained by the evolutionary model proposed by Ryle and Longair (1967) in which it is supposed that two identical plasma clouds are ejected from the nucleus of the galaxy with relativistic velocities. Unless the axis of the system is perpendicular to the line of sight, the two components will subsequently be observed at significantly different ages, with the approaching component at a more advanced stage of evolution than the receding component. In the framework of this model the eastern component of Fornax A is approaching, whilst the western component is receding.

With this in mind a three-dimensional impression of the source can be developed which when combined with the optical data for NGC 1316 suggests that the radio regions were ejected along the minor axis of the galaxy. Searle (1965) has shown that the projected rotational axis of NGC 1316 lies along its minor axis, which is inclined at an angle of about 45^o to the line joining the centroids of the radio components. Relative to the galactic nucleus the north-east side of the galaxy is approaching and the south-west side is receding. It is quite possible that the observed minor axis of the galaxy is not the true minor axis, the latter being inclined to the line of sight at the same angle as the major axis of the radio source. The major axis of the galaxy would then be orthogonal to the major axis of the radio source, but inclined to the plane of the sky such that the south-western side is nearer and the north-eastern side further away. This arrangement would imply that the faint optical radiation emanating in curved pathways from NGC 1316 (Arp, 1964) is not intimately associated with the radio components.

An unresolved source centred on NGC 1316 has been detected at 408 MHz (Cameron, 1969) and at 5000 MHz (WG). The 80 MHz map also shows a weak unresolved source between the main components. However, direct comparison of the main features at 80 MHz and at 408 MHz places it about 1' arc to the south of the 408 MHz position; this discrepancy is possibly due to the change in structure of the central region between 408 and 80 MHz. This source has a flux density at 80 MHz of approximately 2 f.u. which when combined with the estimates at 408 and 5000 MHz gives a spectral index of 0.7 for the emission from NGC 1316 itself.

0349-27

Interferometer observations by Fomalont (1967) have shown this source to consist of three components of almost equal flux density. In the east-west direction the outer components are separated by 3'.9 arc; the third component lies 1'.3 arc to the west of the outer eastern component. Angular sizes given by Fomalont for the eastern, central and western components are 0'.8, 1'.1 and 1'.8 arc respectively.

Figure 4.8(a) shows that the components are not resolved at 80 MHz although the source is clearly elongated in PA = 66°. The position and angular size measurements of Fomalont have been used to estimate the relative flux densities of the components at 80 MHz, using the method adopted for 3C 33. In the present case the analysis is less precise, since two of the components have angular diameters which are an appreciable fraction of the 80 MHz beamwidth. After projecting the east-west distribution on to a position angle of 66° and allowing for the component diameters, their intensities were adjusted until a summed profile of best fit to the observed 80 MHz profile in PA = 66° was obtained. It was found that the relative flux densities of the components are very similar at 80 MHz and 1425 MHz, the only apparent difference being a 10% to 20% decrease in the relative flux density of the western component at 80 MHz. All three components appear to have very similar spectra. There may be a slight decrease in the spectral index of the western component between 1425 MHz and 80 MHz. This would account for the slight flattening in the integrated spectrum (Fig. 4.8(b)) between 408 and 80 MHz.

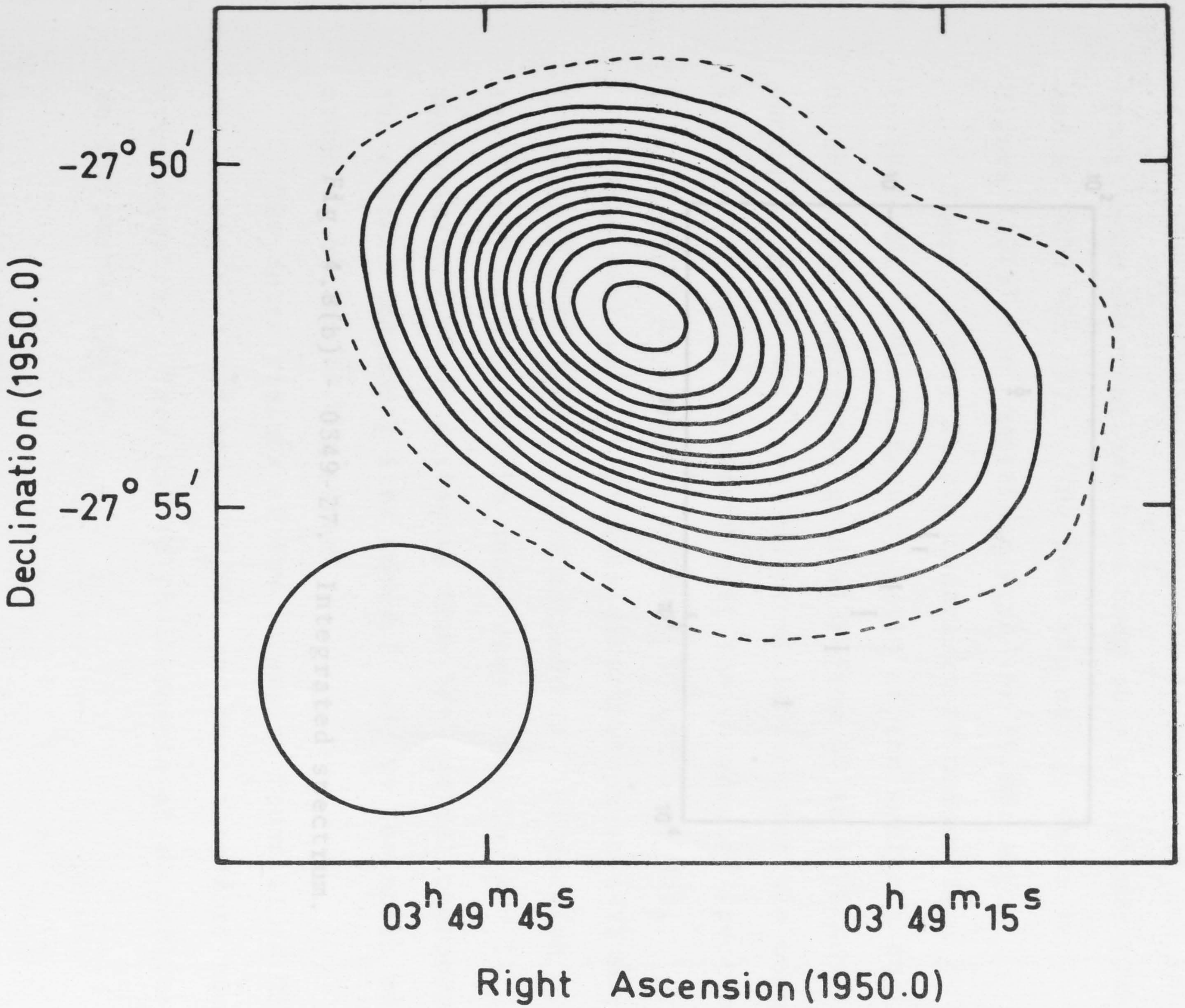

Fig. 4.8(a) - 0349-27.

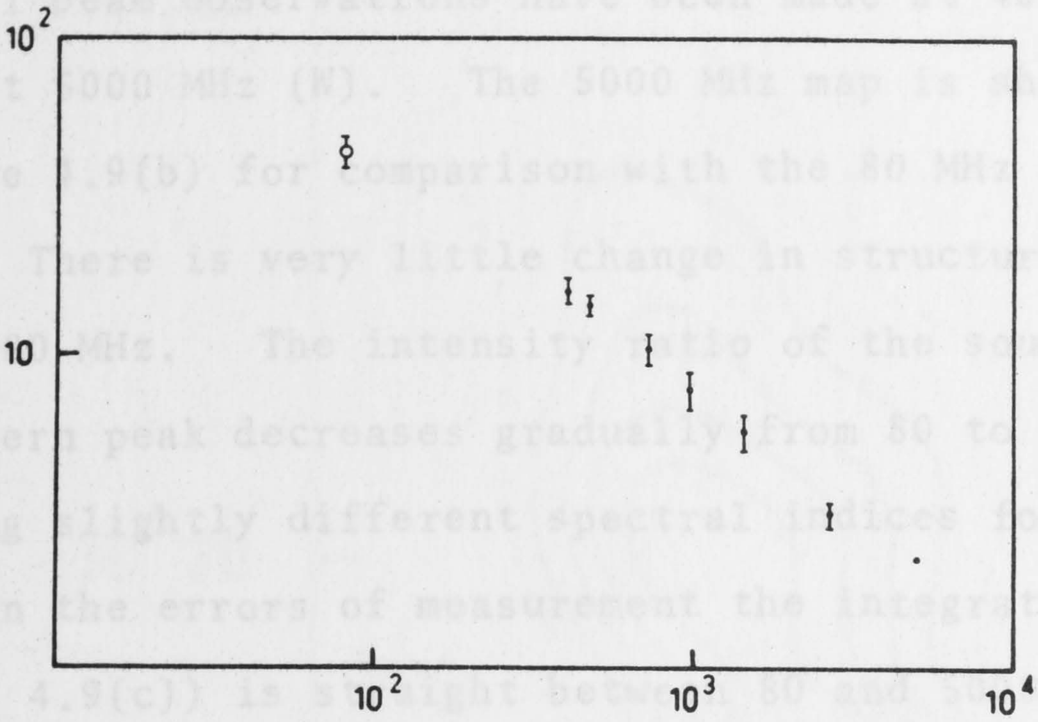

Fig. 4.8(b) - 0349-27. Integrated spectrum.

0511-30

The 80 MHz map is shown in Figure 4.9(a). The source is resolved into two components in PA = 24° with indications of extended low brightness regions to the north and south. Pencil beam observations have been made at 408 MHz (SMb) and at 5000 MHz (W). The 5000 MHz map is shown in Figure 4.9(b) for comparison with the 80 MHz map.

There is very little change in structure from 80 MHz to 5000 MHz. The intensity ratio of the southern to the northern peak decreases gradually from 80 to 5000 MHz, implying slightly different spectral indices for the components. Within the errors of measurement the integrated spectrum (Fig. 4.9(c)) is straight between 80 and 5000 MHz.

The east-west brightness distribution at 1425 MHz (Fomalont, 1967) shows three components. Projection on to the 80 MHz map places the outer components in PA = 22° at approximately equal distances from the central component; the central component lies about 1' arc to the north of the midpoint of the 80 MHz peaks.

The outer regions of low intensity found at 80 MHz are not observed at 408 and 5000 MHz and must therefore have steep spectra. They may be the remnants of an earlier event in the parent galaxy.

0518-45 (Pictor A)

The 80 MHz map (Fig. 4.10(a)) shows two peaks separated by 3'.8 arc in PA = 103°. Fomalont (1967) has shown that at 1425 MHz the structure is very complex with at least five components resolved in the east-west direction. In Figure 4.10(b) the east-west distribution obtained by Fomalont has been projected on to PA = 103°. This distribution, when

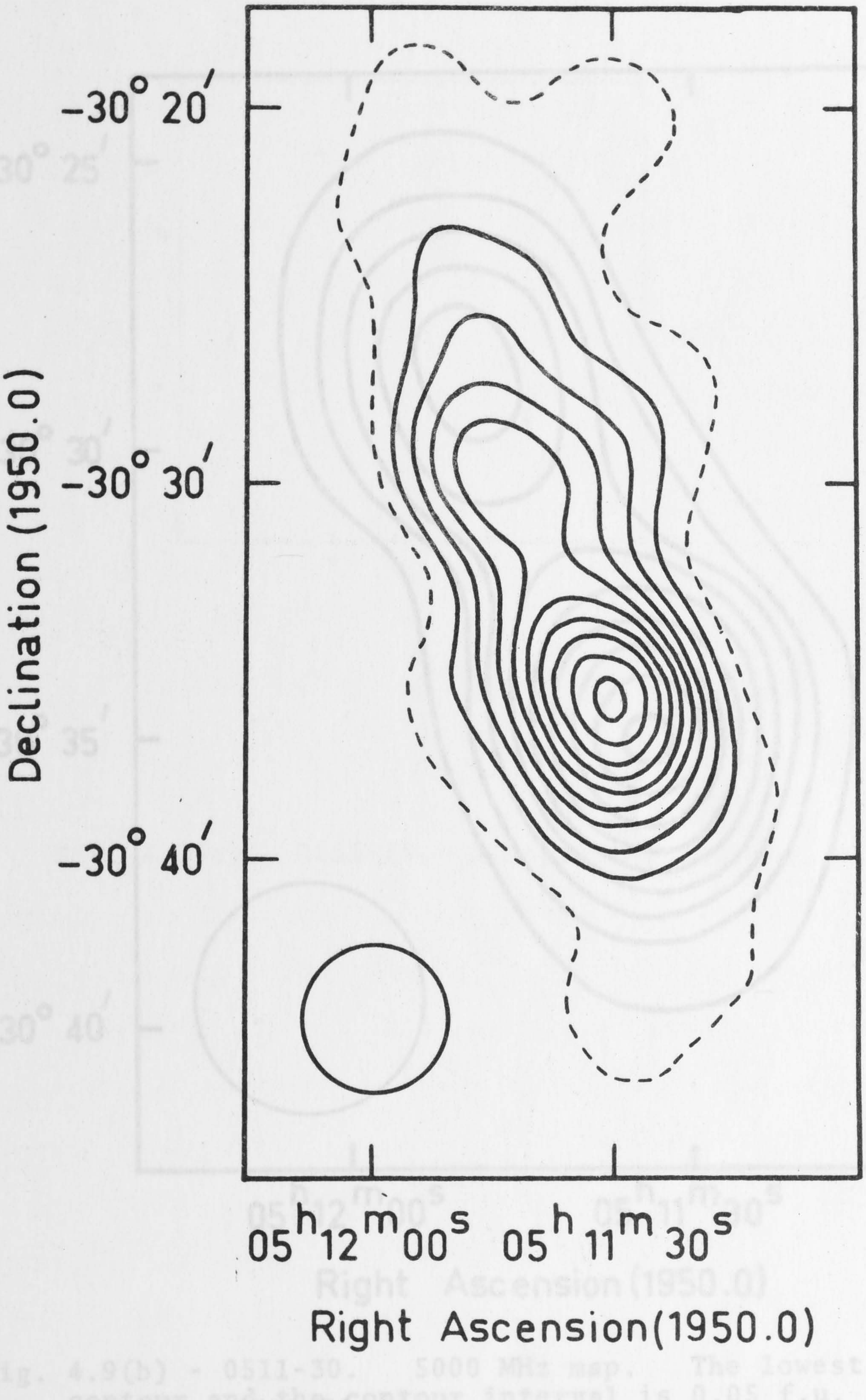

Fig. 4.9(a) - 0511-30.

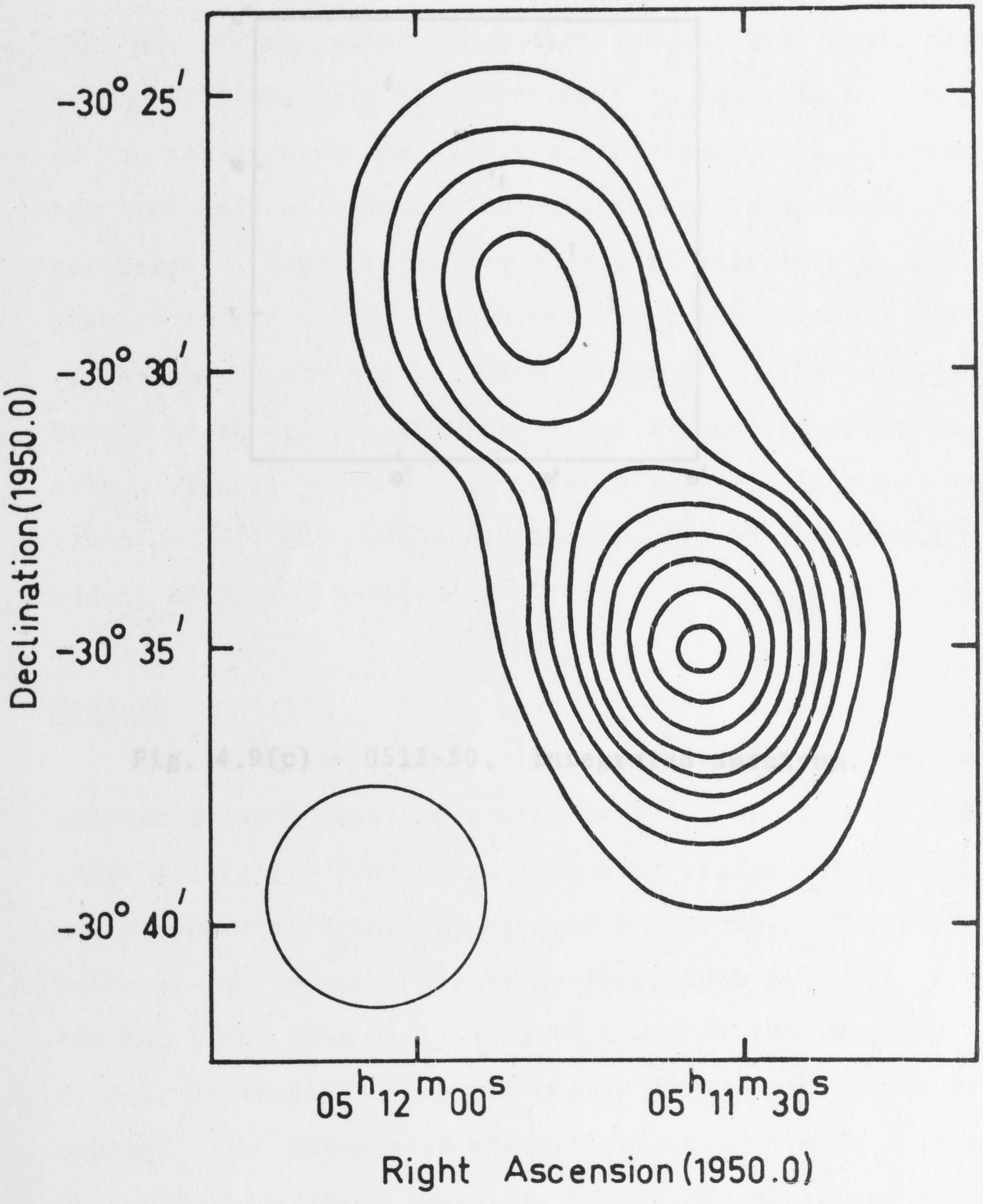

Fig. 4.9(b) - 0511-30. 5000 MHz map. The lowest contour and the contour interval is 0.05 f.u.

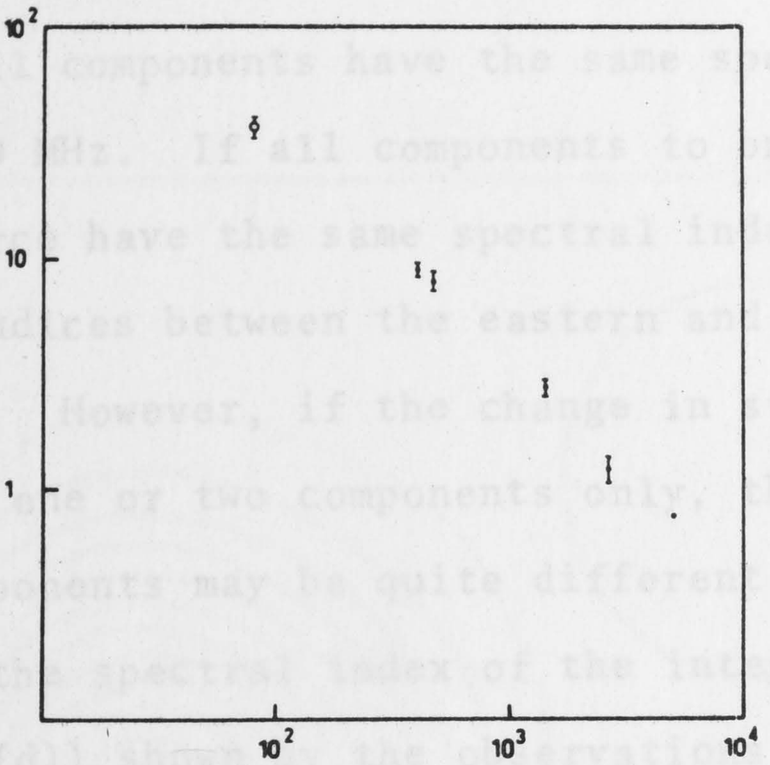

Fig. 4.9(c) - 0511-30, Integrated spectrum.

convolved with a 4' arc Gaussian, is shown in Figure 4.10(c), where comparison is made with profiles in PA = 103^o observed at 80 MHz and at 5000 MHz (WG).

The change in structure shown in Figure 4.10(c) implies that not all components have the same spectral index between 80 and 5000 MHz. If all components to one side of the centre of the source have the same spectral index, the difference in spectral indices between the eastern and western components is not large. However, if the change in structure is due to changes in one or two components only, the spectral indices of the components may be quite different. The marked increase in the spectral index of the integrated spectrum (Fig. 4.10(d)) shown by the observations of Ellis and Hamilton (1966) at 4.7 MHz indicates the presence of components with widely different spectra.

0634-20

At 80 MHz this source is well resolved into two main components with peaks separated by 11'.1 arc in PA = 178^o (Fig. 4.11(a)). The slightly curved region between the peaks suggests further unresolved structure. The intensity ratio of the southern to the northern peak is 1.5:1. At 408 MHz (SMb) this ratio is 1.43:1 and at 5000 MHz (WG) 1.34:1, indicating a gradual change in structure with frequency. The integrated spectrum shown in Figure 4.11(b) is not well defined. However, the 80 MHz measurement suggests that the spectral index of the whole source decreases slightly between 408 and 80 MHz.

In Figure 4.11(a) the position of the optical identification (Bolton, Clarke and Ekers, 1965) is indicated by a cross; its position in relation to the radio components was found

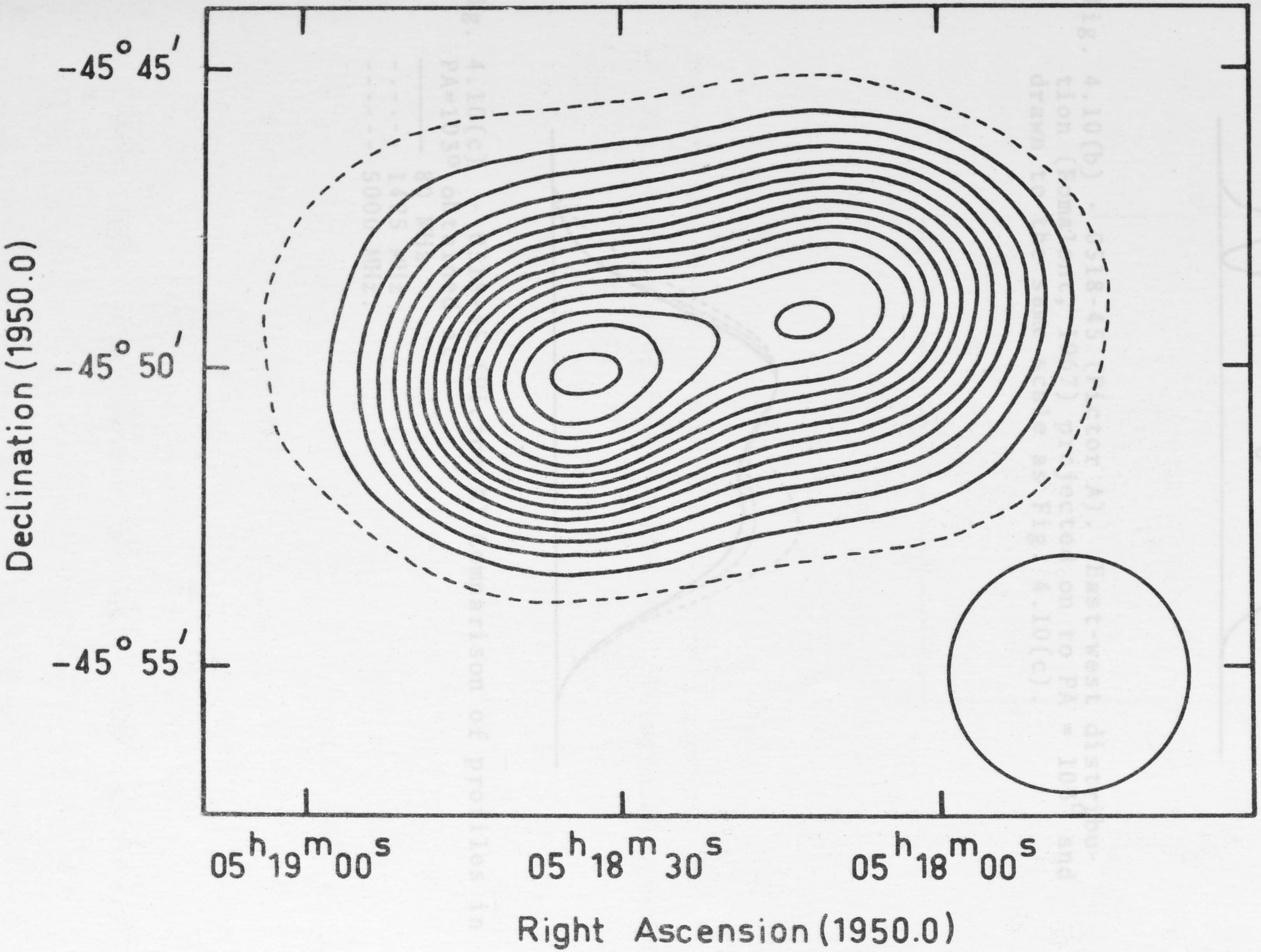

Fig. 4.10(a) - 0518-45 (Pictor A).

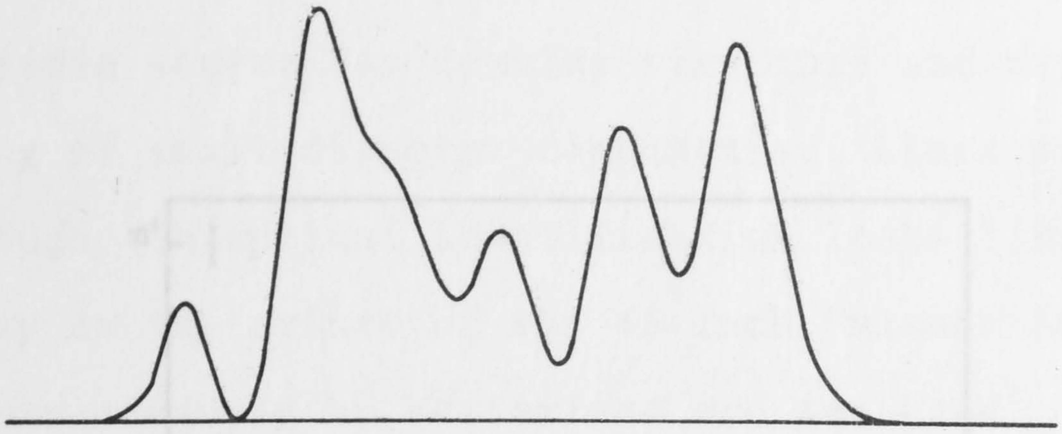

Fig. 4.10(b) - 0518-45 (Pictor A). East-west distribution (Fomalont, 1967) projected on to PA = 103° and drawn to the same scale as Fig. 4.10(c).

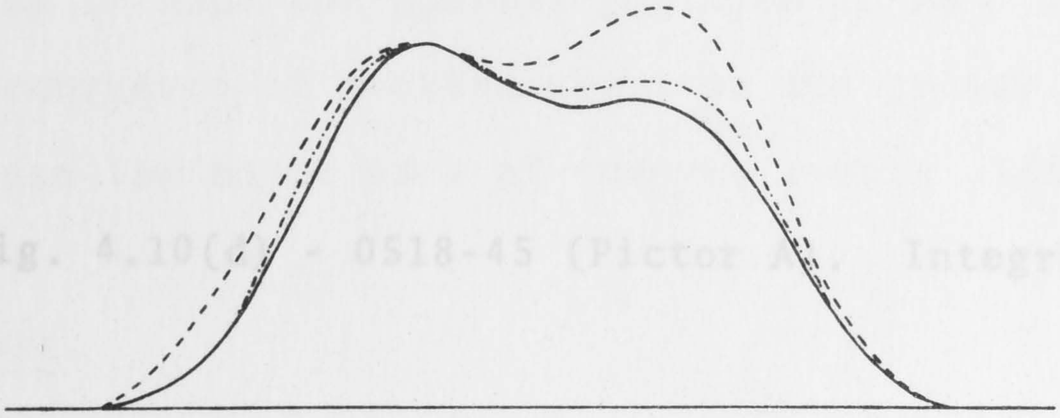

Fig. 4.10(c) - 0518-45 (Pictor A) Comparison of profiles in PA=103° obtained at
——— 80 MHz
-.-.- 1425 MHz
------ 5000 MHz.

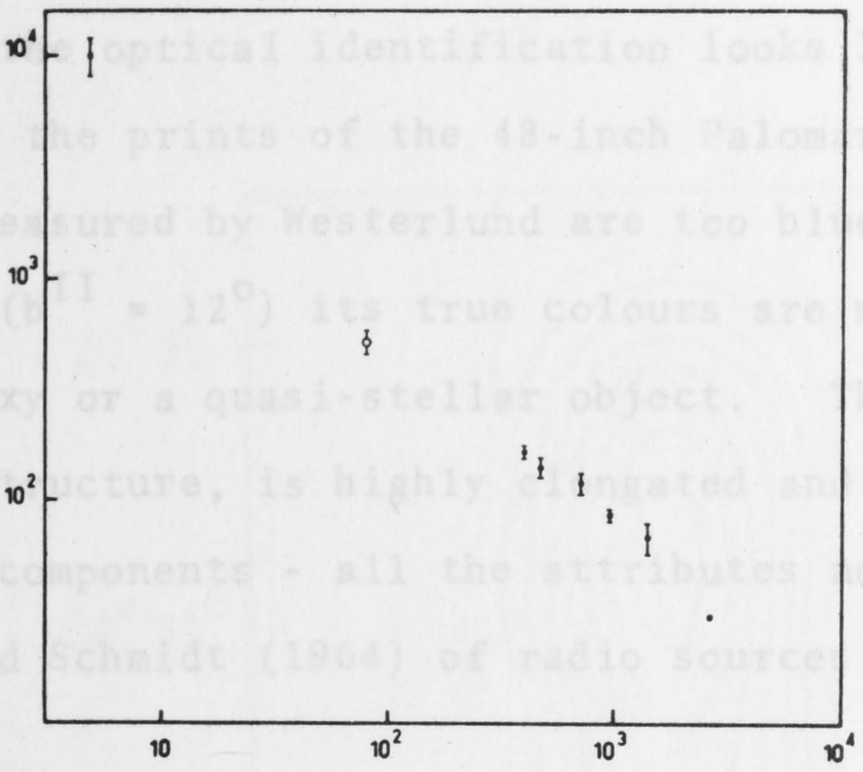

Fig. 4.10(d) - 0518-45 (Pictor A). Integrated spectrum.

by comparison with the 408 MHz map.

Interferometer observations by Ekers (1969) show that the radio source has complex structure and may consist of a string of small diameter components. Ekers points out that although the optical identification looks like an elliptical galaxy on the prints of the 48-inch Palomar Sky Survey, the colours measured by Westerlund are too blue. If it has been reddened ($b^{II} = 12^{o}$) its true colours are more like those of an N galaxy or a quasi-stellar object. The radio source has complex structure, is highly elongated and contains small diameter components - all the attributes noted by Matthews, Morgan and Schmidt (1964) of radio sources identified with N galaxies.

The slight bulging of the 80 MHz contours along a line passing through the optical position in PA = 52^{o} may indicate the occurrence of another event in the galaxy. If this is the case the major axes of the two events differ by 54^{o}.

0800-09

A marked change in structure is found between the 80 MHz map (Fig. 4.12(a)) and a previously unpublished 5000 MHz map (W) (Fig. 4.12(b)). Some evidence of structural changes with frequency is also provided by a comparison of the 5000 MHz map with a 408 MHz map (SMb). As shown in Figure 4.12(b), at 5000 MHz the source appears to be double, with peaks separated by 7'.6 arc in PA = 90^{o}. The intensity ratio of the western to the eastern peak is 0.86:1. Two components are also observed at 408 MHz, but with peaks separated by 7'.1 arc in PA = 90^{o} and an intensity ratio for the western to the eastern peak of 1.48:1. The decrease in the separation of the peaks between 5000 MHz and 408 MHz cannot be explained

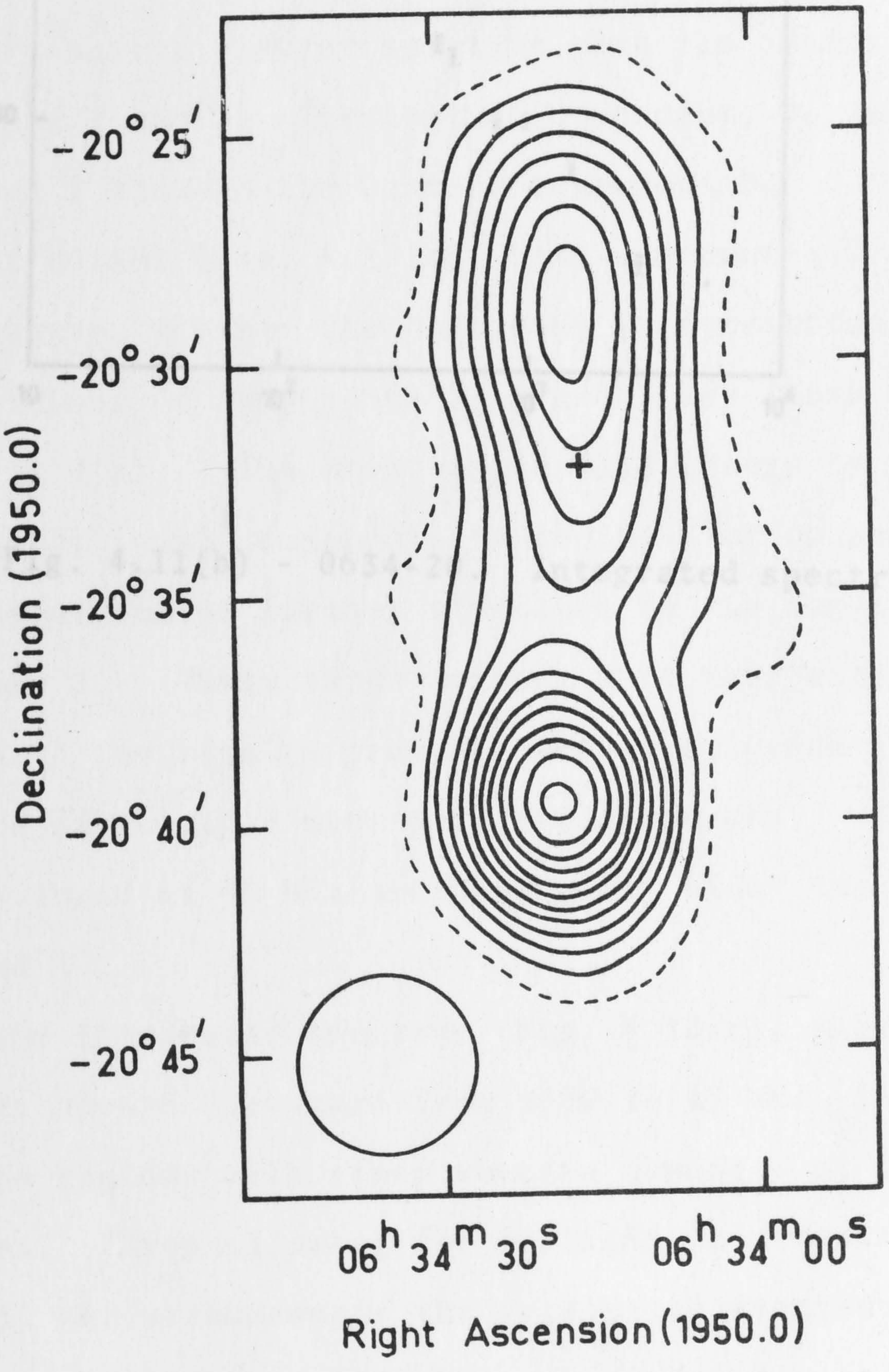

Fig. 4.11(a) - 0634-20. The position of the optical identification is indicated by a cross.

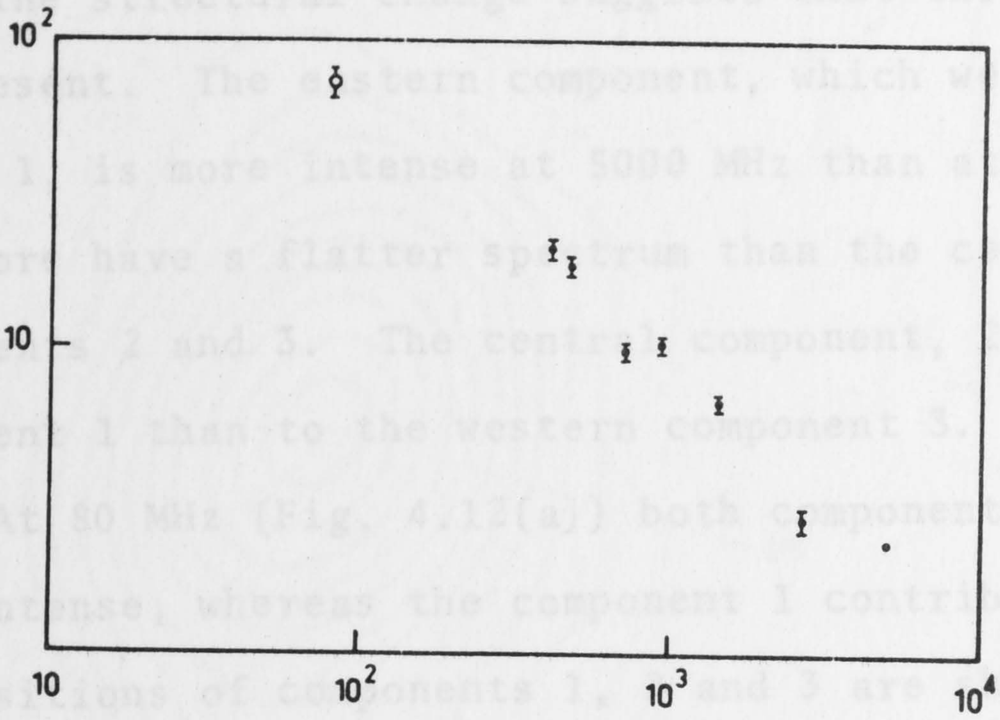

Fig. 4.11(b) - 0634-20. Integrated spectrum.

by the difference in beamwidths. The peaks should if anything be closer at 5000 MHz, since the beamwidth in this case is 4'.0 arc whereas the 408 MHz beamwidth is 2'.86 arc.

The structural change suggests that three components are present. The eastern component, which we shall call component 1, is more intense at 5000 MHz than at 408 MHz and must therefore have a flatter spectrum than the central and western components 2 and 3. The central component, 2, is closer to component 1 than to the western component 3.

At 80 MHz (Fig. 4.12(a)) both components 2 and 3 are very intense, whereas the component 1 contributes very little. The positions of components 1, 2 and 3 are shown in Figure 4.12(a). The most outstanding change is the appearance of two additional components to the east of component 1, and the indications of further structure to the north-west of component 3. These three regions must have extremely steep spectra. The results provide further evidence for the occurrence of multiple events in radio sources. The outer regions found at 80 MHz are presumably older than the regions 1, 2 and 3.

The integrated spectrum (Fig. 4.12(c)) shows a very definite upward curvature from 5000 to 80 MHz, indicating that the regions with steep spectra dominate at low frequencies. Even allowing for a slight underestimation in the 2650 MHz measurements the integrated spectrum is very flat between 1420 and 5000 MHz and presumably at frequencies above 5000 MHz, component 1 contributes strongly to the integrated spectrum.

Possible optical identifications have been discussed by SMb. There is no optical object with which this source can definitely be identified. The field contains several

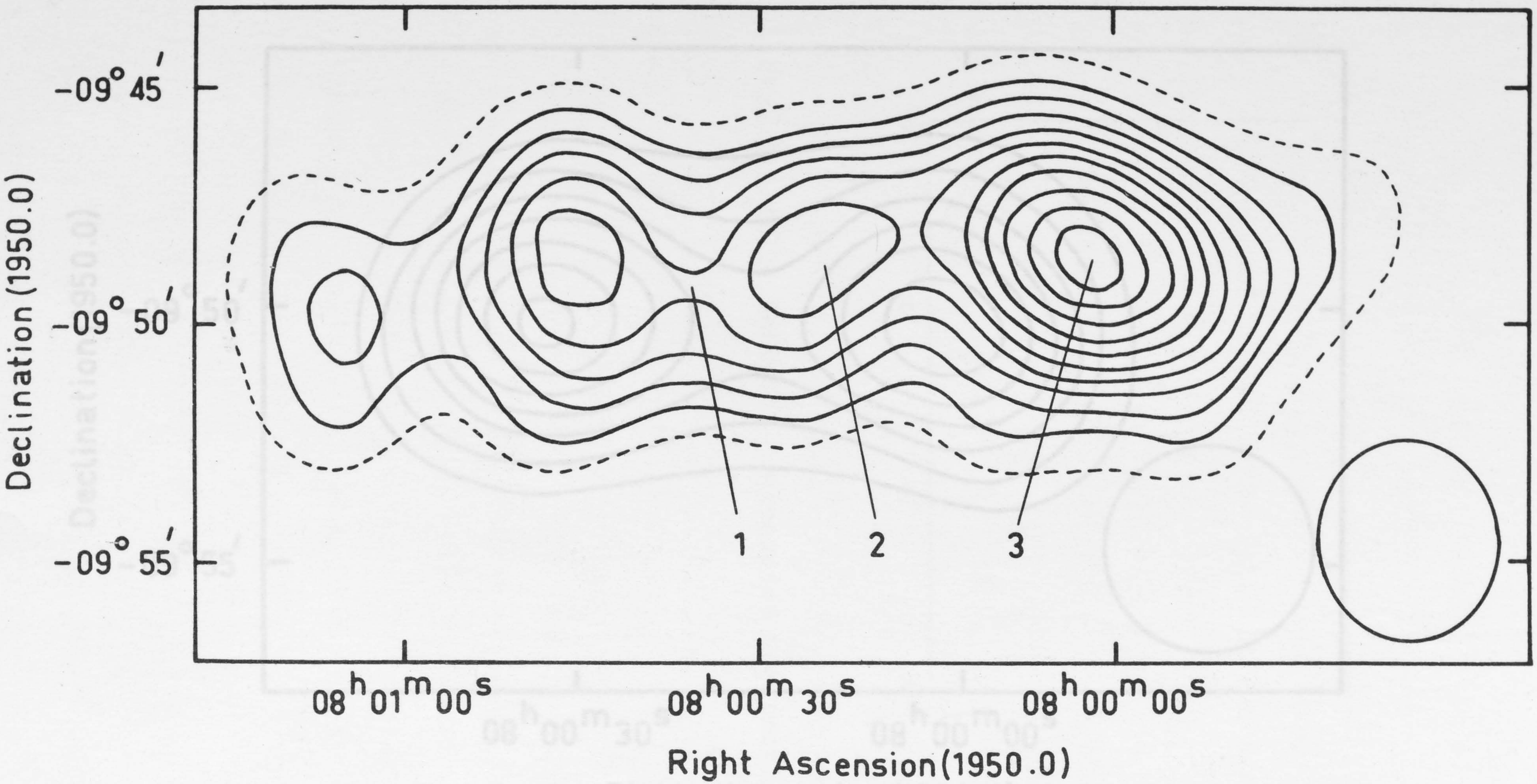

Fig. 4.12(a) - 0800-09. Approximate positions of components 1, 2, 3 are indicated.

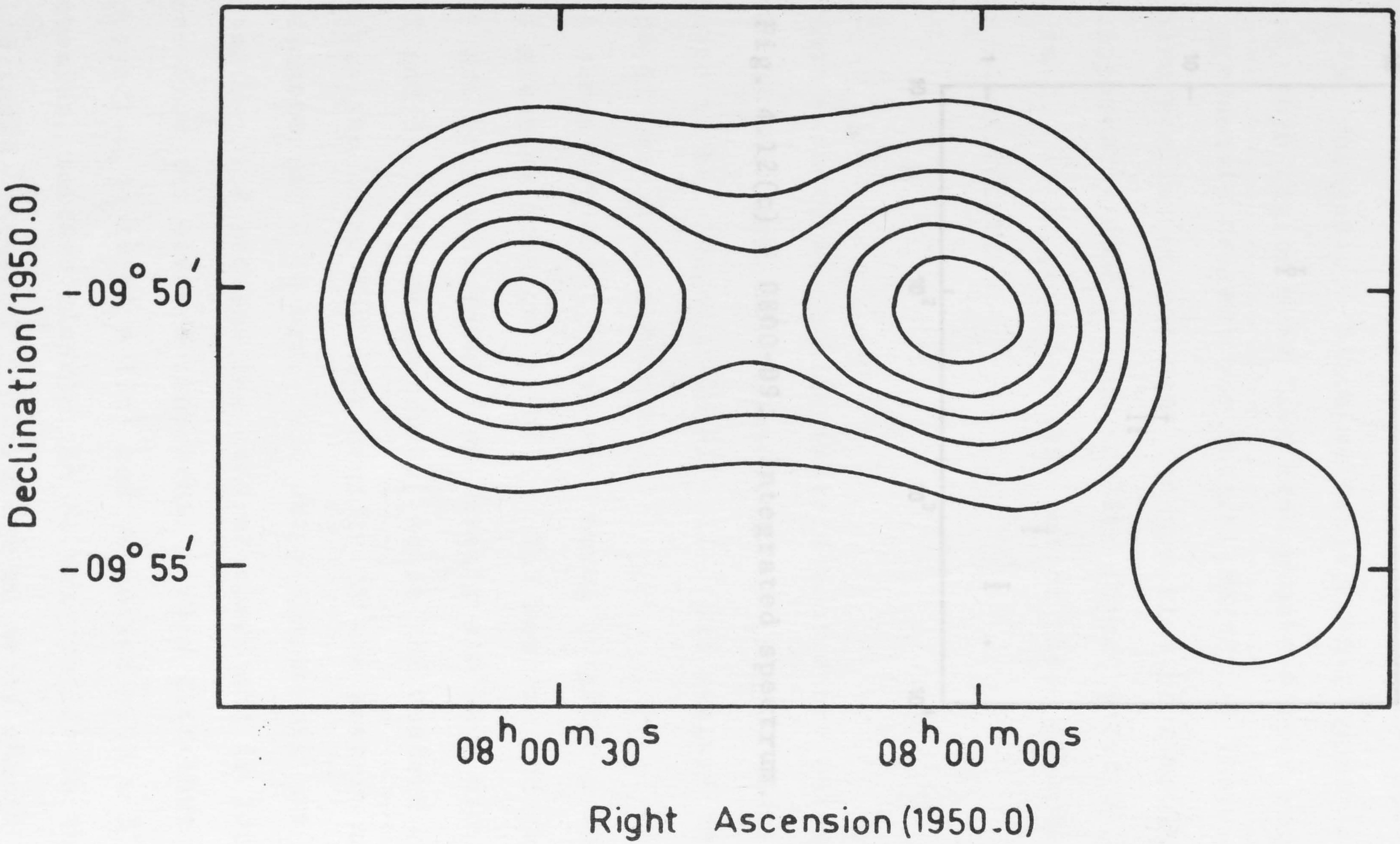

Fig. 4.12(b) - 0800-09. 5000 MHz map. The lowest contour and the contour interval is 0.05 f.u.

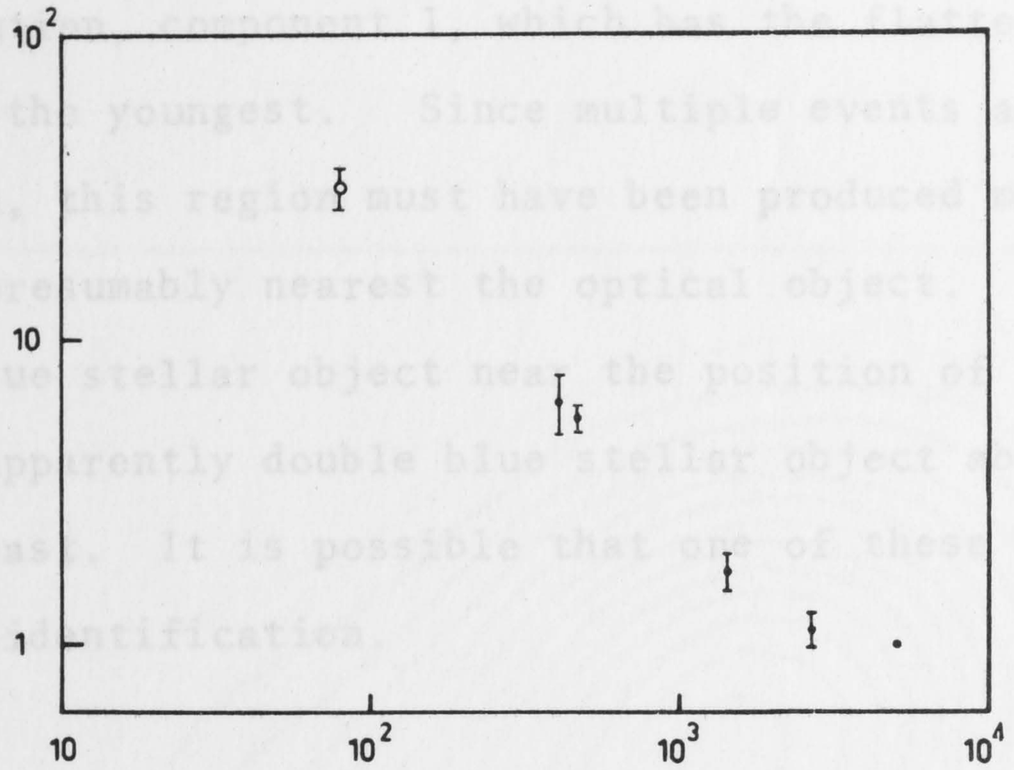

Fig. 4.12(c) - 0800-09. Integrated spectrum.

faint galaxies, one of which was selected by Bolton and Ekers (1966) as the correct identification. If it is assumed that the spectra of the components indicate their stage of evolution, component 1, which has the flattest spectrum, must be the youngest. Since multiple events appear to have occurred, this region must have been produced most recently and is presumably nearest the optical object. There is a $19^m.5$ blue stellar object near the position of component 1 and an apparently double blue stellar object about 0'.5 arc to the east. It is possible that one of these objects is the correct identification.

0819-30

Most structural details of this source are unresolved with the 80 MHz beam. The observations (Fig. 4.13(a)) show the source to be elongated in PA = 126° and suggest the presence of two basic components.

A three-component, east-west model brightness distribution is given by Fomalont (1967). The western and central regions are of almost equal flux density and have diameters of 1'.2 and 3'.7 arc respectively, while the eastern component has one-third the flux density of the western component and a diameter of 0'.6 arc. The outer components are separated by 3'.8 arc and the central component is located 1'.7 arc from the eastern component. This distribution, when projected on to PA = 126° and convolved with a 3'.75 arc Gaussian, matches closely the 80 MHz profile in this position angle. Apparently there are no major changes in structure between 1425 and 80 MHz, a conclusion substantiated by the integrated spectrum (Fig. 4.13(b)) which appears to obey a simple power-law between 80 and 2650 MHz. There may,

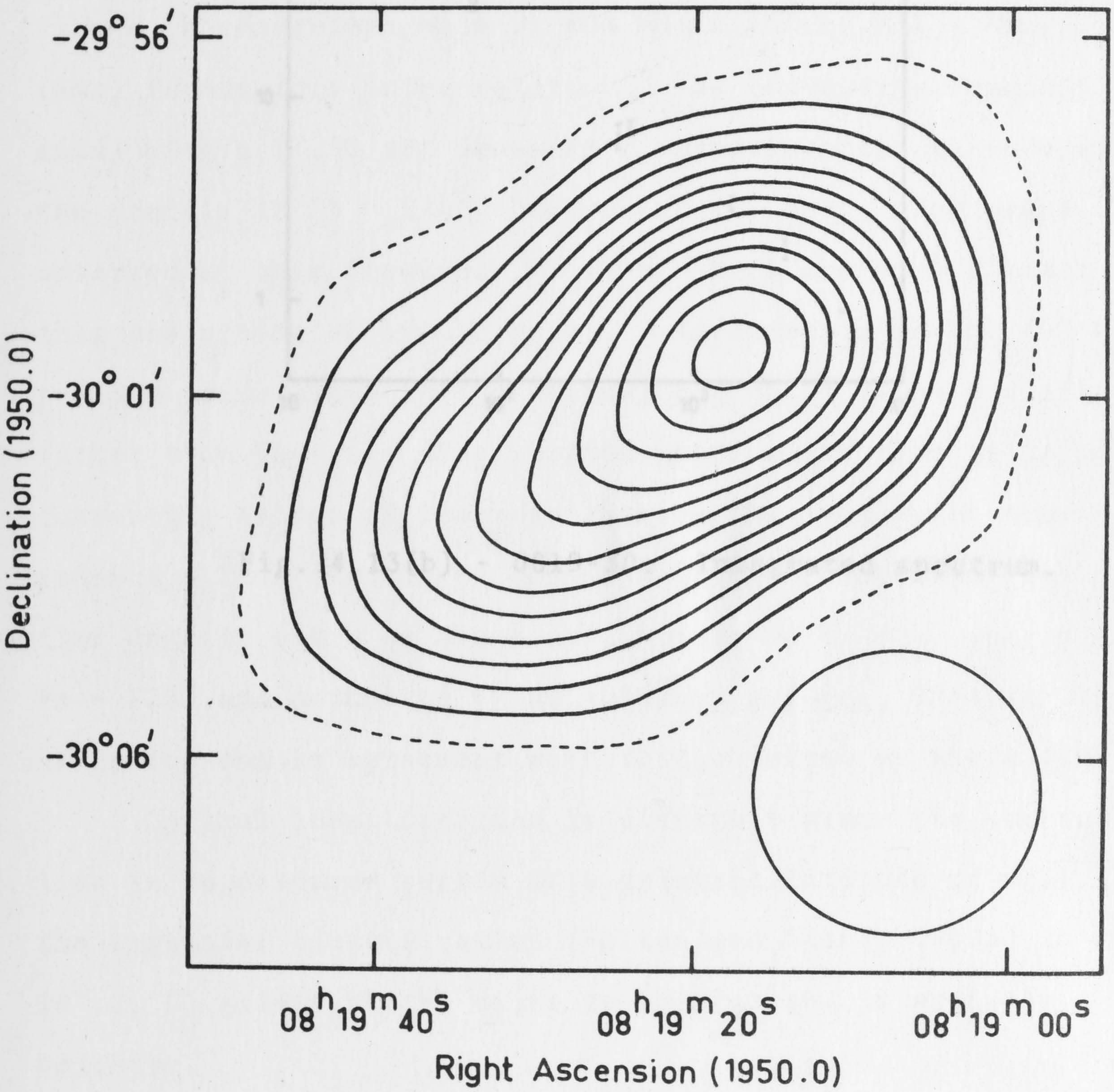

Fig. 4.13(a) - 0819-30.

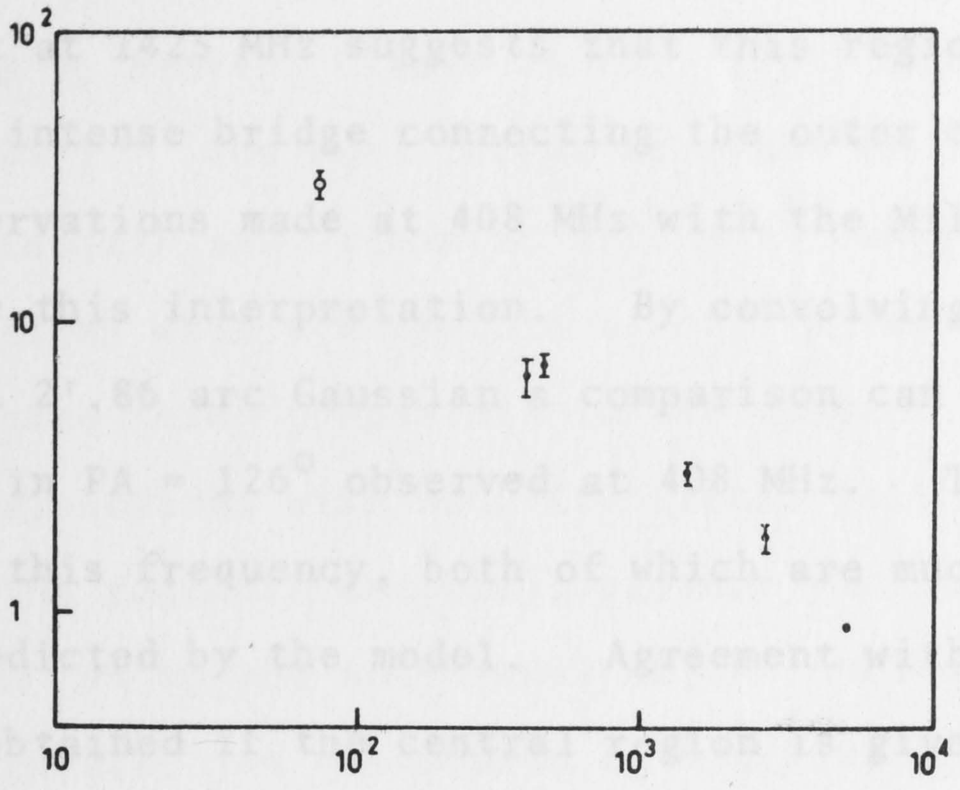

Fig. 4.13(b) - 0819-30. Integrated spectrum.

however, be some increase in spectral index between 2650 and 5000 MHz.

Figure 4.13(a) suggests that the central component is probably elongated along the major axis of the source. Its large extent at 1425 MHz suggests that this region may, in fact, be an intense bridge connecting the outer components. Indeed, observations made at 408 MHz with the Mills Cross (SMa) favour this interpretation. By convolving Fomalont's model with a 2'.86 arc Gaussian a comparison can be made with the profile in PA = 126^{o} observed at 408 MHz. Two peaks are observed at this frequency, both of which are much flatter than are predicted by the model. Agreement with the 408 MHz profile is obtained if the central region is given a flattened rather than Gaussian distribution, indicating that it is a connecting bridge of lower brightness than the outer components. Thus the source consists of two components with a flux density ratio of about 3:1, separated by 4'.7 arc in PA = 126^{o} and connected by an emission bridge. This structure is in reasonable agreement with that obtained by Ekers (1969).

Optical identification is difficult since the source lies in an obscured region at a galactic latitude of only 4^{o}. The suggested identification (Bolton and Ekers, 1966a) is an 18^{m}.2, E3 galaxy which, owing to absorption, is probably brighter.

1228+12 (3C 274, Virgo A)

The radio source Virgo A is associated with the E2 galaxy NGC 4486 (M87), which has a peculiar jet projecting from the nucleus in PA = 290^{o} (Baade and Minkowski, 1954). Essentially the radio structure consists of a compact central component superimposed on an asymmetrical extended component.

The compact source structure has been investigated in detail both by aperture synthesis (MKN; Hogg, Macdonald, Conway and Wade, 1969) and by the use of very long baseline interferometers (e.g. Cohen, Moffet et al., 1969; Miley, Hogg and Basart, 1970; Broten, Clarke et al., 1967; Donaldson, Miley et al., 1969). The most recent aperture synthesis observations by Longair and Graham at 4995 MHz (Komesaroff, private communication) with a beamwidth of only a few seconds of arc, have revealed three components in the compact source, one of which is associated with NGC 4486 itself (although apparently not with the galactic nucleus), another with the parts of the well-known jet to the north-west of the nucleus, and the third with the counter jet discovered by Arp (1967).

Information on the structure of the extended component is less complete and no recent study has been made of the individual component spectra. The present observations are of sufficiently high angular resolution to show the general structure of the extended component and to allow an estimate to be made of the 80 MHz flux density of both the compact and extended components.

The 80 MHz map is shown in Figure 4.14(a). Our observations show that both components are present at this frequency, although the intensity of the compact component in relation to the extended component is less than is found at higher frequencies. The extended component has the same shape and dimensions at both 80 and 408 MHz (Cameron, 1969).

Two alternative methods of computer analysis were used to estimate the relative flux densities of the components at 80 MHz. With the first method it was assumed that the compact source was completely unresolved by the radioheliograph, allowing the components to be separated by subtraction of

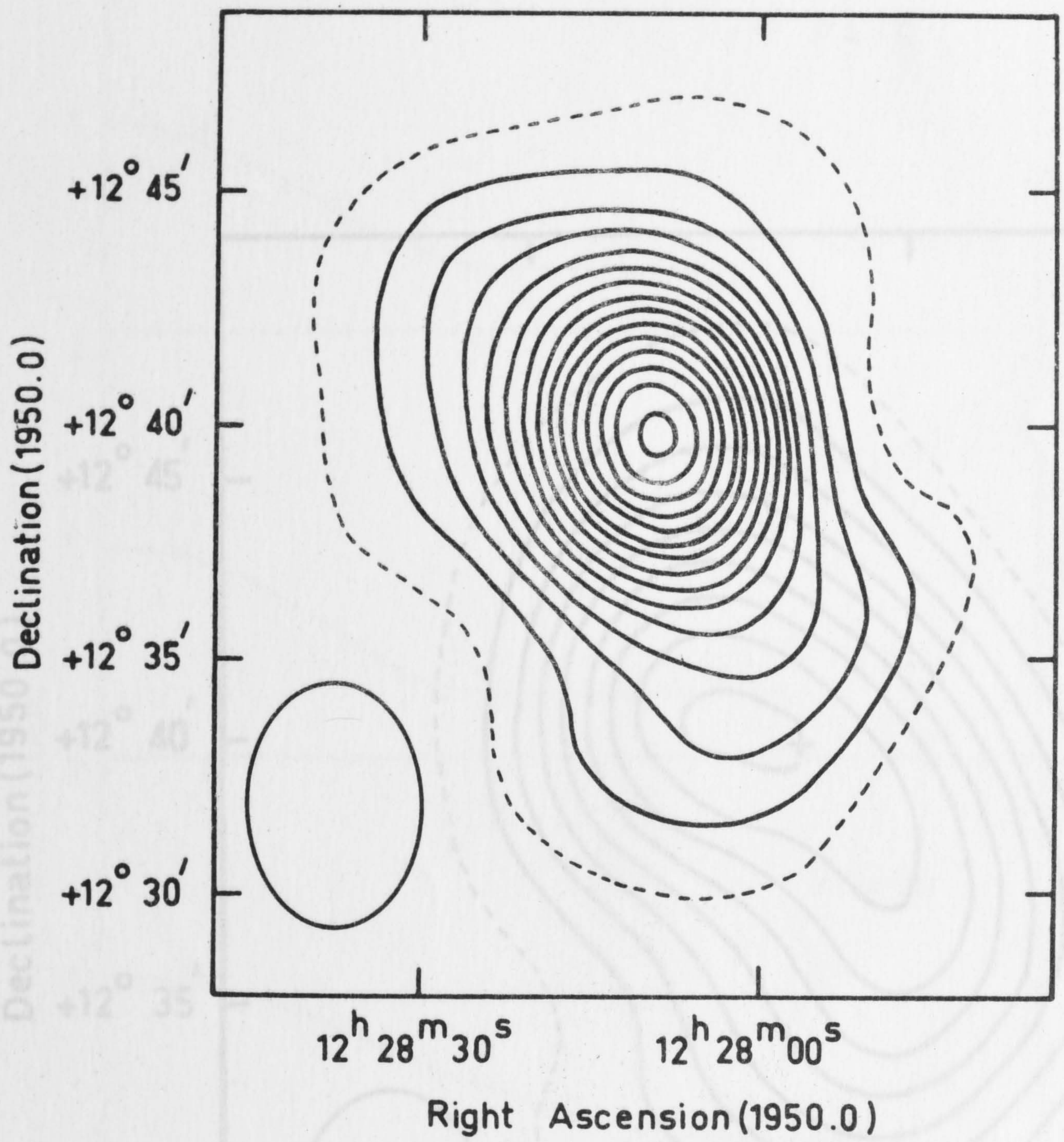

Fig. 4.14(a) - 1228+12 (3C 274, Virgo A).

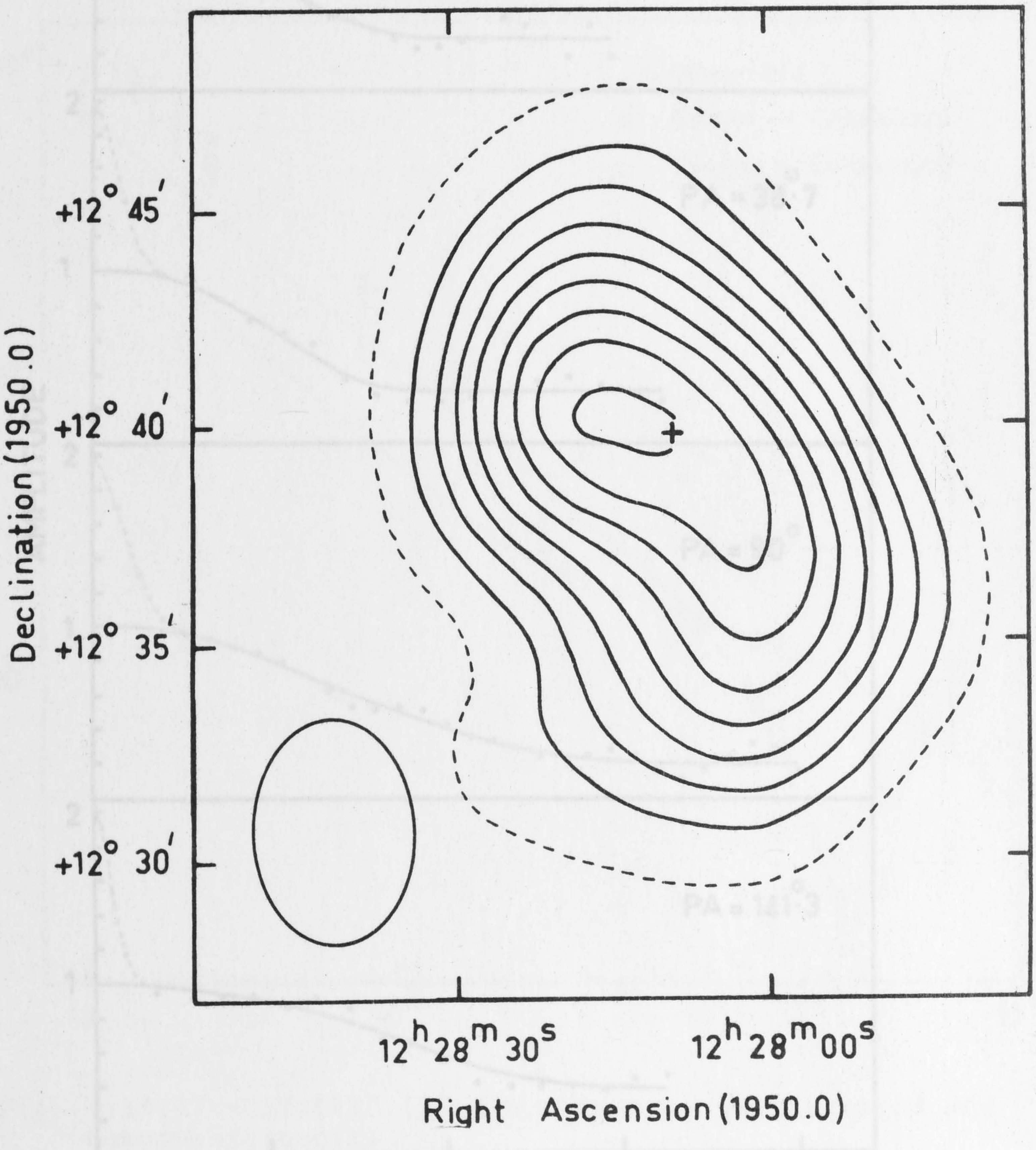

Fig. 4.14(b) - 1228+12 (3C 274, Virgo A). Map of the extended component. The position of the centre of the compact component is marked with a cross.

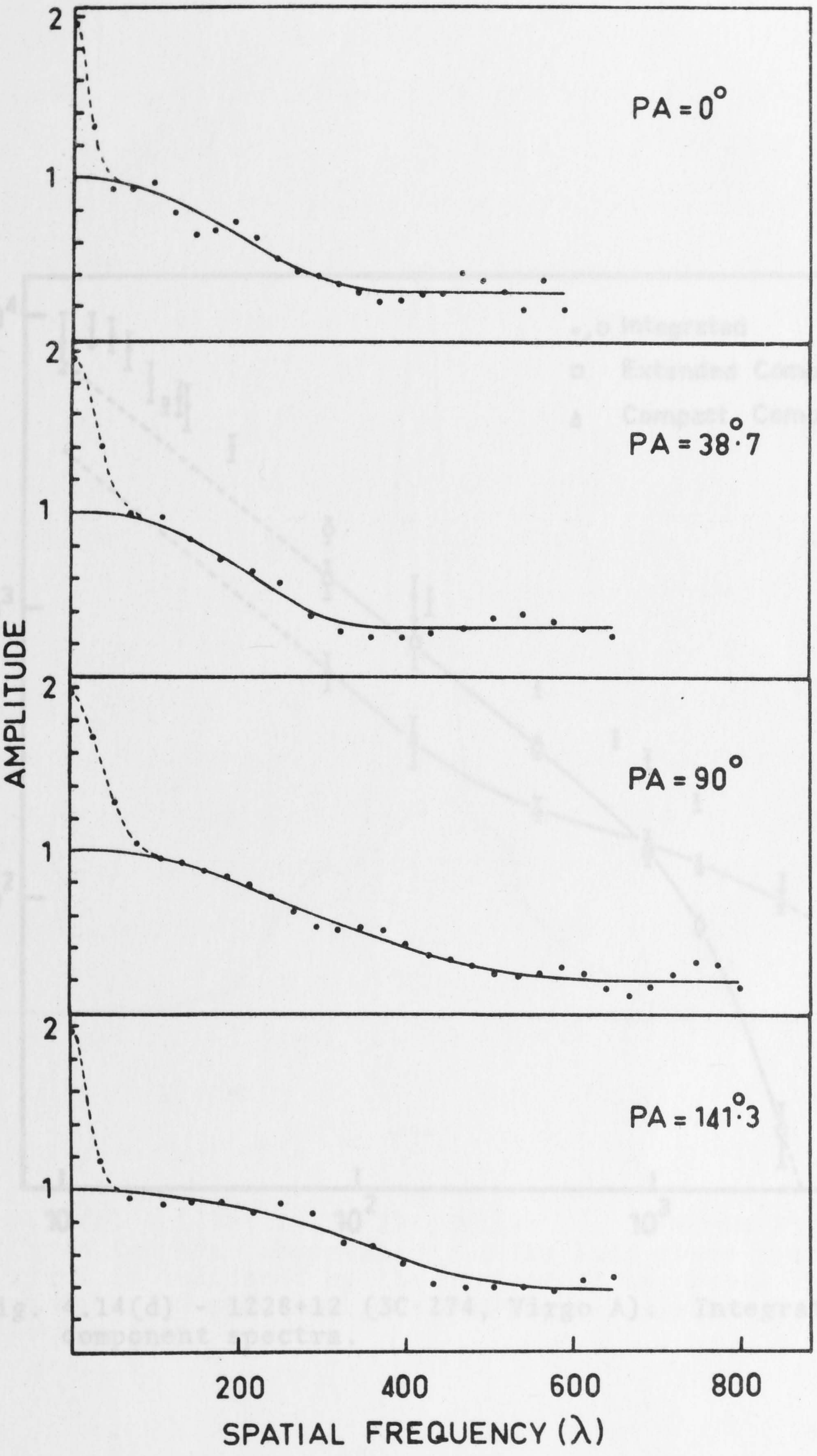

Fig. 4.14(c) - 1228+12 (3C 274, Virgo A). Spatial frequency measurements at 80 MHz in selected position angles.

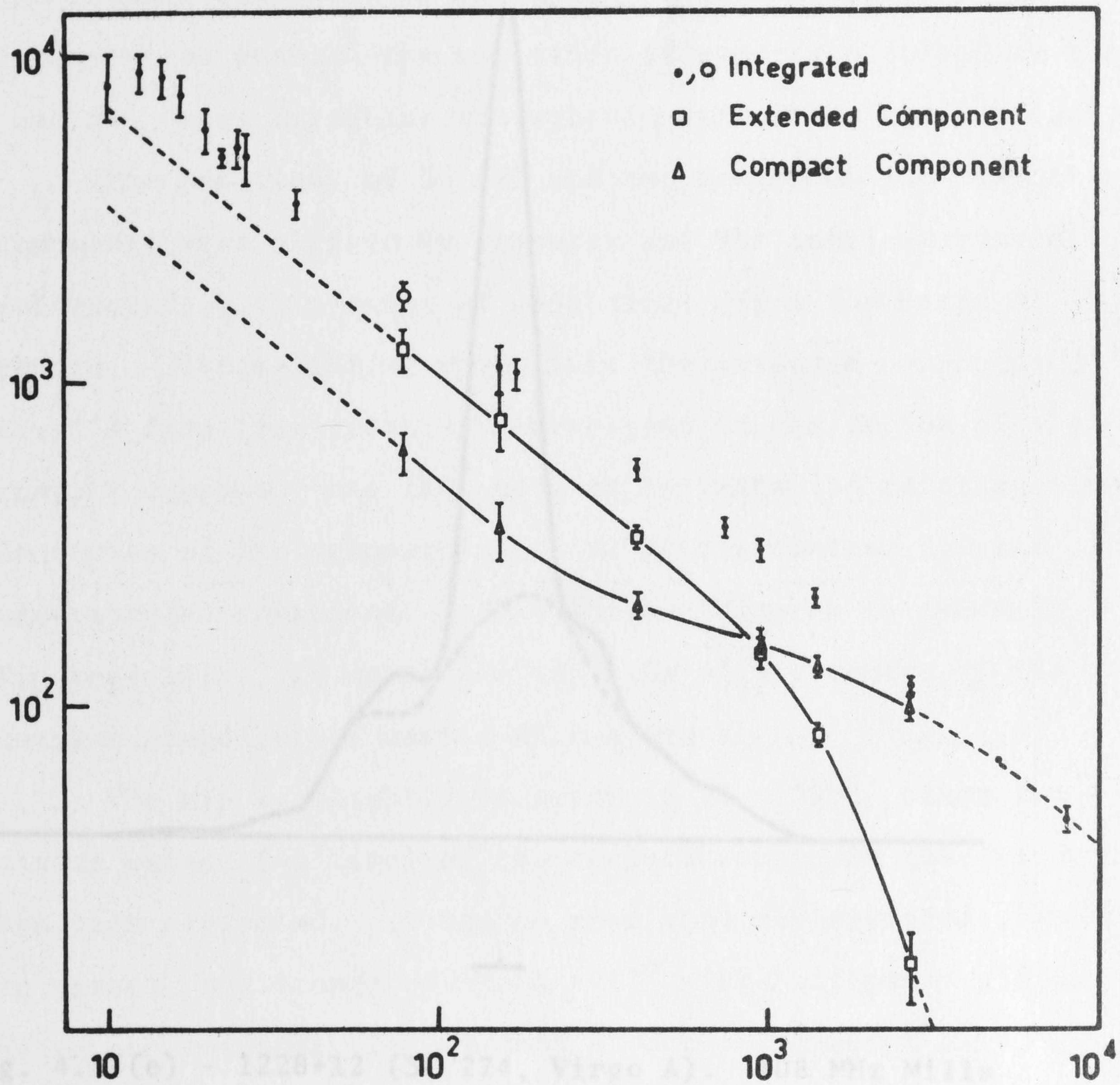

Fig. 4.14(d) - 1228+12 (3C 274, Virgo A). Integrated and component spectra.

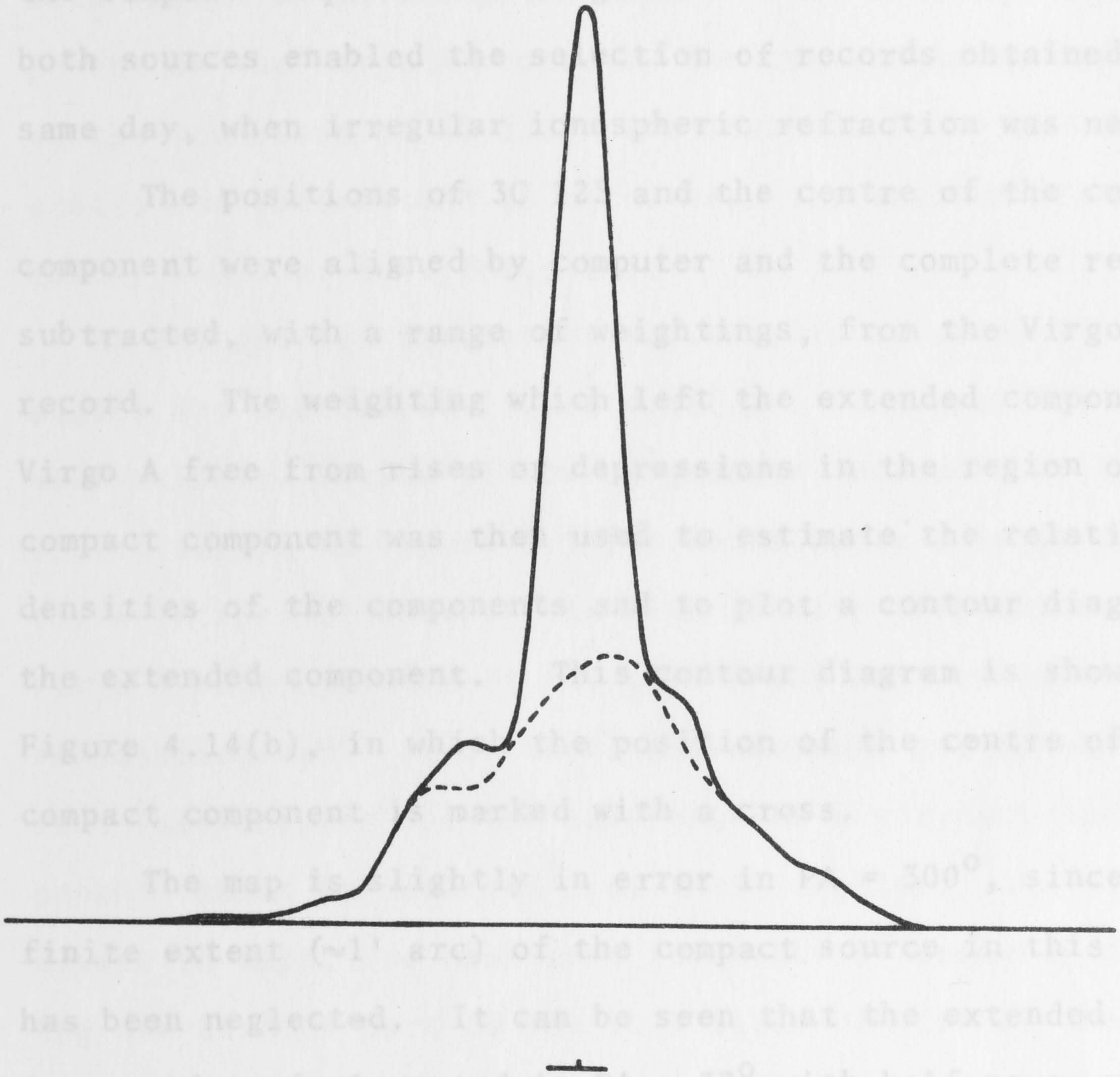

Fig. 4.14(e) - 1228+12 (3C 274, Virgo A). 408 MHz Mills Cross fan-beam observation. The half-power beam-width is indicated by the horizontal bar below the profile. Separation into components is shown by the broken line.

the true polar diagram, with a selected weighting, from the Virgo A record. A record of 3C 123 was selected for this purpose, since this source is relatively strong, of diameter 0'.25 arc (Fomalont, 1967) and has a northern declination, so that its sidelobe structure should resemble closely that of the compact component of Virgo A. Numerous observations of both sources enabled the selection of records obtained on the same day, when irregular ionospheric refraction was negligible.

The positions of 3C 123 and the centre of the compact component were aligned by computer and the complete record subtracted, with a range of weightings, from the Virgo A record. The weighting which left the extended component of Virgo A free from rises or depressions in the region of the compact component was then used to estimate the relative flux densities of the components and to plot a contour diagram of the extended component. This contour diagram is shown in Figure 4.14(b), in which the position of the centre of the compact component is marked with a cross.

The map is slightly in error in PA = 300^o, since the finite extent (~1' arc) of the compact source in this direction has been neglected. It can be seen that the extended component is curved, and elongated in PA = 37^o with half-power widths along and perpendicular to this direction of about 11'.5 and 6'.5 arc respectively. It is of note that the halo is extended almost orthogonally to the nucleus-jet axis of NGC 4486.

This analysis gave a flux density contribution of 64% for the extended component. To check this result an alternative method was used. For a source consisting of two superimposed components with significantly different diameters, a flux density estimate for each component is readily obtained from the amplitude-spatial frequency diagram, provided the larger component is fully resolved at the greatest spatial frequencies measured. In the present case, the spatial frequencies measured by the array, which are normally weighted during beam-shaping, were restored to their full values by dividing the amplitude of each Fourier component of the Virgo A record by the corresponding amplitude of the transform of 3C 123. The analysis is by no means exact, and errors tend to occur near the maximum spatial frequency and near zero frequency.

The spatial frequency measurements in several position angles are plotted in Figure 4.14(c). The presence of a very extended region of low brightness indicated by the broken curves in Figure 4.14(c) would imply a large discrepancy (by a factor ~2) between the flux density measurements of Virgo A made by Yates et al. (1968) and those made with the radioheliograph. Since these measurements are in close agreement (see Chapter 3), the existence of a very extended component cannot be inferred from these results: the sharp increase in amplitude near zero frequency is probably due to the use of only part of the full field of view of the radioheliograph in this analysis, with slightly different offset adjustments made for Virgo A and 3C 123.

In PA = $38^{\circ}.7$ the extended component is fully resolved, whereas the compact component, which is extended in PA = 300° is effectively unresolved. This plot gives an estimate of about 70% for the contribution from the extended component, in satisfactory agreement with the previous estimate of 64%. Combining the results, a value of 67% ± 5% has been adopted for the contribution from the extended component. With a total flux density at 80 MHz of 1850 f.u. the component flux densities are then 1240 f.u. and 610 f.u.

These results have been combined with measurements at higher frequencies in order to derive the spectrum of the individual components. The component spectra are shown in Figure 4.14(d), together with measurements of the integrated spectrum from 10 to 8000 MHz. A summary of the various component flux density measurements is presented in Table 4.5.

According to Shimmins et al. (1969), the extended component is not detected at 5009 MHz. At 2695 MHz, measurements of the compact component flux density by Hogg et al. (1969) give a flux density for the extended component of 16 f.u. if a value of 114 f.u. is adopted for the integrated flux density. If the 1420 MHz measurements of Biraud et al. (1960) are scaled up so that their sum agrees with the integrated flux density given by Fomalont (1967), it is found that all three sets of measurements near 1400 MHz are in close agreement. The values at 958 MHz were obtained from Maltby and Moffet (1962) who estimate a contribution of 48% ± 3% from the extended component.

The 408 MHz measurements are not in good agreement. Our values were obtained from a specially requested fan-beam observation made with the Mills Cross. The east-west fan beam of the Mills Cross has a half-power width of 1'.43 arc and a well-defined beam shape, allowing a precise separation of the two components. Analysis of this observation is shown in Figure 4.14(e), in which the separation into components is indicated by the broken line. Assuming Gaussian distributions for both the compact and extended components, this observation gives east-west half-power widths of 0'.41 and 6'.5 arc respectively. The east-west half-power width of the compact component at 4995 MHz is about 0'.87 arc but

TABLE 4.5

FLUX DENSITIES* OF THE COMPONENTS OF VIRGO A

Frequency (MHz)	Integrated Flux Density	Compact Component Flux Density	Extended Component Flux Density	Reference
80	1850 ± 180	610 ± 90	1240 ± 190	Present measurement
158	1100 ± 180	350 ± 70	750 ± 150	Allen et al. (1962)
408	550 ± 55	350 ± 35	200 ± 20	MKN
408	527 ± 37	203 ± 20	324 ± 24	Present measurement (Mills Cross)
958	300 ± 21	156 ± 15	144 ± 15	Maltby and Moffet (1962)
1400	214 ± 11			Kellermann et al. (1969)
1407		130		MKN
1420	186	112	74	Biraud et al. (1960)
1425	213	133	80	Fomalont (1967)
2695	110 ± 6			Horton et al. (1969)
"		98		Hogg et al. (1969)
"	118.3 ± 5.6			Kellermann et al. (1969)
4995	65 ± 5			Horton et al. (1969)
5000	72.1 ± 3			Kellermann et al. (1969)
5009	67.6 ± 1.2		No halo (scans)	Shimmins et al. (1969)
8000	44.7 ± 5			Dent and Haddock (1966)

---

* In units of 10^{-26} Wm^{-2} (Hz)$^{-1}$

the brightness distribution is more or less rectangular, which will not broaden the 1'.43 arc beam by as much as a Gaussian distribution. The east-west dimensions of both components at 408 MHz are therefore similar to those found at other frequencies. The discrepancy between the present results and those of MKN is probably due to the use in the latter case of spacings too small to fully resolve the extended component. The component dimensions given by MKN are too large, which strengthens this argument.

Finally, we have obtained approximate values for the component flux densities at 158 MHz from the rather limited measurements of Allen et al. (1962). Here, fringe amplitudes at 300λ and 2200λ have been analysed with the aid of the east-west visibility function at 1425 MHz (Fomalont, 1967), by assuming that the dimensions of the compact and extended components are the same at both frequencies. The 300λ fringe amplitude at 158 MHz is 0.45 (Lequeux, 1962) which when compared with Fomalont's data gives a contribution from the central component of 26%. At 2200λ the fringe amplitude at 158 MHz is 0.1, giving a central component contribution of 35%. A mean value of 31% has been adopted.

Figure 4.14(d) shows that the spectra of both components are well defined between 80 and 5000 MHz. The extended component has a pronounced "break" in the spectrum near 1300 MHz, where the spectral index changes from about 0.82 at low frequencies to a value of 2.5 to 2.9 at high frequencies. The compact component spectrum is even more complex, with a flattening around 3000 MHz and a further steepening again near 250 MHz.

The physical conditions within the extended component were discussed by Lequeux (1962). Although the spectrum derived by Lequeux is in reasonable agreement with that shown in Figure 4.14(d) the more recent measurements contain no evidence of a change in the dimensions of the extended component with frequency as was found by Lequeux.

The present analysis strongly suggests that an evolutionary model such as that proposed by Kellermann (1966) is applicable. The model assumes that the radio spectrum is initially rather flat with $\alpha \sim 0.25$ and that gradual steepening occurs from a combination of synchrotron radiation losses and repeated particle injection. The extended component is presumably much older than the central regions and has reached a stage of evolution where the low frequency spectrum has been steepened to near the expected value of $\alpha = 0.75$ (Kellermann, 1966). The cut-off in the spectrum at high frequencies implies that either particle injection has ceased altogether and that synchrotron radiation losses alone are influencing the spectrum or that we are observing the extended component between periods of particle injection. Its large dimensions would favour the former idea unless the source of relativistic particles lies within the radio region itself rather than in NGC 4486.

The spectrum of the compact component may be interpreted in terms of two (or more) regions with very different spectra. One region has a spectrum which, at least at low frequencies, closely resembles that of the extended component. The other region appears to have a cut-off in the spectrum towards low frequencies with a turnover near 1400 MHz.

Perhaps the latter region is to be associated with the regions of small angular size detected by long baseline interferometry (Donaldson, Miley et al., 1969; Cohen, Moffet et al., 1969), and by aperture synthesis (Hogg et al., 1969)

However, the flux density of these regions is only 5% or so of the total flux density of the compact component so that the model proposed above is clearly oversimplified. Nevertheless it is clear that both the structure and spectrum of the compact component is complex, with evidence of repeated activity in the galaxy. On the other hand, the extended component has a spectrum and structure indicating that it is at an advanced stage of evolution and is now evolving independently of any recent activity in NGC 4486.

1559+02 (3C 327)

The east-west model given by Fomalont (1967) consists of two components separated by 3'.51 arc. The diameter of the eastern component is 1'.2 arc and the western component diameter is 2'.2 arc. The flux density ratio of the eastern to the western component is 2.5:1.

Observations have been made at both 80 MHz and 5000 MHz (W); these maps are shown in Figures 4.15(a) and (b) respectively. The 5000 MHz map shows that the source is elongated in PA = 96^{o}. Although the 80 MHz beam is somewhat elliptical, the beamwidth in the east-west direction is slightly less than at 5000 MHz. Comparison of the two maps shows that relative to the eastern component the western component is much less intense at 80 MHz than at 5000 MHz. The western component must therefore have a flatter spectrum than the eastern component although its rather small contribution to the total flux density does not lead to any marked change in the spectral index of the whole source (Fig. 4.15(c)).

1648+05 (3C 348, Hercules A)

Interferometer observations at 960 MHz (Maltby and

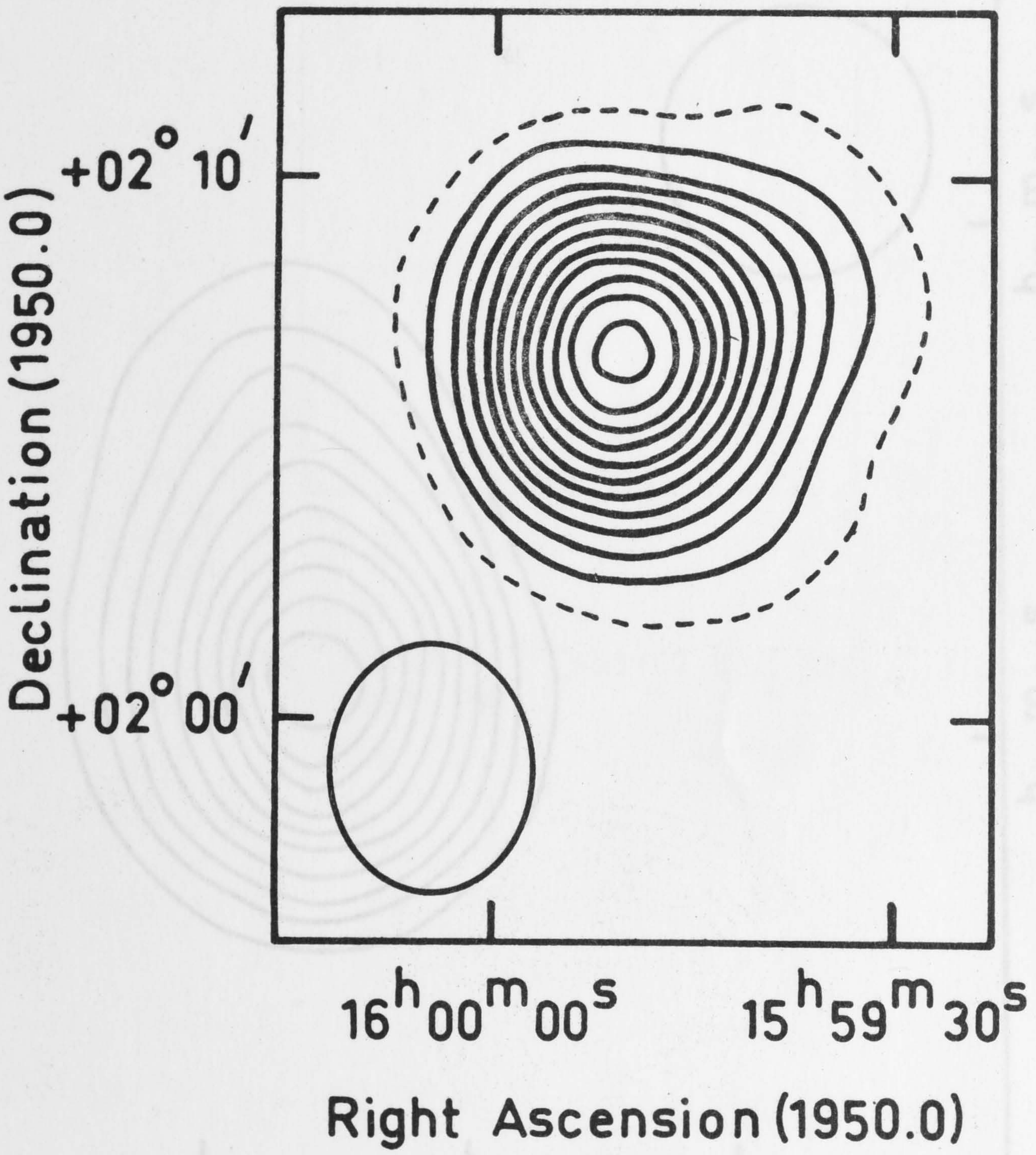

Fig. 4.15(a) - 1559+02 (3C 327).

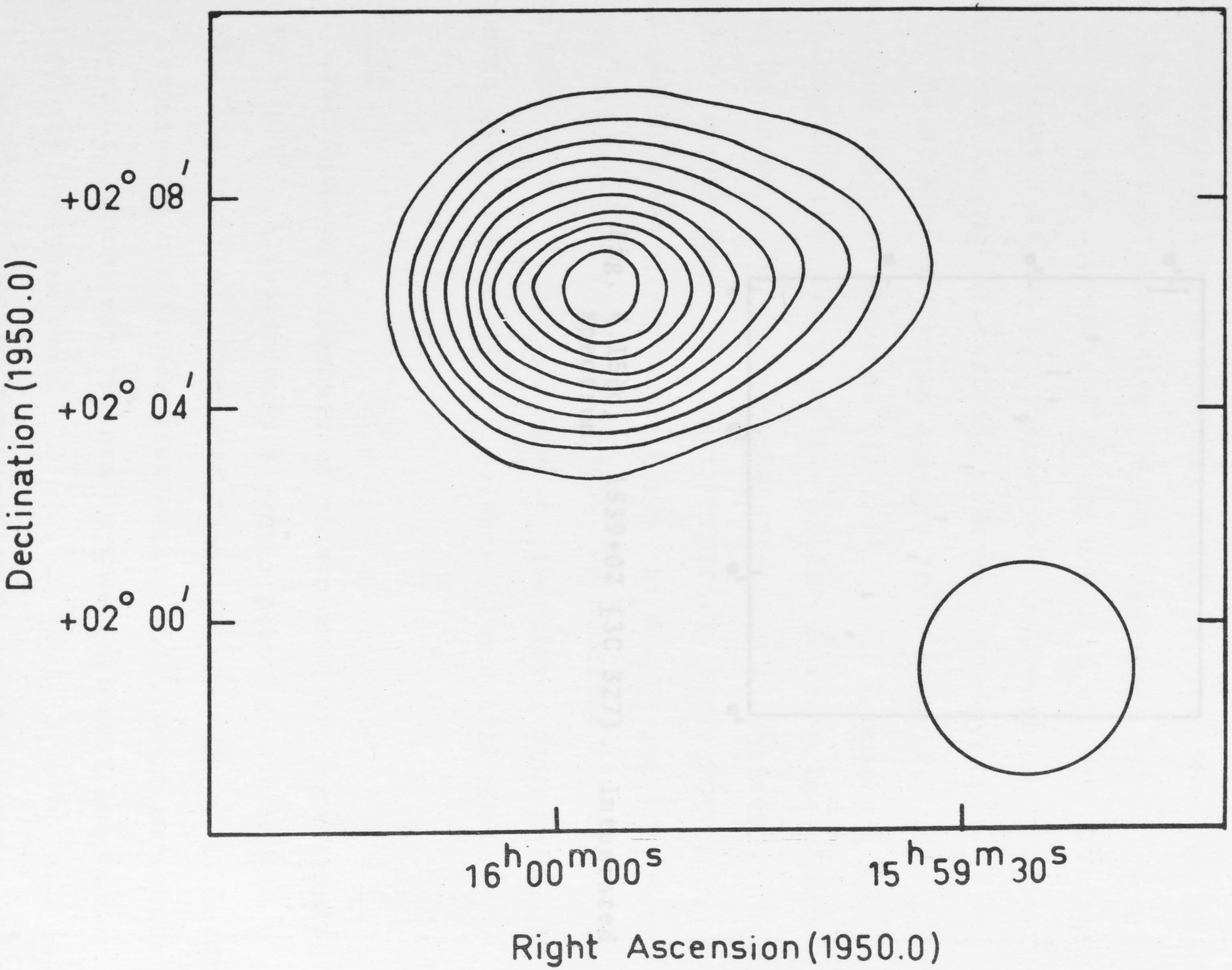

Fig. 4.15(b) - 1559+02 (3C 327). 5000 MHz map.

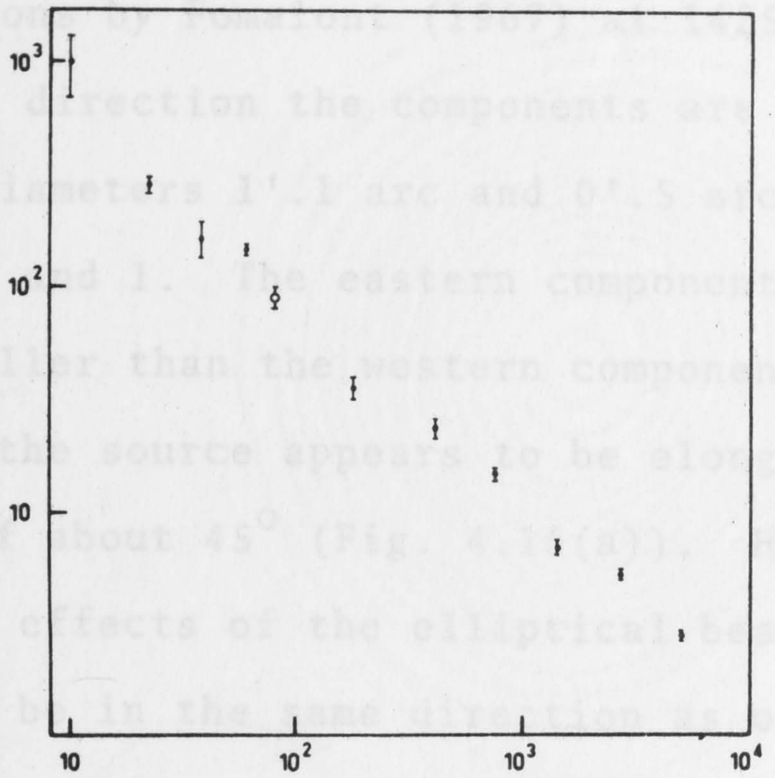

Fig. 4.15(c) - 1559+02 (3C 327). Integrated spectrum.

Moffet, 1962) showed that Hercules A consists of two components with relative intensities 1.4 ± 0.1 and 1, equal diameters of 0'.75 ± 0'.20 arc and a separation of 1'.95 ± 0'.10 arc along a major axis is PA = 100°.5 ± 1°.5. More recent observations by Fomalont (1967) at 1425 MHz show that in the east-west direction the components are separated by 1'.84 arc with diameters 1'.1 arc and 0'.5 arc and relative intensities 1.46 and 1. The eastern component is more intense and is smaller than the western component.

At 80 MHz the source appears to be elongated in a position angle of about 45° (Fig. 4.16(a)). However, by allowing for the effects of the elliptical beam the elongation is found to be in the same direction as observed at higher frequencies. The model brightness distribution at 960 and 1425 MHz reproduce closely the 80 MHz map if corrections are made in the latter case for sidelobe structure near the main beam. It seems probable, therefore, that both components have similar spectra between 80 and 1425 MHz.

2058-28

The intense components of this source lie approximately in PA = 175°. Although only a single peak is observed at 80 MHz (Fig. 4.17(a)) there are clear indications of at least two components in this position angle. Additional structure of lower brightness may be seen to the south-west and to the east of the southern peak.

The interferometer observations do not allow a detailed comparison with the structure at 80 MHz. At 1425 MHz the east-west model of Fomalont (1967) consists of two components, separated by 1'.08 arc with a flux density ratio of about 1.4:1. The eastern component is more intense than the western

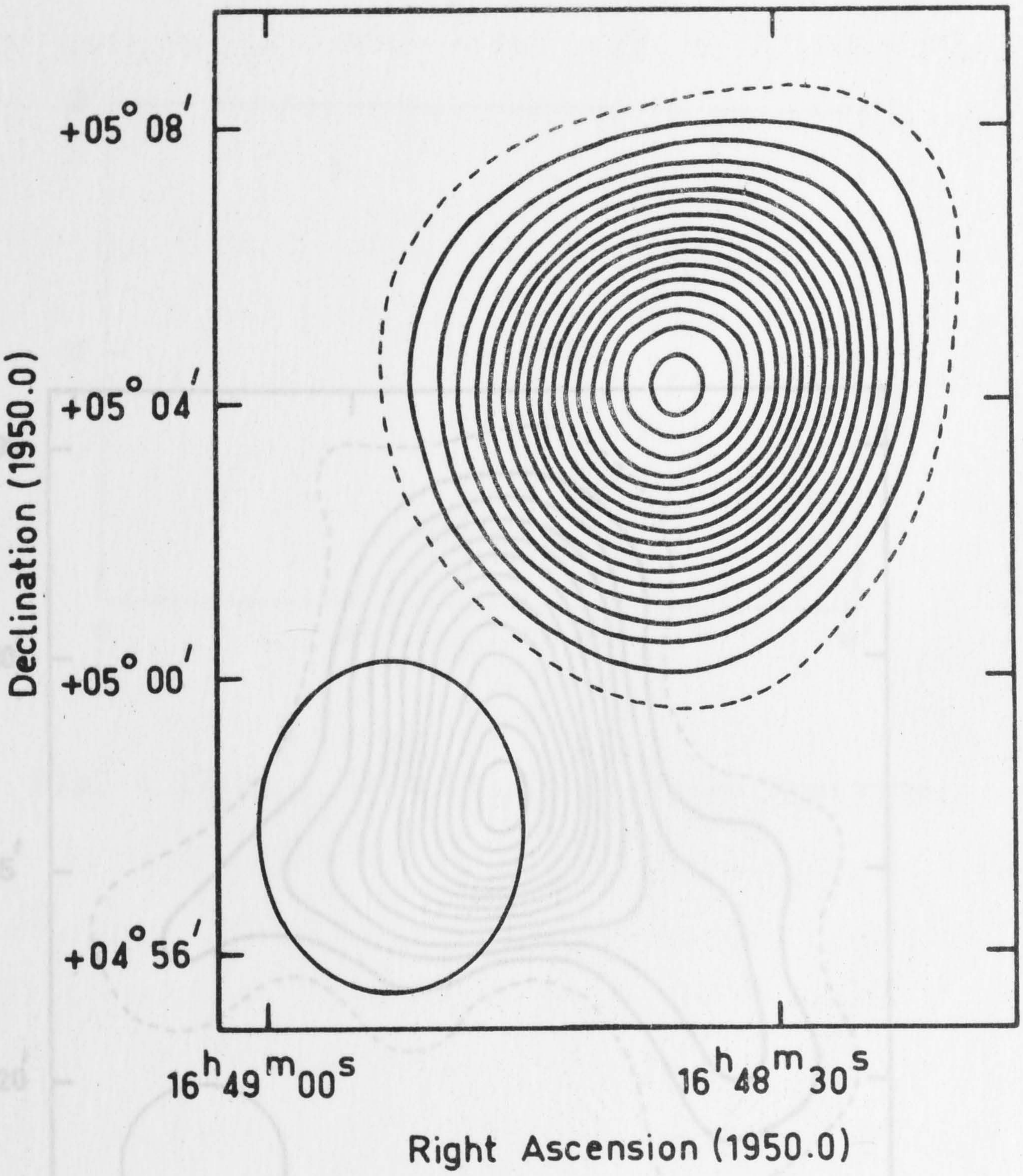

Fig. 4.16(a) - 1648+05 (3C 348, Hercules A).

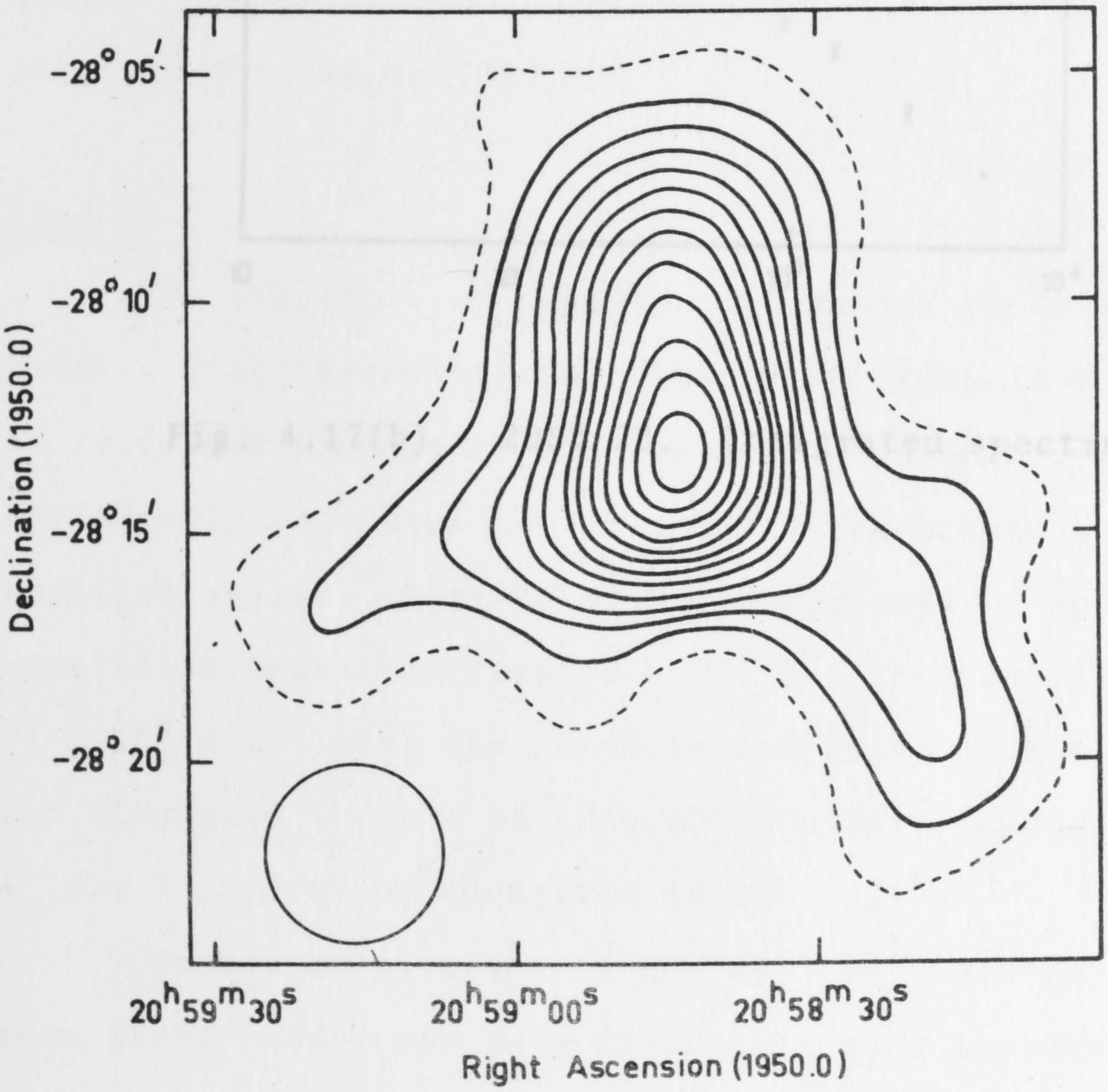

Fig. 4.17(a) - 2058-28.

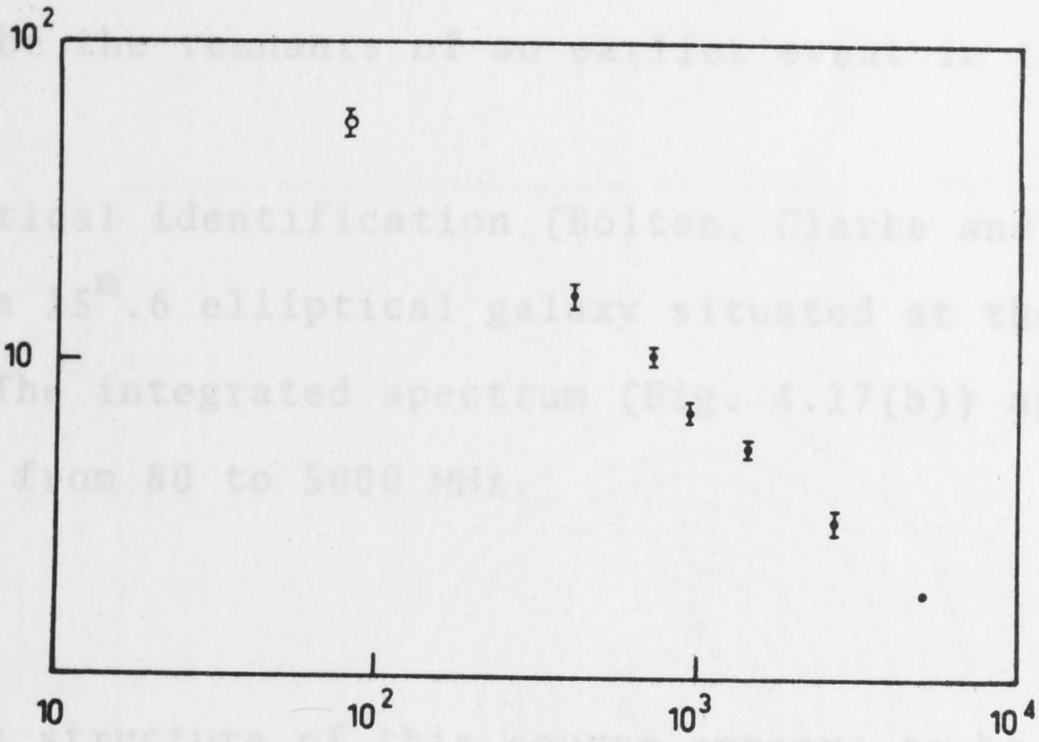

Fig. 4.17(b) - 2058-28. Integrated spectrum.

component. This structure is consistent with that found in the present observations except that the extensions to the south-west and to the east observed at 80 MHz are apparently not detected at 1425 MHz. These regions may have steep spectra and may be the remnants of an earlier event in the parent galaxy.

Optical identification (Bolton, Clarke and Ekers, 1965) is with a $15^{m}.6$ elliptical galaxy situated at the radio centroid. The integrated spectrum (Fig. 4.17(b)) appears to be straight from 80 to 5000 MHz.

2104-25

The structure of this source appears to be rather unusual. Interferometer observations by Ekers (1969) show that at least two components are present. His model, which does not closely reproduce the visibility measurements in some position angles, consists of two components of approximately equal flux density separated by 3'.3 ± 0'.3 arc in PA = $16^{o} \pm 10^{o}$ with the northern component 1'.1 x 1'.8 arc and elongated in PA = 35^{o} and the southern component 6'.0 x 1'.9 arc and elongated in PA = 135^{o}.

Comparison with the 80 MHz map (Fig. 4.18(a)) suggests that Ekers' model may be a reasonably good assessment of the true structure. Although components are not resolved at 80 MHz, the map shows an intense, curved ridge running to the south-east of the peak and also a weak extension to the north. The model requires slight alteration to be consistent with the present observations. The southern component must be arc-like in shape and probably very elongated, while the northern component must have a weak extension to the north. The visibility function in PA = 90^{o} obtained by Ekers suggests that

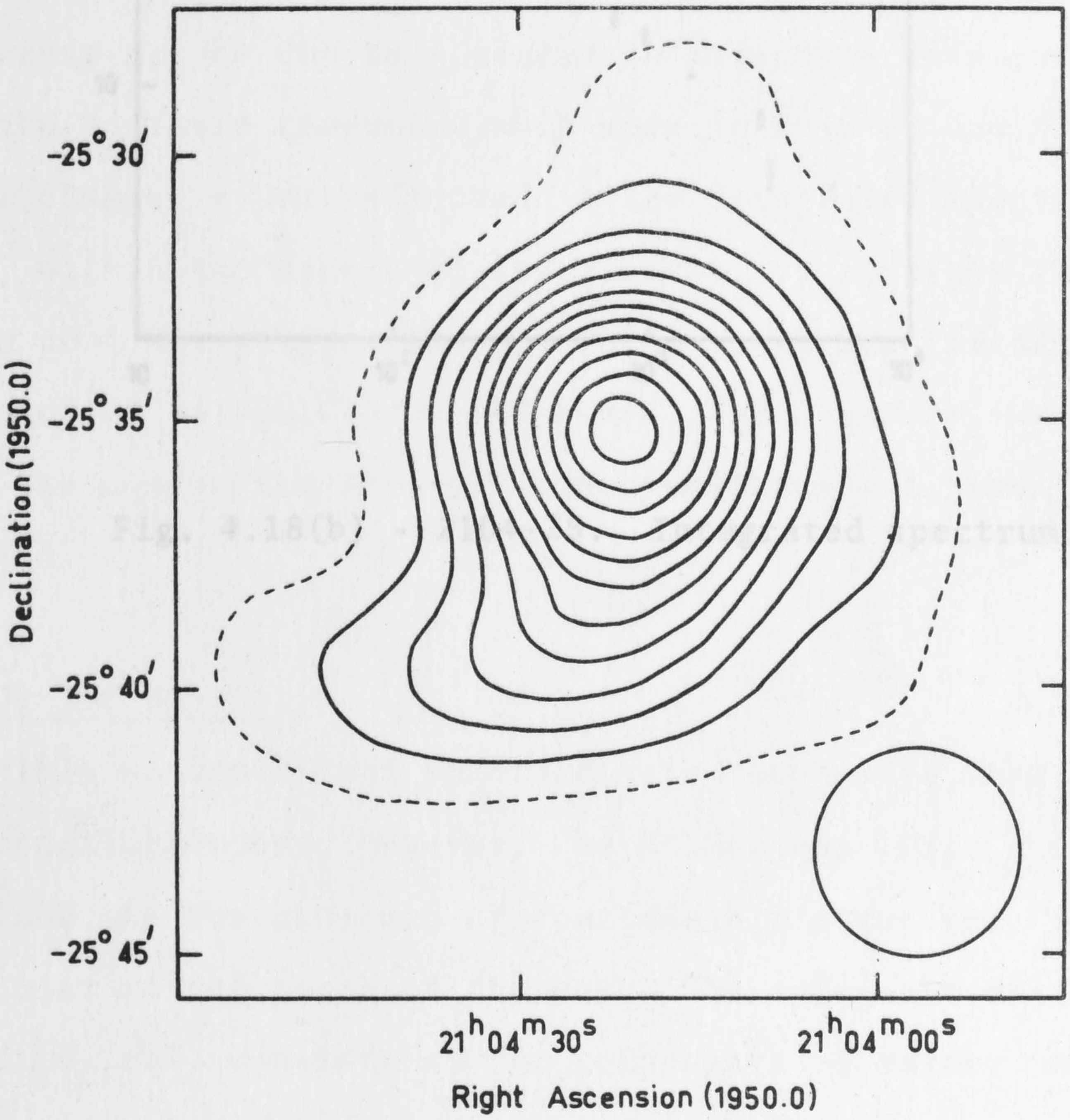

Fig. 4.18(a) - 2104-25.

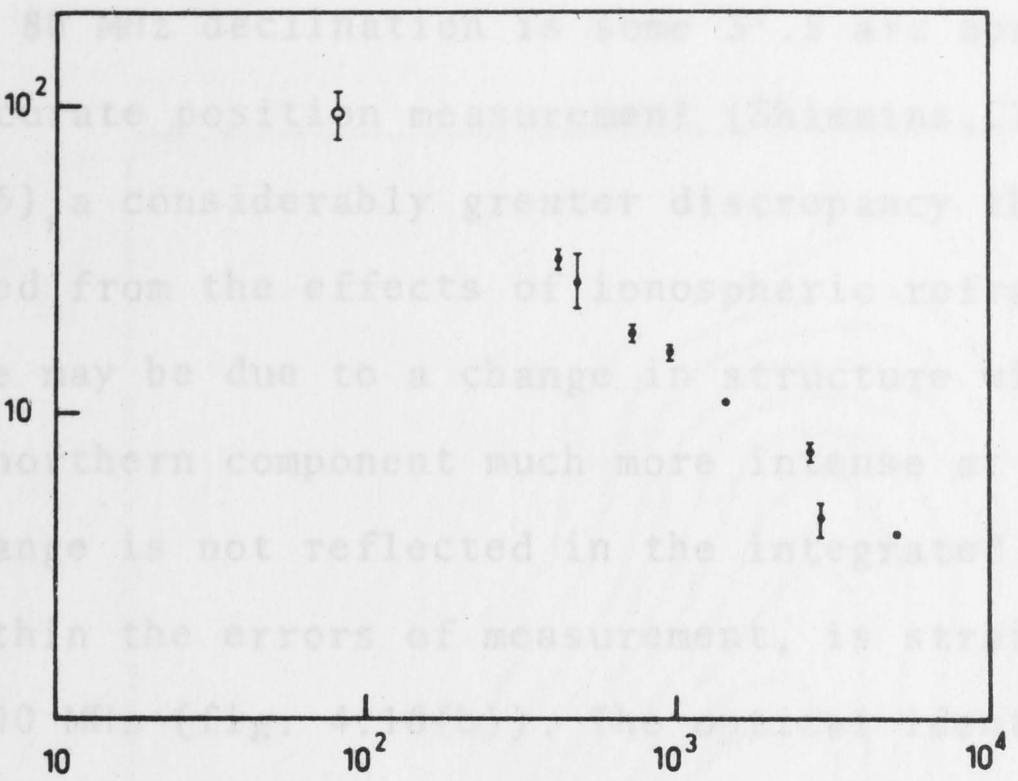

Fig. 4.18(b) - 2104-25. Integrated spectrum.

the arc-like component has a number of sub-components.

The 80 MHz declination is some 3'.5 arc north of the Parkes accurate position measurement (Shimmins,Clarke and Ekers,1966), a considerably greater discrepancy than is to be anticipated from the effects of ionospheric refraction.The difference may be due to a change in structure with frequency, with the northern component much more intense at low frequencies. Such a change is not reflected in the integrated spectrum, which, within the errors of measurement, is straight from 80 MHz to 5000 MHz (fig. 4.18(b)). The optical identification suggested by Bolton,Clarke and Ekers (1965) may be incorrect, since the components straddle other brighter and peculiar galaxies.

2221-02 (3C 445)

This source is not resolved into components despite its large angular extent. However, the 80 MHz map (Fig. 4.19(a)) does indicate the presence of considerable structure, in particular to the south of the peak. The east-west distribution (Fomalont,1967) consists of two components of rather uncertain angular size separated by 1'.01 arc with the eastern component more intense than the western component.

Figure 4.19(a) shows that the two-dimensional brightness distribution is more complex than this model. If only two components are present, each must be quite extended. It is likely that the source consists of more than two components. Some of the structure observed at 80 MHz may be regions with steep spectra. The integrated spectrum (Fig. 4.19(b)) shows

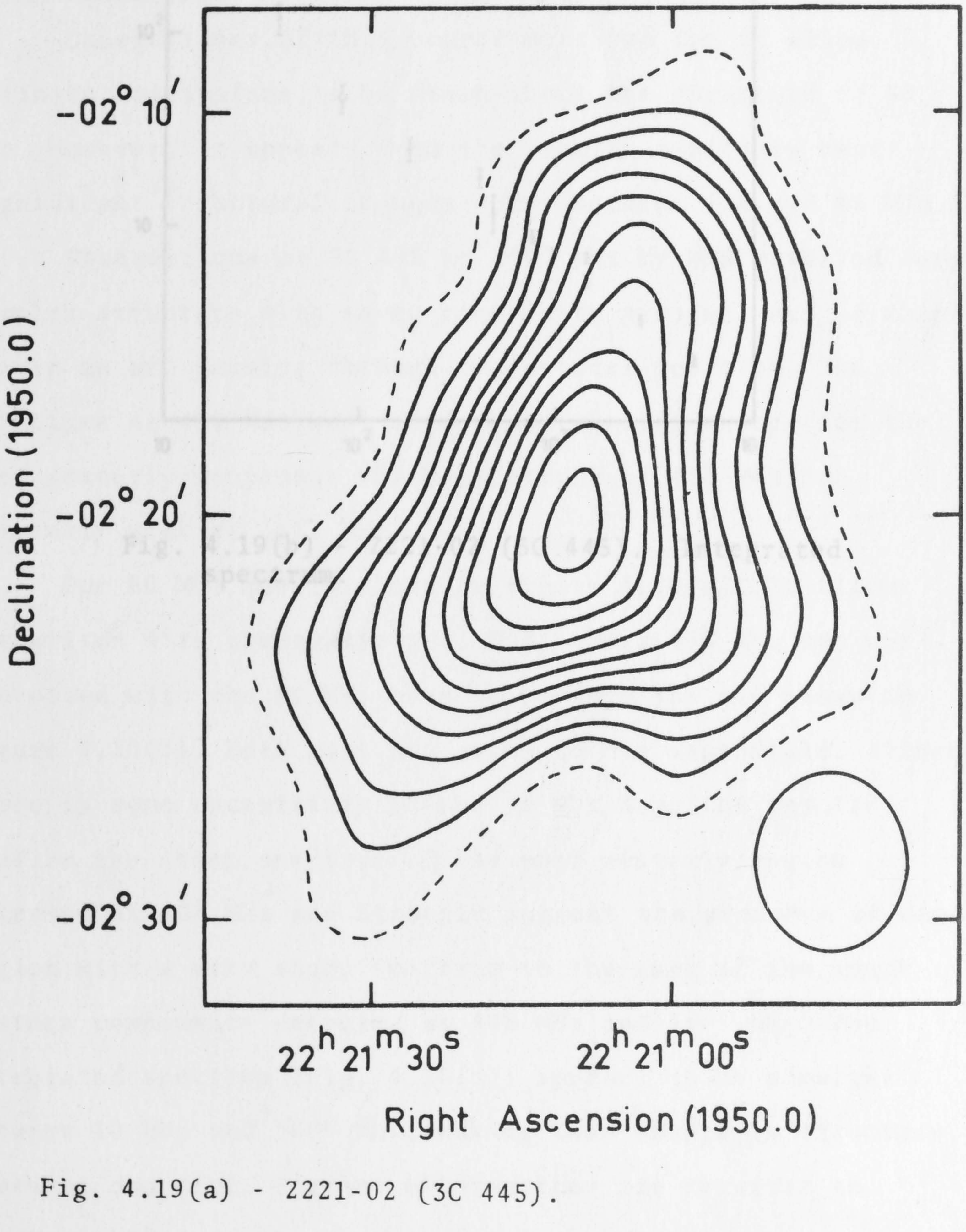

Fig. 4.19(a) - 2221-02 (3C 445).

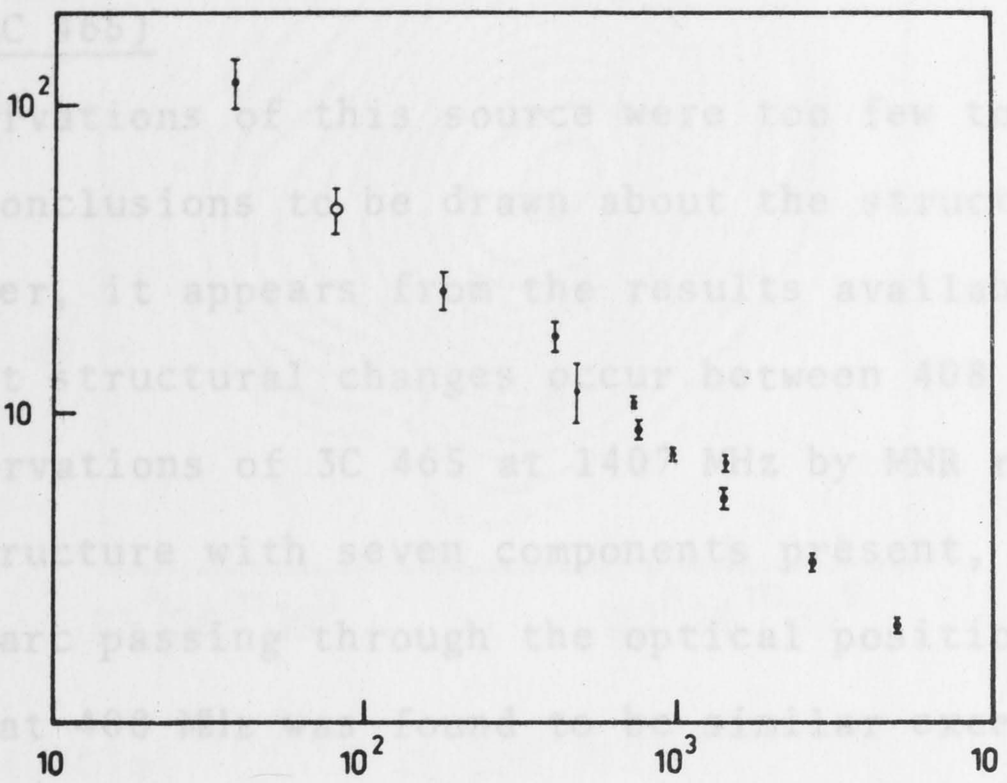

Fig. 4.19(b) - 2221-02 (3C 445). Integrated spectrum.

some scatter but appears to be straight from 38 MHz to 5000 MHz.

2335+26 (3C 465)

Observations of this source were too few to allow definite conclusions to be drawn about the structure at 80 MHz. However, it appears from the results available that significant structural changes occur between 408 and 80 MHz.

Observations of 3C 465 at 1407 MHz by MNR revealed very complex structure with seven components present, six of which lie in an arc passing through the optical position. The structure at 408 MHz was found to be similar except for the most westerly component which is strong at 408 MHz but extremely weak at 1407 MHz.

Our 80 MHz map is shown in Figure 4.20(a). To allow comparison with observations of MNR, their 408 MHz map was convolved with the 80 MHz beam to produce the map shown in Figure 4.20(b). Both maps are drawn to the same scale. Although there is some uncertainty in the 80 MHz map, the results confirm the steep spectrum of the most westerly region detected at 408 MHz and strongly suggest the presence of another region with a very steep spectrum to the east of the south-eastern components detected at 408 MHz and 1407 MHz. The integrated spectrum (Fig. 4.20(c)) appears to be straight between 10 MHz and 5000 MHz, making this change in structure somewhat doubtful. Further observations are required to confirm this result.

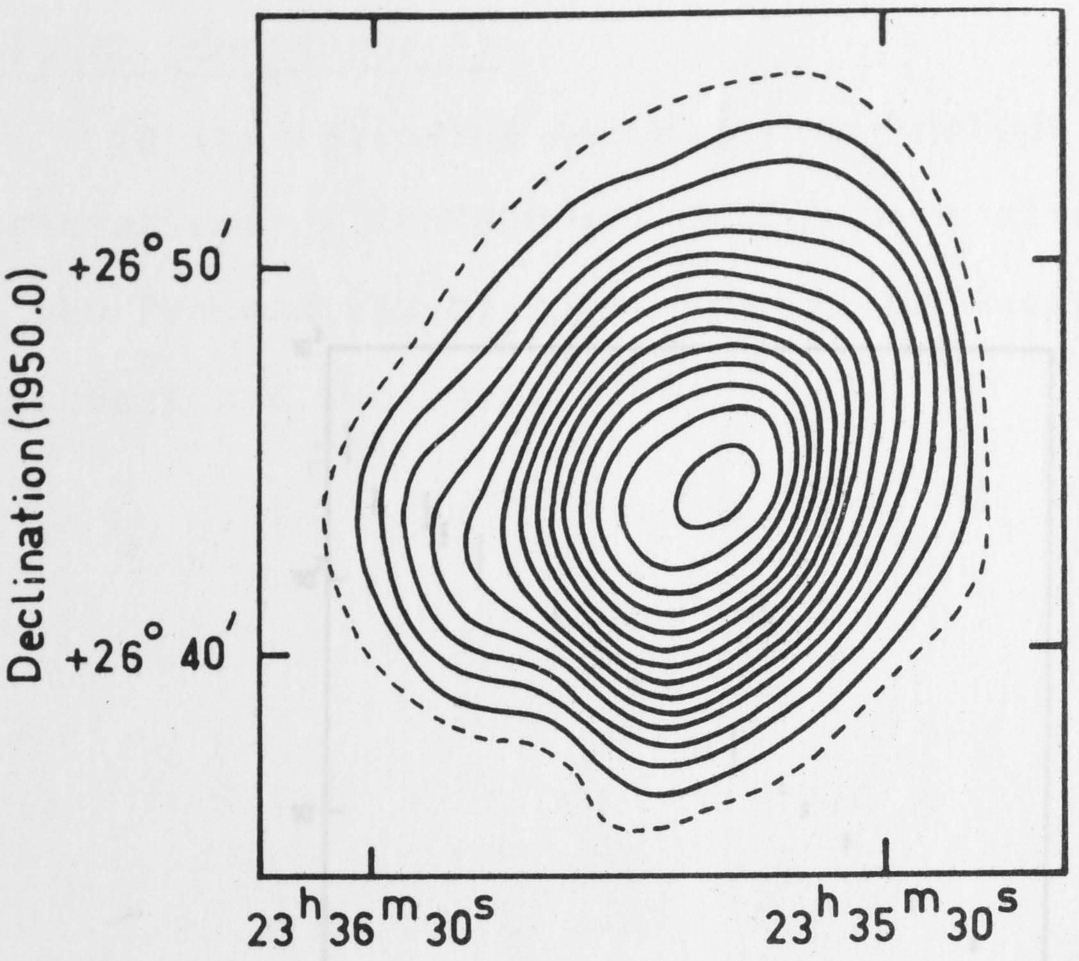

Fig. 4.20(a) - 2335+26 (3C 465).

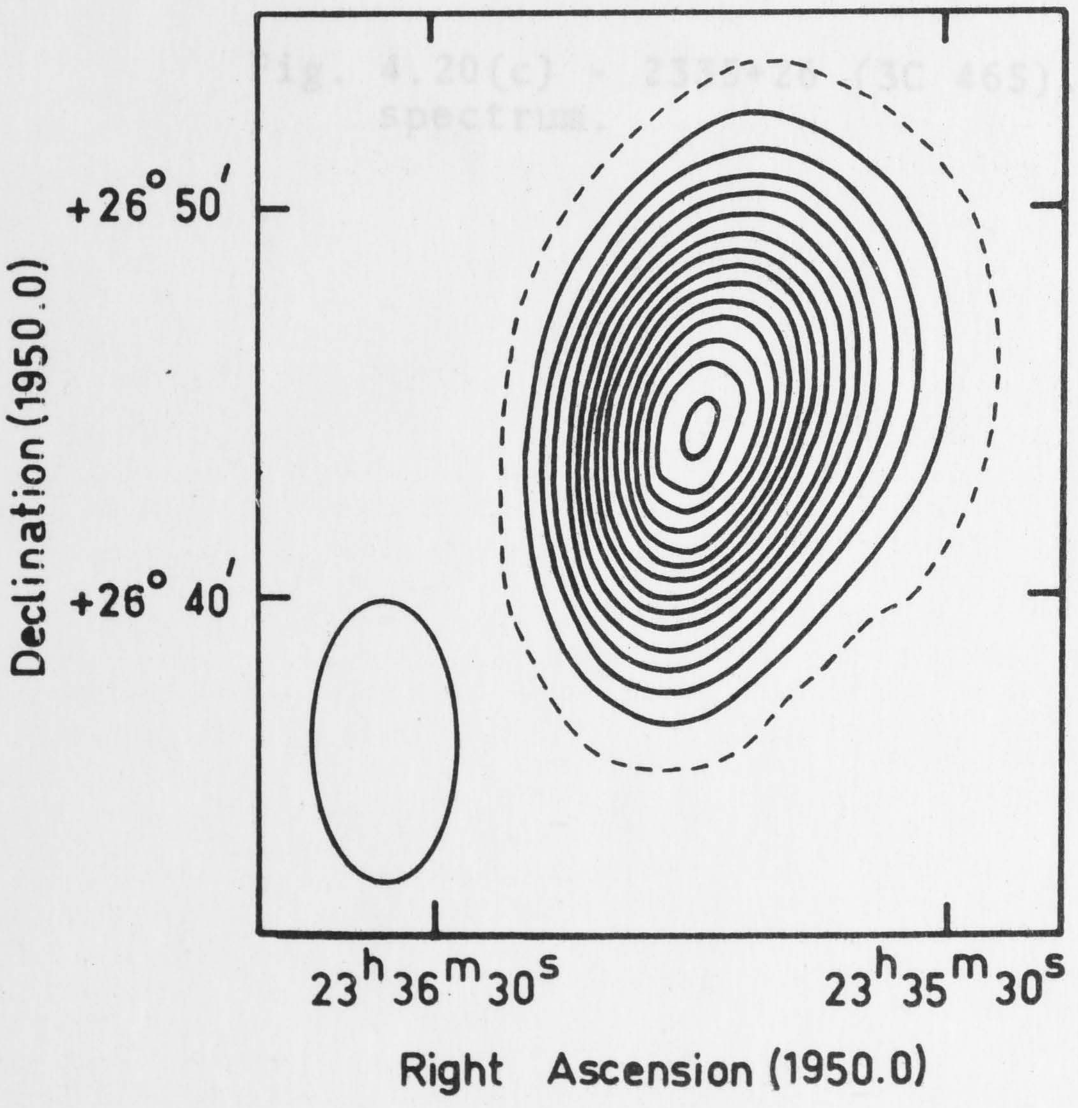

Fig. 4.20(b) - 2335+26 (3C 465). 408 MHz map (MNR) smoothed to 80 MHz beamwidth.

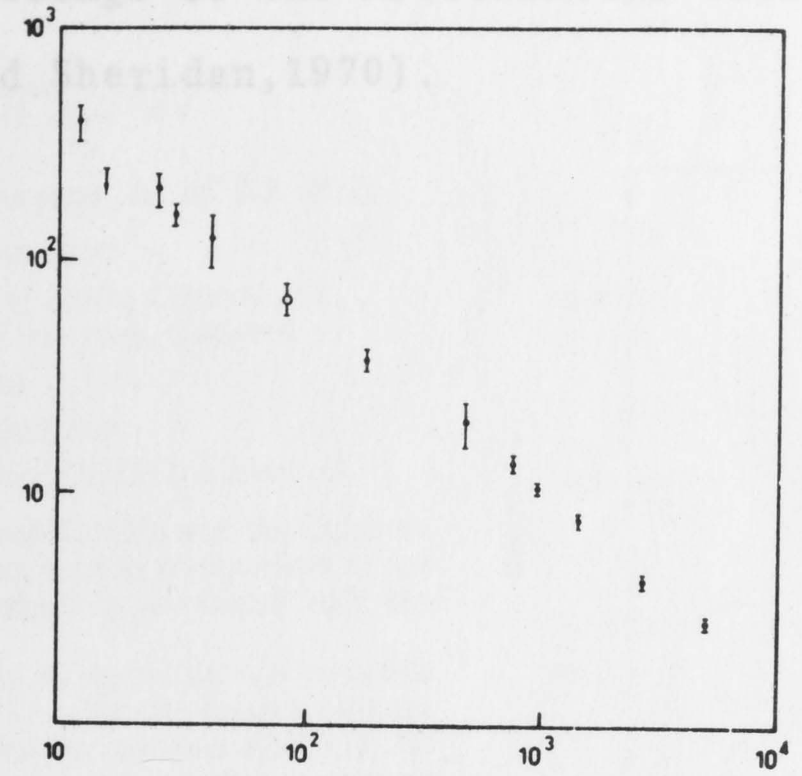

Fig. 4.20(c) - 2335+26 (3C 465). Integrated spectrum.

1322-42 (Centaurus A)

In the following two pages we include the results of observations of Centaurus A which have already been published in the Proceedings of the Astronomical Society of Australia (Lockhart and Sheridan,1970).

Reprinted from
Proceedings of the Astronomical Society of Australia
Volume 1, *Number* 7, *pages* 344-345, *April* 1970

Observations of Centaurus A at 80 MHz

I. A. LOCKHART
Mount Stromlo and Siding Spring Observatories,
Australian National University, Canberra

AND

K. V. SHERIDAN
Division of Radiophysics, CSIRO, Sydney

We present observations made at 80 MHz with the Culgoora radioheliograph of the compact central components of the radio source Centaurus A, which is associated with the peculiar galaxy NGC 5128.

The radioheliograph records, in digital form, a complete image of a 2° × 2° field in 1 s.[1] For the present purpose the field was centred on the published position of NGC 5128[2] and maps were obtained by integrating 900 successive images. Eight such maps were produced at various times during 1969. Each differs slightly owing to the effects of ionospheric refraction and that given in Figure 1 was selected for reasons given below. From these data the following quantities were derived:

Intensity ratio (NE component/SW component)	1.47 ± 0.03
Component separation	7′.10 ± 0′.10
Position angle	43°.9 ± 0°.4
Right ascension	$13^h\ 22^m\ 30^s.0$ (1950 epoch)
Declination	—42° 43′ 48″.2 (1950 epoch)
Integrated flux density	1680 ± 180 f.u.

(The right ascension and declination refer to the midpoint of the intensity maxima of the two components.)

The first three quantities, which agree closely with those derived at 408 MHz by Cameron,[3] are accurate to within a few per cent. The contour map of Figure 1 was selected from the set of observations because it appeared to be undisturbed by the ionosphere and had parameters very close to the averaged values given above.

At 80 MHz one of the most severe limitations imposed by the ionosphere is upon the determination of absolute positions to an accuracy comparable with those derived at higher frequencies. In addition to random refraction effects, which are typically ≲1′ arc with time scales of from minutes to hours, there appears to be a constant component of ionospheric refraction (not eliminated by the recording procedure) which displaces objects towards the zenith and becomes more severe with increasing zenith angle. Observations were restricted to near the meridian to minimize refraction in right ascension. We find that our position differs in right ascension by $1^s.6$ from the optical centre of NGC 5128[2] and by $0^s.3$ from the radio source centre derived by Labrum, Krishnan, Payten and Harding[4] at 21 cm; however there is a discrepancy of $3^s.8$ between our value and that quoted by Cooper, Price and Cole[2] at 5000 MHz,[2] and $5^s.5$ from that of Cameron[3] at 408 MHz, and of Little, Cudaback and Bracewell[5] at 3300 MHz. In declination we have merely included a scale with zero corresponding to the centre of the source, as our average position falls approximately 1′ arc north of positions derived from 5000 MHz and 408 MHz observations mentioned above.

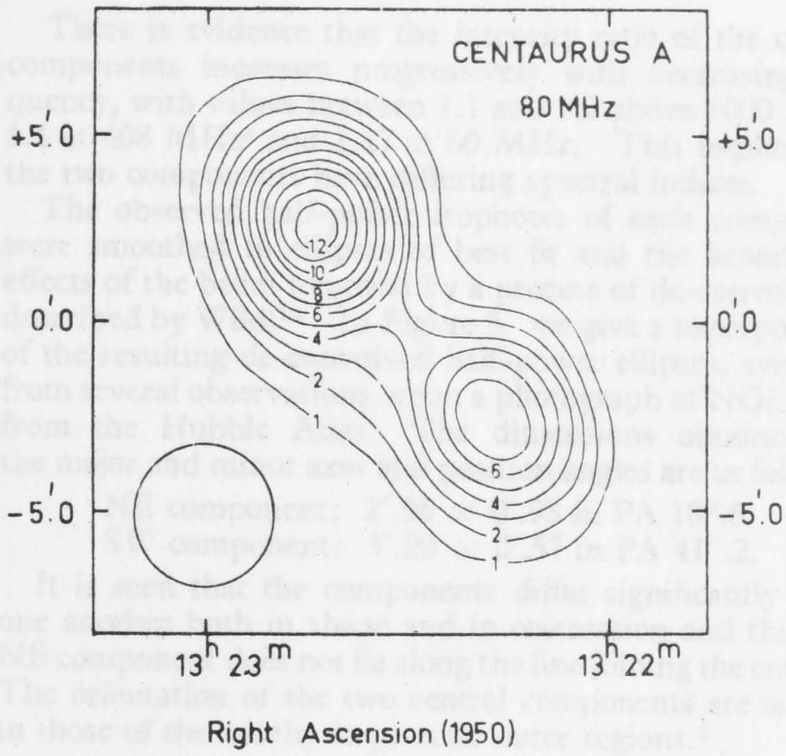

Figure 1. Isophotes of brightness temperature for the central component of Centaurus A. The first contour and the contour interval are ≃2.2 × 10^5 °K. The map is on equiangular coordinates with north at the top. The aerial half-power beamwidth is 3′.75.

To obtain the absolute value of flux density given above for the combined central components, the radioheliograph intensities were calibrated using four standard sources observed with the 210-ft telescope at Parkes by Yates, Wielebinski and Landecker[6] and Landecker (private communication) at 85.5 and 150 MHz in which they performed detailed experiments to determine an accurate temperature scale. Our value of flux density has been included in Figure 2, which is a logarithmic plot of flux density vs frequency of published observations. It is in close agreement with the 85 MHz flux density for the unresolved central component obtained by multiplying the flux density estimated by Sheridan,[7] by 0.82, the scaling factor suggested by Kellermann[8] to harmonize the flux density scale of the 85 MHz survey of Mills, Slee and Hill[9, 10] with the currently accepted flux scale for northern sources. This agreement suggests that at frequencies at least as low as 80 MHz the spectral index of the combined central components is more probably 0.64 compared with the value of 0.6 suggested by Cooper, Price and Cole.[2] However, the 19.7 MHz flux density for the central components derived by Shain[11] if correct, implies a considerable flattening in the spectrum below 80 MHz. This may be explained by the mechanism which has been discussed by Kellermann,[8] whereby, in the early life of certain sources, the rate of injection of energetic particles has not reached equilibrium with the radiation losses. In such a case the spectral slope is expected to flatten towards the low frequency end, but as the source ages and equilibrium is reached, the spectral curvature disappears. The

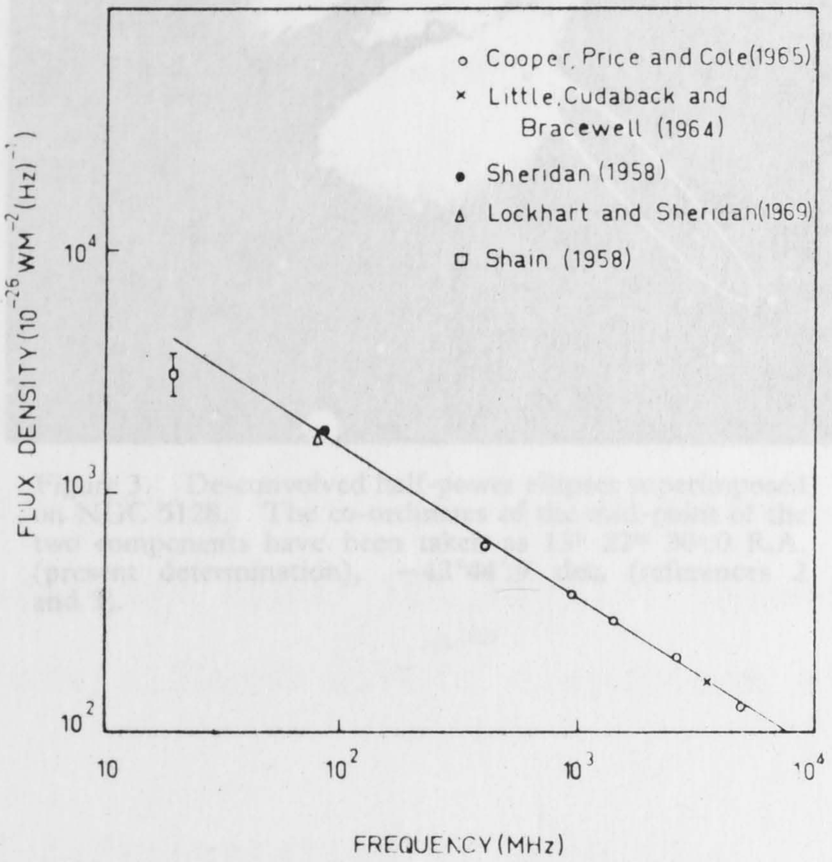

Figure 2. The spectrum of the total flux of the central components of Centaurus A.

extended component of Centaurus A exhibits a relatively straight spectrum from 1410 MHz to 19.7 MHz,[2] so that the central components may be at this early stage of development, whereas the outer parts have reached equilibrium.

There is evidence that the intensity ratio of the central components increases progressively with decreasing frequency, with values between 1.1 and 1.2 above 1000 MHz, 1.4 at 408 MHz[3] and 1.47 at 80 MHz. This implies that the two components have differing spectral indices.

The observed half-power isophotes of each component were smoothed to ellipses of best fit and the broadening effects of the beam removed by a process of de-convolution described by Wild.[12] In Figure 3 we give a superposition of the resulting de-convolved half-power ellipses, averaged from several observations, upon a photograph of NGC 5128 from the Hubble Atlas. The dimensions obtained for the major and minor axes and position angles are as follows:

NE component: 2′.56 × 0′.93 in PA 18°.6
SW component: 3′.20 × 0′.57 in PA 41°.2.

It is seen that the components differ significantly from one another both in shape and in orientation and that the NE component does not lie along the line joining the centres. The orientation of the two central components are similar to those of the nearby large-scale outer regions.[2]

---

[1] Wild, J. P., '*The Culgoora Radioheliograph*', *Proc. IREE Aust.*, **28** (1967).
[2] Cooper, B. F. C., Price, R. M. and Cole, D. J., *Aust. J. Phys.*, **18**, 589 (1965).
[3] Cameron, M. J., *Proc. ASA*, **1**, 229 (1969).
[4] Labrum, N. R., Krishnan, T., Payten, W. J. and Harting, E., *Aust. J. Phys.*, **17**, 323 (1964).
[5] Little, A. G., Cudaback, D. D. and Bracewell, R. N., *Proc. Nat. Acad. Sci.*, **52**, 690 (1964).
[6] Yates, K. W., Wielebinski, R. and Landecker, T. L., *Aust. J. Phys.*, **20**, 595 (1967).
[7] Sheridan, K. V., *Aust. J. Phys.*, **11**, 400 (1958).
[8] Kellermann, K. I., *Astrophys. J.*, **140**, 969 (1964).
[9] Mills, B. Y., Slee, O. B. and Hill, E. R., *Aust. J. Phys.*, **11**, 360 (1958).
[10] Mills, B. Y., Slee, O. B. and Hill, E. R., *Aust. J. Phys.*, **13**, 676 (1960).
[11] Shain, C. A., *Aust. J. Phys.*, **11**, 517 (1958).
[12] Wild, J. P., *Aust. J. Phys.*, **23**, in press, 1970.

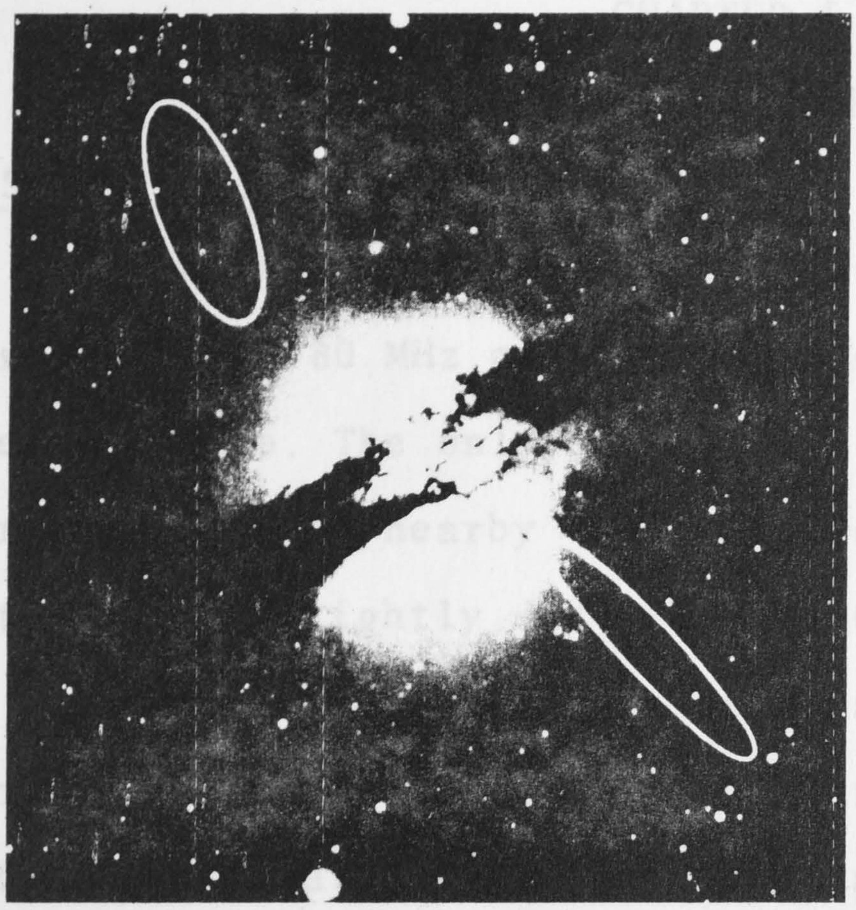

Figure 3. De-convolved half-power ellipses superimposed on NGC 5128. The co-ordinates of the mid-point of the two components have been taken as 13h 22m 30s.0 R.A. (present determination), −42°44′.9 dec. (references 2 and 3).

Simmons Limited, Glebe, Sydney.

CHAPTER 5

GALACTIC SOURCES

5.1 Introduction

In this chapter we give results for 6 galactic radio sources. An 80 MHz contour map and flux density is given for each source. The only source felt to be affected by grating responses from nearby strong sources is 1905+07, which appears to be very slightly disturbed by Cygnus A grating lobes.

Comparison has again been made with higher frequency observations of comparable angular resolution. References to these observations are given in Table 5.1 together with the operating frequencies and beamwidths or range of aerial spacings used. The similar beamwidths at 80,408 and 5000 MHz have allowed direct comparison of maps in some cases.

5.2 Presentation of Results.

5.2.1 Contour diagrams

Contour diagrams are presented in the same format as those in Chapter 4. All details given under the above subheading in Chapter 4 are applicable to the sources discussed below with the exception of the estimate of the error introduced by noise. For galactic sources the enhanced background noise introduces errors in the zero-level determination and in the contours themselves of between one-half and one contour level.

5.2.2 Source list

The sources observed are listed in Table 5.2, whose sucessive columns give:

(1) The source number in the Parkes nomenclature.

(2) The source number in the revised 3C catalogue or

TABLE 5.1

Frequency (MHz)	Instrument	Beamwidth or range of aerial spacings	Ref. No.
408	Sydney University Mills Cross	Elliptical 2'.86 x 2'.86 sec z arc	1
"	"	"	2
1425	Caltec variable baseline interferometer(EW)	Baselines 144λ-2626λ	3
5000	Parkes 210 ft paraboloid	4'.0 arc	4
"	"	"	5
"	"	"	6
"	"	"	7

References for Table 5.1

1. Shaver, P.A., and Goss, W.M., (1970), Aust. J. Phys. Astrophys. Suppl. No 14, (Paper II)
2. Kestevan, M.J.L., (1968), Aust. J. Phys. 21, 739
3. Fomalont, E.B., (1968), Astrophys. J. Suppl. Ser., 15, 203
4. Milne, D.K.,(1969),Aust. J. Phys., 22,613
5. Milne, D.K., (1971a), Aust. J. Phys. In press
6. Milne, D.K., (1971b), Astrophys. Letters. In press
7. Whiteoak, J.B., and Gardner, F.F., private communication

TABLE 5.2

SOURCE LIST

(1) Parkes Number	(2) 3C or other name	(3) S_{80}*	±p.e.	(4) Peak T_B $(10^{4\,\circ}K)$	±p.e.	(5) Contour Interval $(10^{3\,\circ}K)$	(6) Error in RA (sec)	(7) Error in Dec('arc)	(8) α whole source
0821-42	Puppis A	533	33	6.4	0.7	5.82	0.0	2.2	0.54
1711-38	CTB 37	235	23	10	1	10.00	-5.2	1.1	
1727-21	358,Kepler's N	118	12	29	4	22.30	-0.7	1.2	0.68
1757-23	W28	780	120	9.6	1	8.00	-3.0	-0.7	0.37
1853+05	392,W44	720	70	9.4	1	7.83			0.46
1905+07	397	61	6	10	2	8.33	1.4	-0.8	

* In units of $10^{-26}\,Wm^{-2}\,(Hz)^{-1}$

any alternative source name.

(3) The measured 80 MHz flux density with probable error.

(4) The peak brightness temperature at 80 MHz.

(5) The contour interval used in plotting the contour diagram.

(6) The estimated error in the measured right ascension.

(7) The estimated error in the measured declination.

(8) The approximate spectral index α for the whole source, where α is defined in the sense $S \propto \nu^{-\alpha}$. No value is given for sources with non-linear spectra.

5.2.3 Spectral index diagrams

The format used for the extragalactic sources has been adopted for the galactic sources. For each source, measurements at different frequencies by various authors are summarized in either Milne and Hill(1969), Milne(1969), Milne(1971a,b) or in Holden and Caswell(1969).

5.3 Results

0821-42 (Puppis A)

Observations with the Parkes 210 ft telescope at 2650 MHz (Milne and Hill,1969) and at 2700 and 5000 MHz (Milne, 1971a) show Puppis A to have an annular structure with the most intense emission originating along the eastern boundary. The 80 MHz map (Fig.5.1(a)) is generally very similar to the 5000 MHz map obtained by Milne although some regions are clearly different at the two frequencies.

The beamwidths at 80 MHz and 5000 MHz are 3'.75 and 4'.0 arc respectively, allowing direct comparison of the structure observed at these frequencies. To reveal changes in structure we have computed the temperature spectral index,β, at various points across the source, where β is defined by

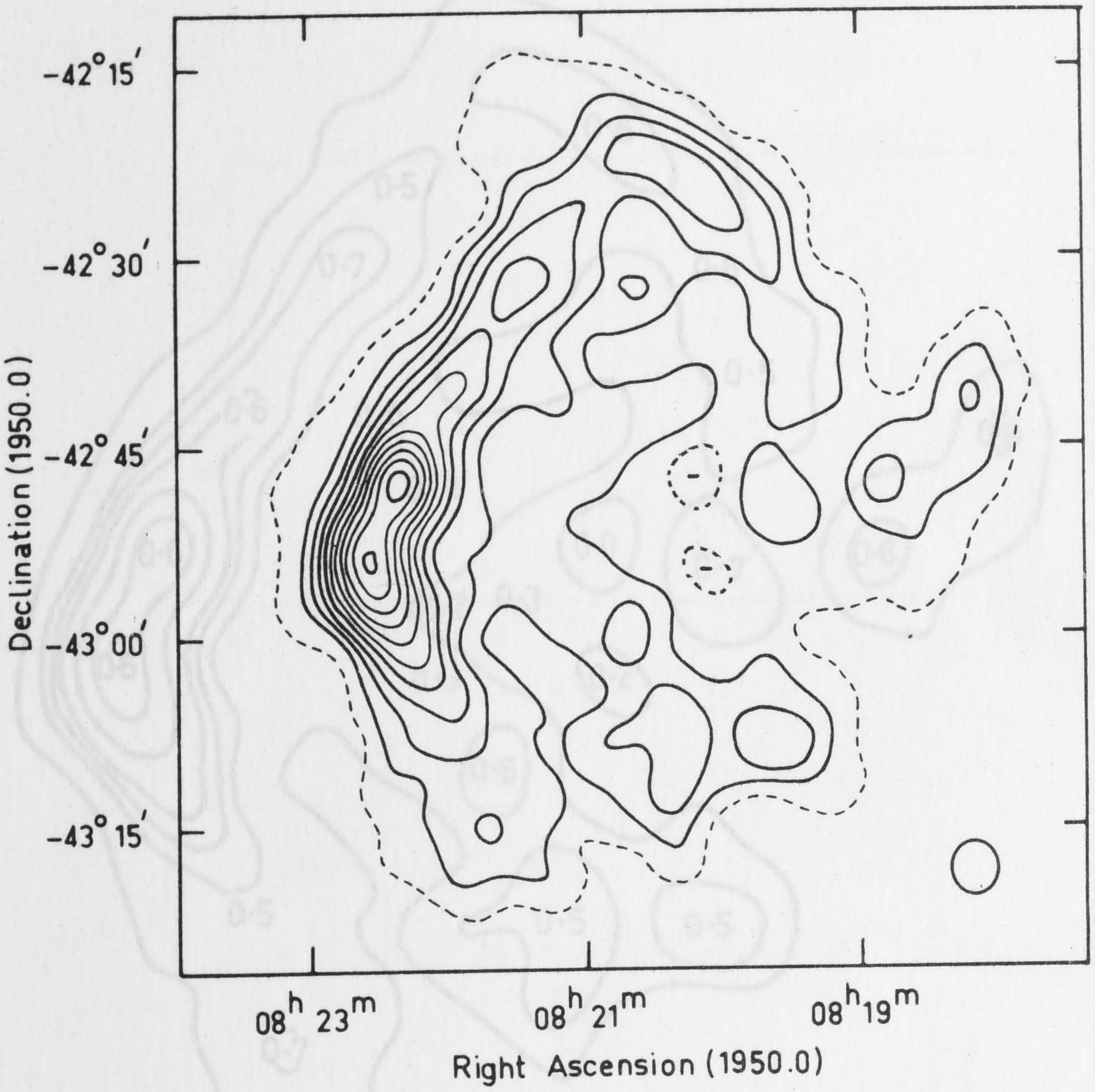

Fig. 5.1(a) - 0821-42 (Puppis A).

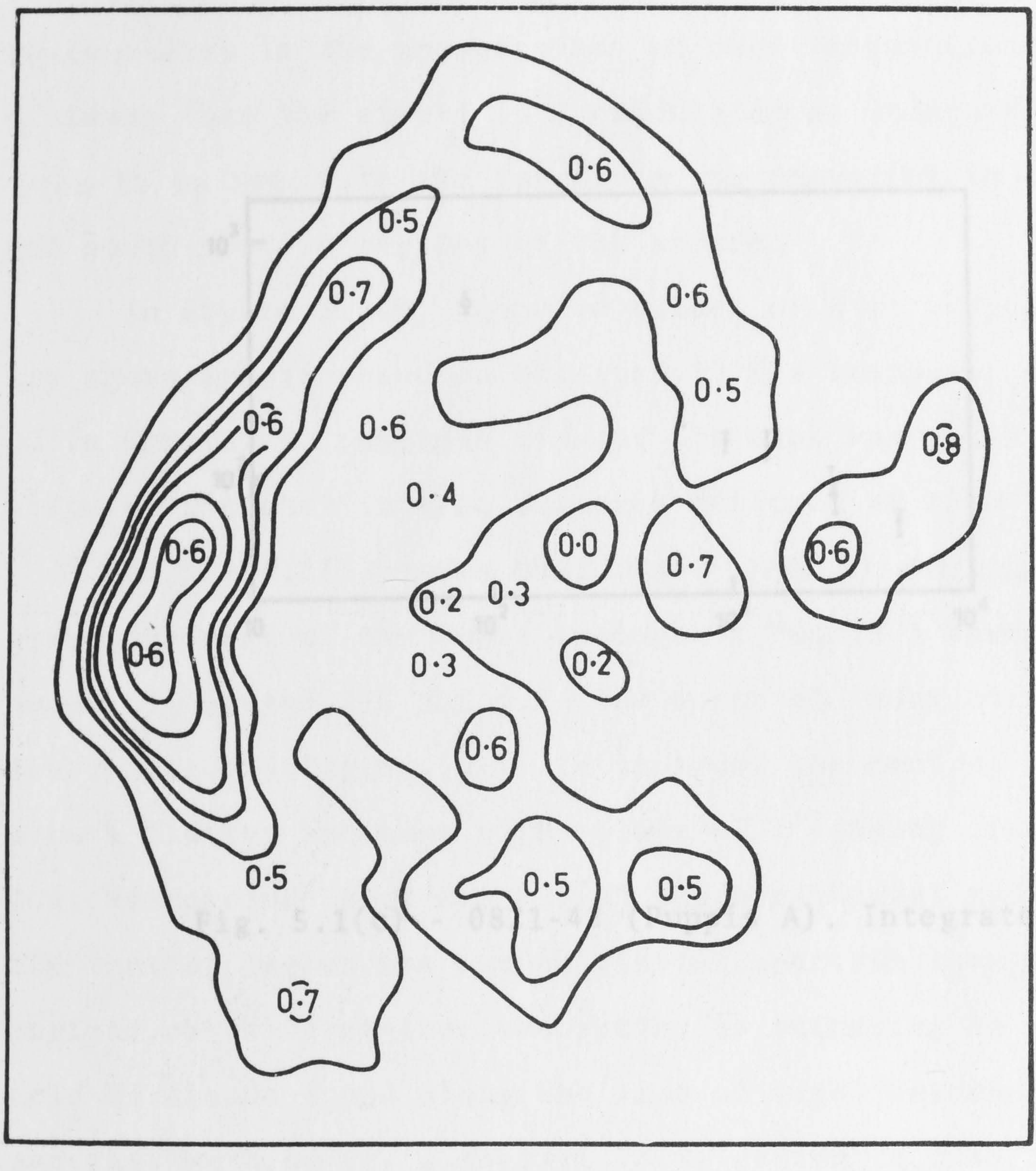

Fig. 5.1(b) - 0821-42 (Puppis A). Values of β, the temperature spectral index, at various points across the source.

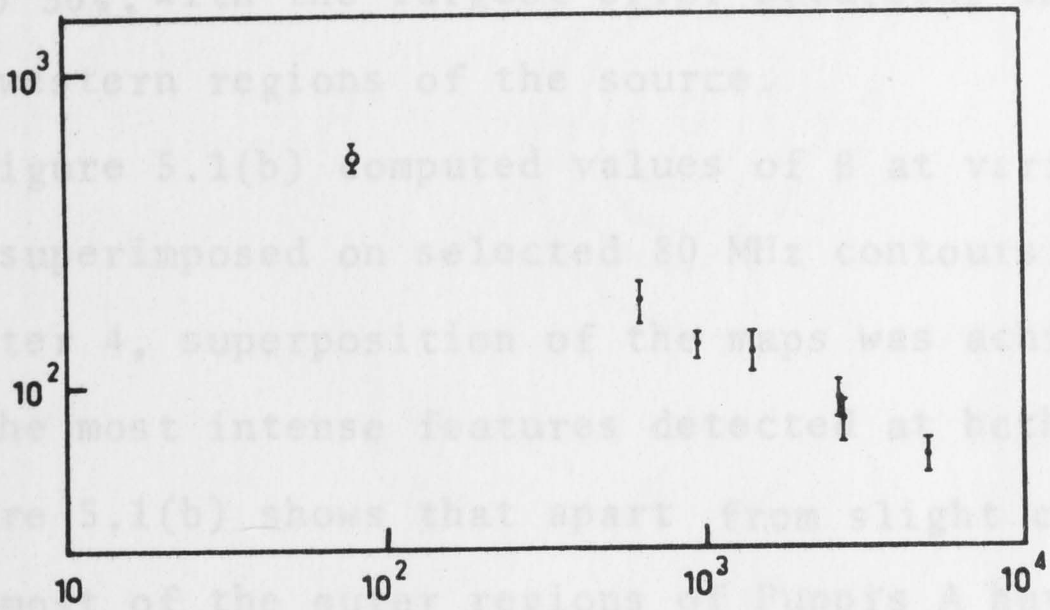

Fig. 5.1(c) - 0821-42 (Puppis A). Integrated spectrum.

$$\frac{T_{80}}{T_{5000}} = \left(\frac{5000}{80}\right)^{\beta+2} = 62.5^{\beta+2}$$

Such a comparison is bound to involve errors arising from inaccuracies in the measurements at both frequencies. We estimate that the errors in β calculated as indicated above are from 10 to 30%, with the largest error occurring in the central and south-western regions of the source.

In Figure 5.1(b) computed values of β at various points are shown superimposed on selected 80 MHz contours. As discussed in Chapter 4, superposition of the maps was achieved by aligning the most intense features detected at both frequencies.

Figure 5.1(b) shows that apart from slight changes in structure most of the outer regions of Puppis A have a spectral index of between 0.5 and 0.6. The spectral index of the whole source is 0.54(Fig.5.1(c)). In contrast the central region has a much flatter spectrum with values of β ranging from 0.0 to 0.4. We conclude that either (a) the non-thermal radiation in the central region has a much flatter spectrum than the outer regions, or (b) free-free absorption is occurring in patchy, cold HI clouds found along the line of sight between the source and the Earth, or (c) a thermal (HII) region is also present. Possibility (c) is unlikely since there are no HII regions discernible on photographs taken of the Puppis A region. Observations of high angular resolution and at intermediate frequencies would determine the exact nature of the spectrum in the central region and allow a choice between possibilities (a) and (b).

1711-38 (CTB 37)

In Figure 5.2(a) we present the 80 MHz map of this

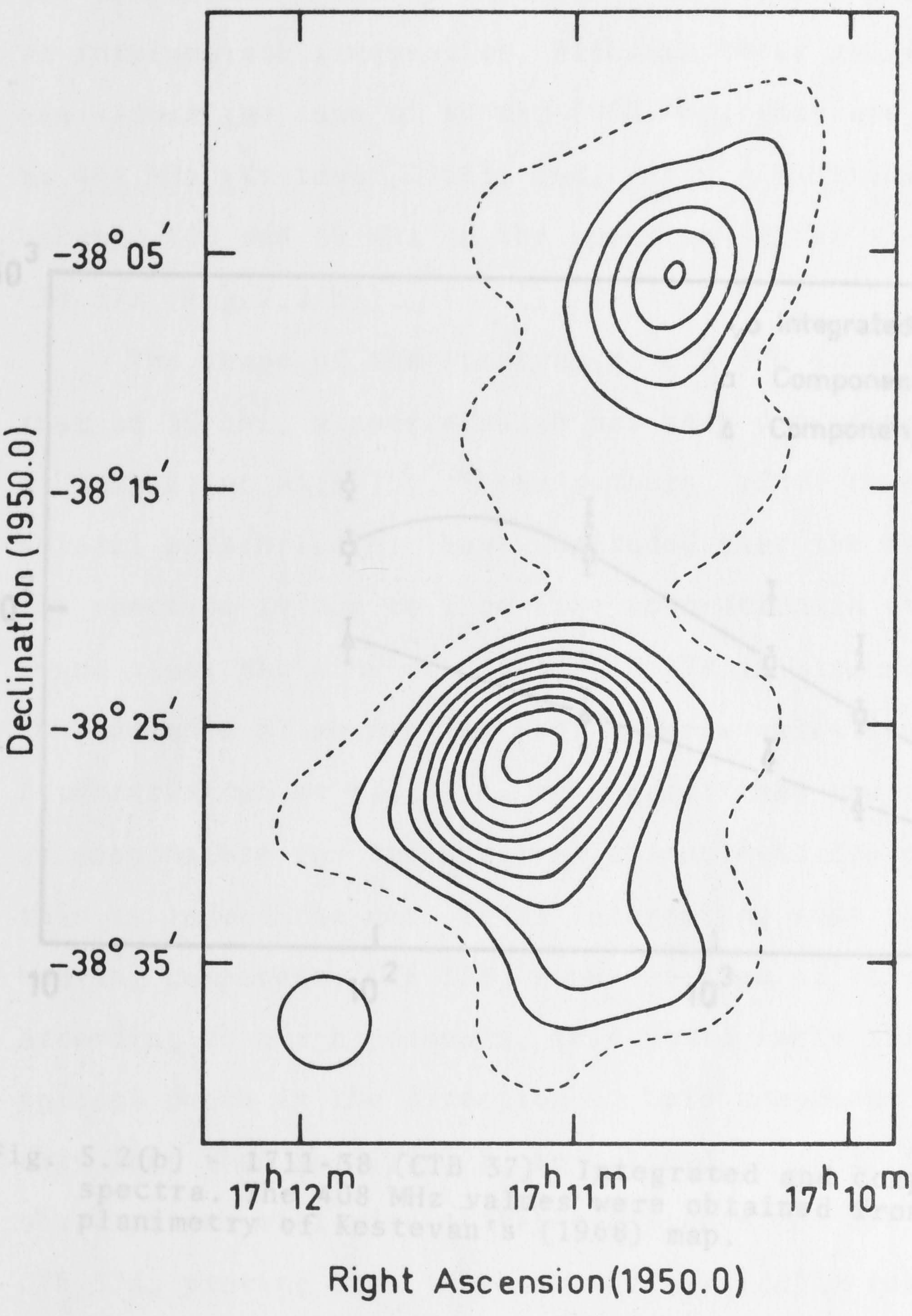

Fig. 5.2(a) - 1711-38 (CTB 37).

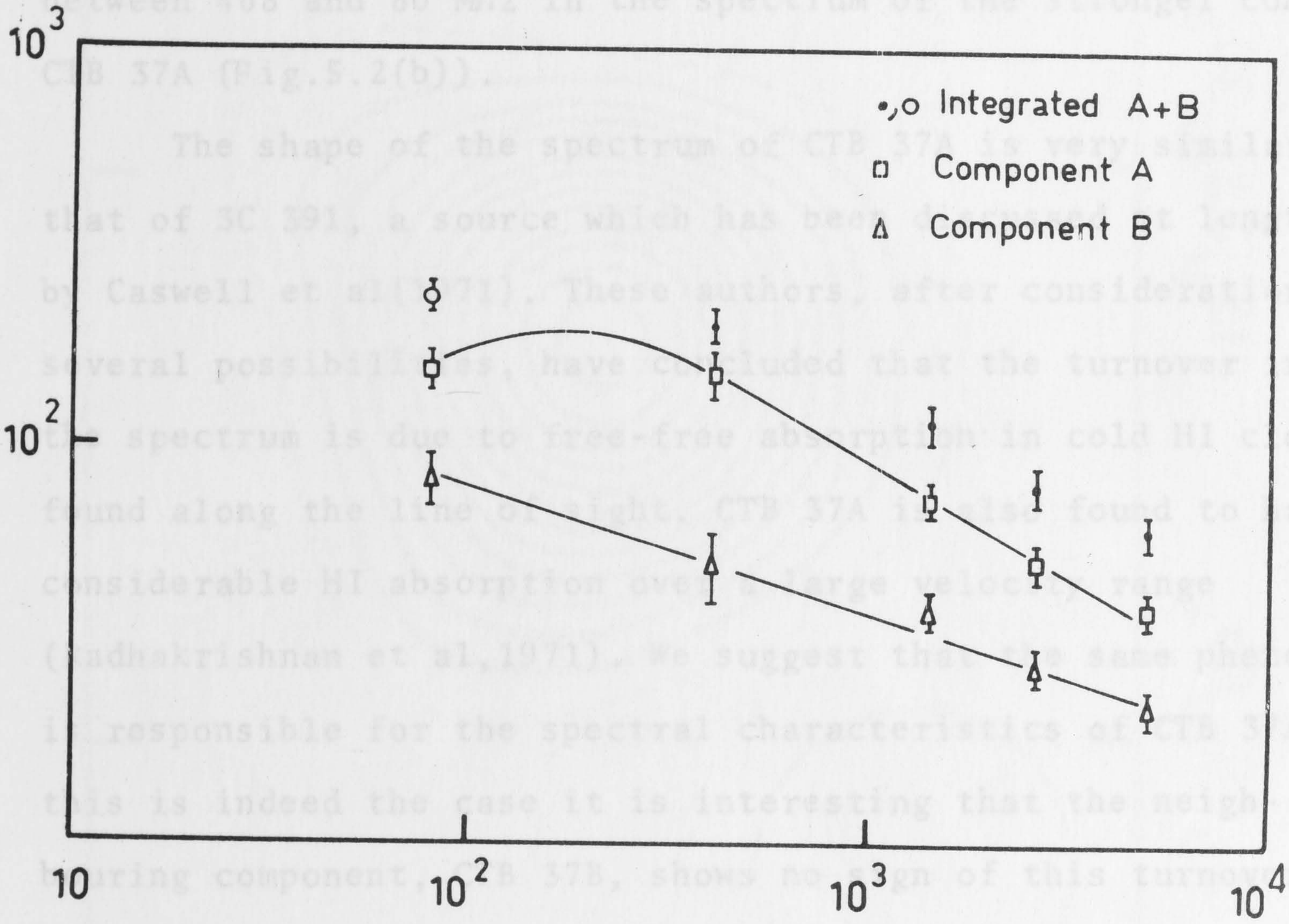

Fig. 5.2(b) - 1711-38 (CTB 37). Integrated and component spectra. The 408 MHz values were obtained from planimetry of Kestevan's (1968) map.

double source. The contours are remarkably similar to those at 5000 MHz obtained by Milne(1969). However the spectra of the components are very different, as evidenced by measurements at intermediate frequencies. Although their relative strengths are almost the same at 80 and 5000 MHz, they are very different at 408 MHz (Kestevan,1968), indicating a flattening-off between 408 and 80 MHz in the spectrum of the stronger component, CTB 37A (Fig.5.2(b)).

The shape of the spectrum of CTB 37A is very similar to that of 3C 391, a source which has been discussed at length by Caswell et al(1971). These authors, after consideration of several possibilities, have concluded that the turnover in the spectrum is due to free-free absorption in cold HI clouds found along the line of sight. CTB 37A is also found to have considerable HI absorption over a large velocity range (Radhakrishnan et al,1971). We suggest that the same phenomenon is responsible for the spectral characteristics of CTB 37A.If this is indeed the case it is interesting that the neighbouring component, CTB 37B, shows no sign of this turnover. According to our hypothesis, this would imply that the 21cm optical depth in the direction of this component is considerably less than for CTB 37A. We believe, in fact, that 21cm observations will give a lesser distance for CTB 37B than for CTB 37A, proving that they are not physically related. Future observations should show whether these predictions are correct.

1727-21 (3C 358,Kepler's Nova)

The remnant of Kepler's Nova has been observed extensively at higher frequencies but is essentially unresolved at 80 MHz (Fig. 5.3(a)). Our observations of this source contribute

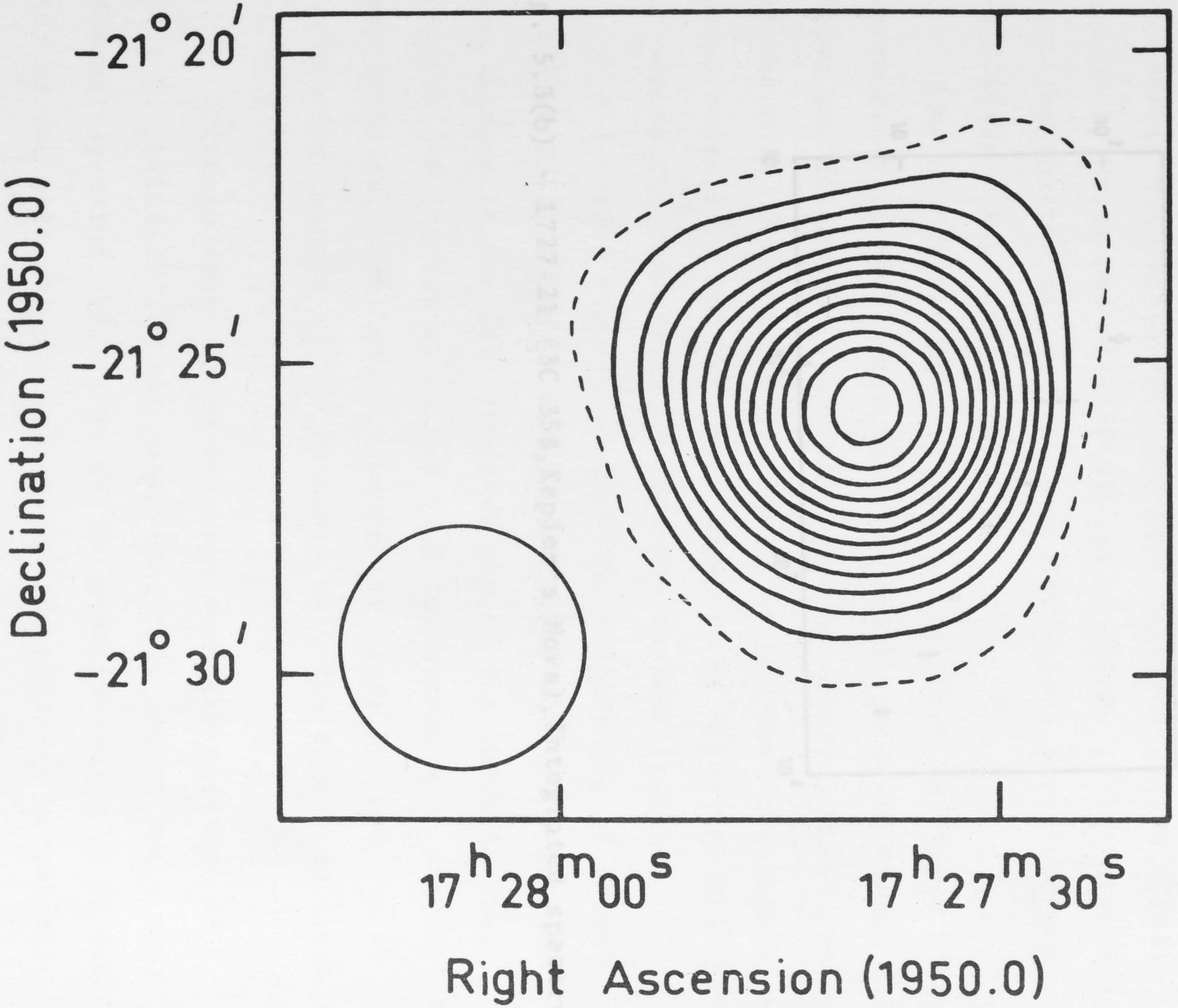

Fig. 5.3(a) - 1727-21 (3C 358,Kepler's Nova).

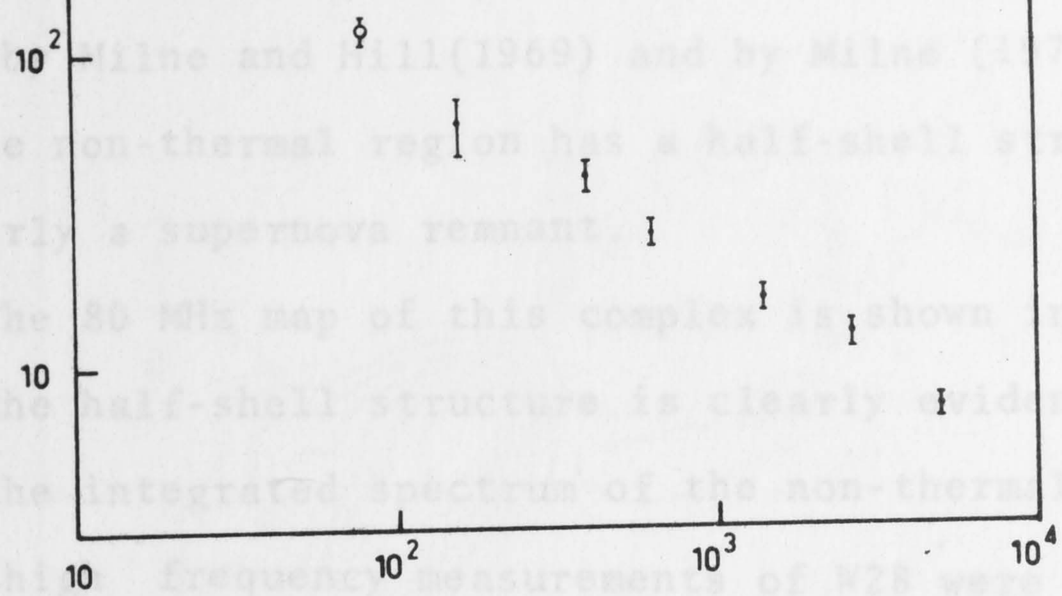

Fig. 5.3(b) - 1727-21 (3C 358,Kepler's Nova).Integrated spectrum.

only an integrated flux density which has been plotted in Figure 5.3(b). We obtain a spectral index of 0.68, somewhat higher than Milne's(1969) value of 0.58.

1757-23 (W28)

The radio source W28 (Westerhout,1958) is a combination of thermal and non-thermal regions. High resolution observations by Milne and Hill(1969) and by Milne (1971b) have shown that the non-thermal region has a half-shell structure and is clearly a supernova remnant.

The 80 MHz map of this complex is shown in Figure 5.4(a) where the half-shell structure is clearly evident. Figure 5.4(b) shows the integrated spectrum of the non-thermal shell. Some of the high frequency measurements of W28 were obtained with large beamwidths and have been adjusted by Milne and Hill (1969) to remove the contributions from the thermal regions.

A detailed comparison with the 408 MHz map of Shaver and Goss(1970) shows no major structural changes apart from the absence in the low frequency map of the known thermal regions and the source G6.4-0.5. A comparison with the 5000 MHz map of Milne(1971b) shows a number of minor but not really surprising changes in the contours with the exception again of G6.4-0.5.

Although there is an HII region at the position of G6.4-0.5, Milne(1971b) has shown that this source has a non-thermal spectrum. The ratio of the peak intensity of G6.4-0.5 to the two most intense regions of the shell is essentially unaltered between 5000 MHz and 408 MHz. At 80 MHz its relative intensity has dropped by a factor of about 4,perhaps due to absorption by the HII region. On this interpretation the HII region would be closer to us than the non-thermal source so

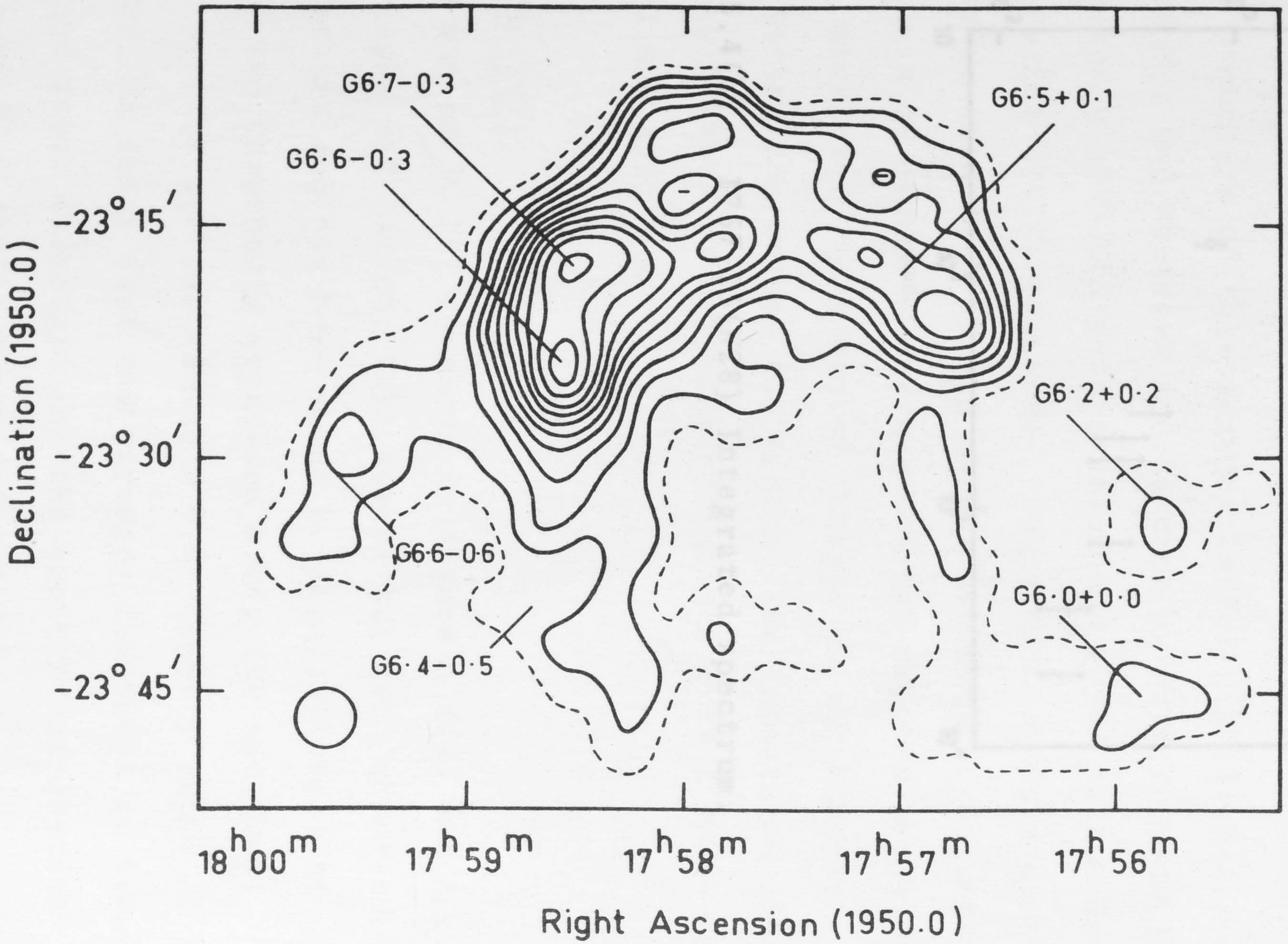

Fig. 5.4(a) - 1757-23 (W28).

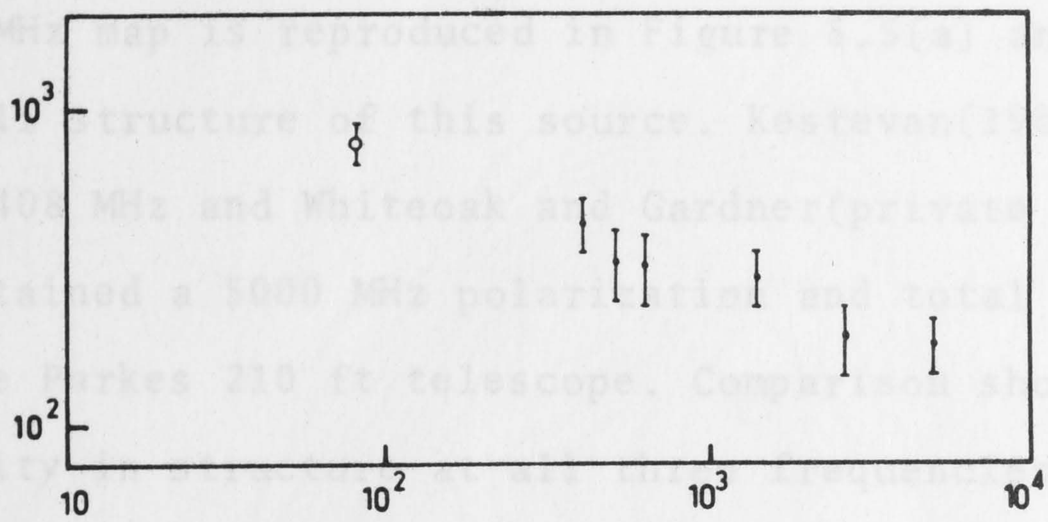

Fig. 5.4(b) - 1757-23(W28) Integrated spectrum.

that a recombination line measurement of the HII region should lead to a kinematic distance less than the distance to W28.

1853+01 (3C 392,W44)

W44 is another well-known galactic supernova remnant. The 80 MHz map is reproduced in Figure 5.5(a) and shows clearly the shell structure of this source. Kestevan(1968) has observed W44 at 408 MHz and Whiteoak and Gardner(private communication) have obtained a 5000 MHz polarization and total intensity map with the Parkes 210 ft telescope. Comparison shows a close similarity in structure at all three frequencies. We conclude that there is no evidence for any thermal regions superimposed on this source or for any marked changes in the electron energy distribution across the source. The integrated spectrum (Fig. 5.5(b)) shows no striking variations from a power-law between 80 and 8350 MHz.

1905+07 (3C 397)

Our map of 3C 397 is shown in Figure 5.6(a) and appears to show slight resolution. This source has been observed by several authors and has been shown by Fomalont(1967) to consist of two components separated along the east-west direction by 6'.5 arc and having a flux density ratio of 3:1 at 1425 MHz. He finds that the stronger component is towards the east and gives diameters for the eastern and western components of 3'.0 and 4'.0 arc respectively.

Holden and Caswell(1969) have suggested that this source is a supernova remnant in which case on would expect a reasonably constant spectral index across it. In our 80 MHz observations there was no evidence of any weaker component displaced

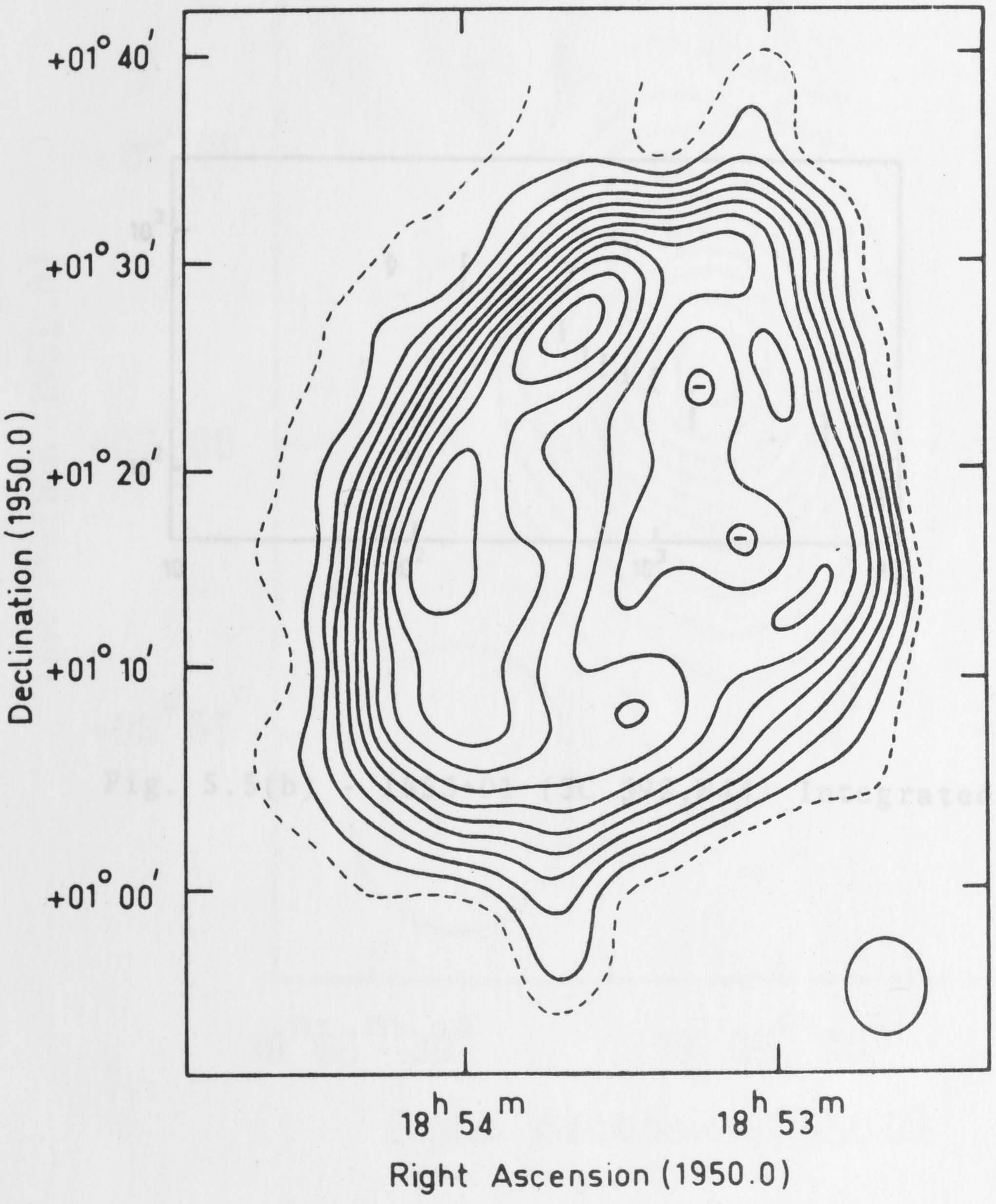

Fig. 5.5(a) - 1853+01 (3C 392,W44).

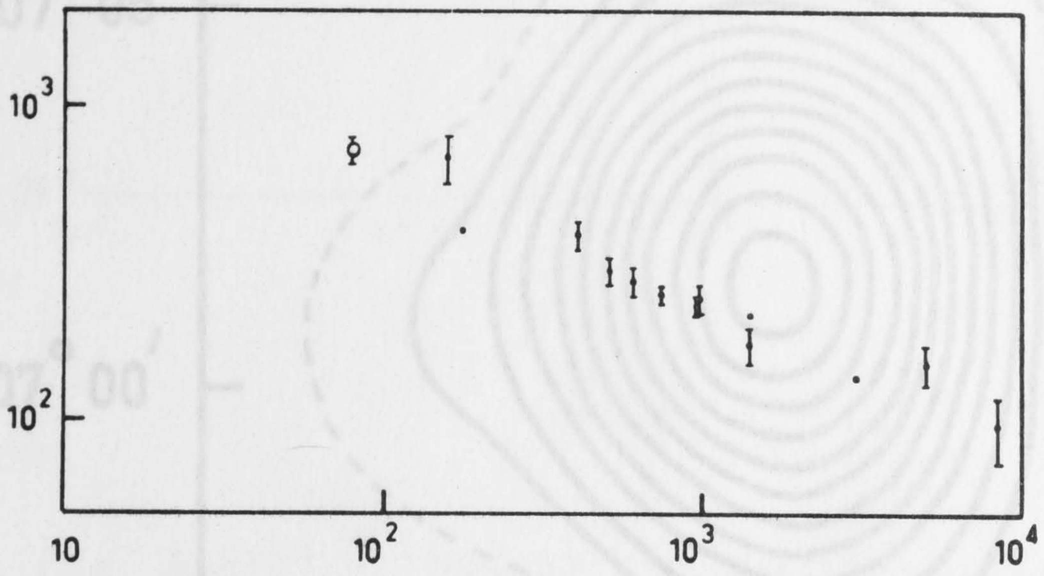

Fig. 5.5(b) - 1853+01 (3C 392,W44) Integrated spectrum.

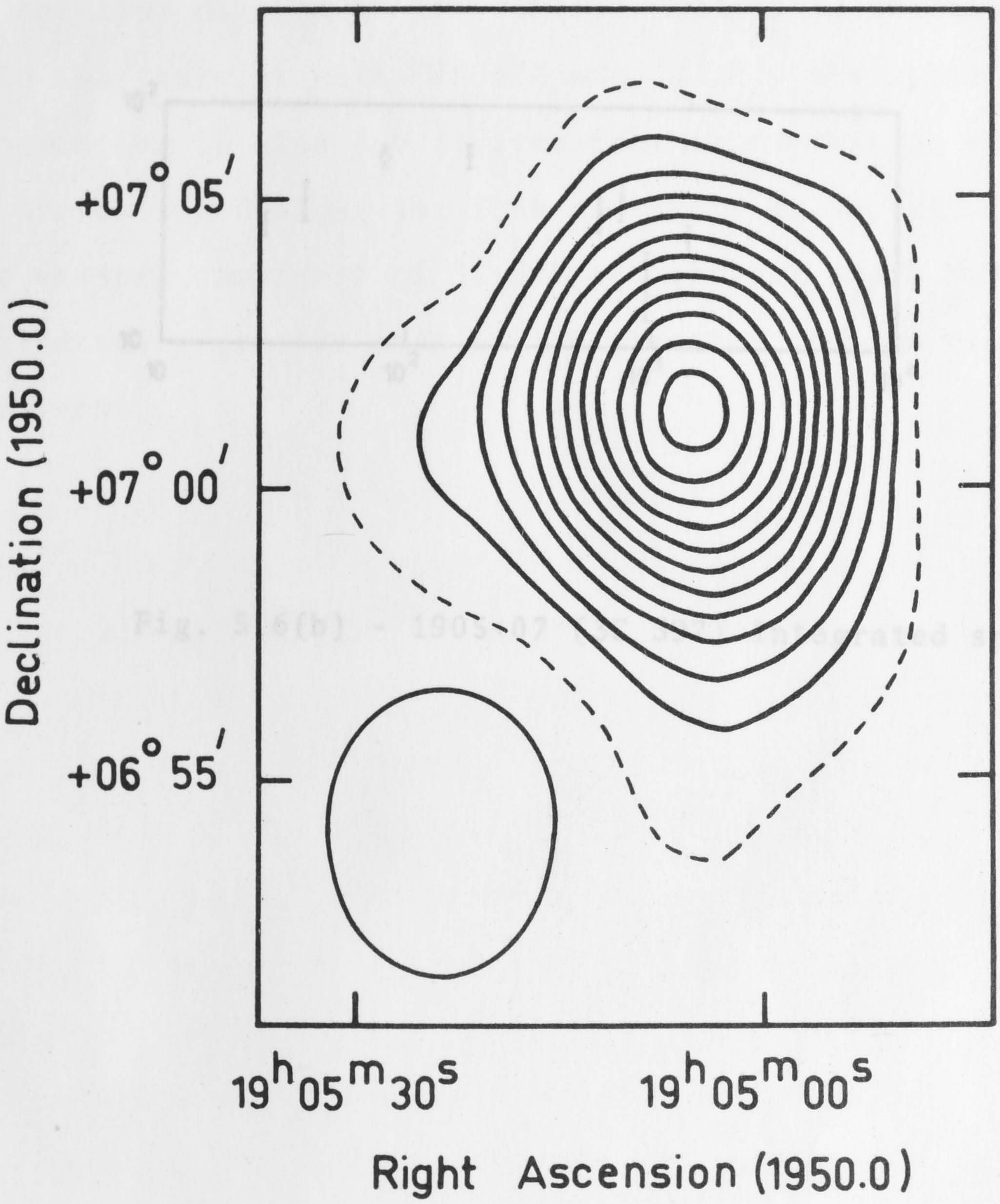

Fig. 5.6(a) - 1905+07 (3C 397).

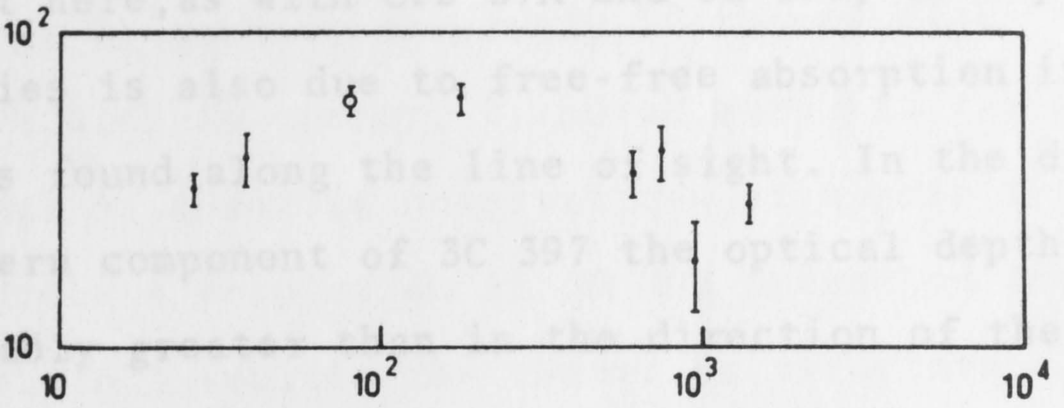

Fig. 5.6(b) - 1905+07 (3C 397) Integrated spectrum.

6'.5 arc to the west. The 80 MHz flux density is therefore entirely that of Fomalont's eastern component. The available measurements show that the integrated flux density of 3C 397 decreases at frequencies below 80 MHz, implying a decrease in the flux density of the eastern component. It seems probable that here,as with CTB 37A and 3C 391, absorption at low frequencies is also due to free-free absorption in patchy cold HI clouds found along the line of sight. In the direction of the western component of 3C 397 the optical depth must be considerably greater than in the direction of the eastern component.

CHAPTER 6

CONCLUSIONS

6.1 Extragalactic sources

Our observations of extragalactic sources have provided ample evidence for variations in structure with frequency. Out of the 21 sources observed, 10 showed clear variations in structure with frequency, 4 showed marginal variations and for 7 the lack of adequate observations at higher frequencies or the inadequate resolution at 80 MHz prevented detailed comparisons. In 3 sources the change in structure can be attributed either in part or in full to the onset of synchrotron self-absorption in one of the components. In all other cases changes in the electron energy spectrum across the source would adequately explain the observations.

We have looked for possible systematic patterns in the disposition of the components with steeper spectra relative to those with flatter spectra, but there appears to be no universal trend. In 3 sources components with very steep spectra appear at the outer extremities of a line or arc-like brightness distribution as would be expected on an evolutionary model where the outermost components have been radiating for the longest time. In other sources the components with the steeper spectra appear to be located at random within the brightness distribution.

The various brightness distributions encountered suggest that not all sources could have resulted from a series of consecutive ejections along some preferred direction. On such a simple model one would expect a gradation of spectral index from the outer to the inner components unless a continued supply of relativistic particles is maintained within the separate components.

6.2 Galactic sources

Of the 6 galactic sources observed, 2 appear to be completely non-thermal and have power-law spectra, 1 contains both thermal and non-thermal components and for 3, the change in structure can possibly be attributed to free-free absorption in cold HI clouds situated between the source and the Earth. For the source containing both thermal and non-thermal components, parts of the non-thermal radiation appear to be absorbed at low frequencies by foreground HII regions.

6.3 Future observations

Inaccuracies in position measurements at 80 MHz introduce uncertainties in the comparisons that we have made. It has been necessary to assume, perhaps incorrectly in some cases, a coincidence in position of the most intense features observed at the comparison frequencies.

Future observations with the radioheliograph should help to overcome this difficulty. The conversion to multi-frequency operation at present underway will allow effectively simultaneous observations of a source at frequencies of 43,80 and 160 MHz. From the relative position measurements at these three frequencies an absolute position should be derivable without having to assume the form of the wavelength dependence of ionospheric refraction.

Observations at these three frequencies should prove valuable in flux density measurements of sources with anomalous low frequency spectra. Galactic source observations may prove particularly interesting, since absorption at low frequencies appears to be relatively common. For many galactic and extragalactic sources, the 1'.9 arc beam of the radioheliograph operated at 160 MHz is expected to reveal important details of structure and to add significantly to our knowledge of discrete radio sources.

APPENDIX I

We wish to show that the flux density of a source observed with the radioheliograph is always given by summation of the sampled values which completely specify the observed source brightness distribution. Bracewell (1956) has treated the special case in which the true sky coordinates are approximated by a rectangular coordinate system and the observed brightness distribution is sampled on a rectangular raster.

In the general case, when a source is observed away from the meridian, the beam elongation is no longer in the north-south direction and the sampling raster becomes skew. We now show that, by adopting the coordinate system in which a direction is specified by two of its directional cosines (l, m, n) with respect to the (x, y, z) axes, both the beam and the sampling remain undistorted everywhere on the sky. We follow the nomenclature adopted by Christiansen and Hogbom (1969) and choose the x and y axes to be in the antenna aperture plane. The field pattern, F(l, m) of an array with "grading" or current distribution g(x, y) is then given by (Christiansen and Hogbom, 1969)

$$F(l,m) = K\,F_e(l,m) \iint_{-\infty}^{\infty} g(x,y)\, e^{2\pi i(xl+ym)}\,dx\,dy \qquad (1)$$

where $F_e(l,m)$ is the field pattern of an array element and where K has the value that makes $|F(l,m)|_{max} = 1$. If the array is now pointed to (l_0,m_0), g(x,y) is multiplied by $e^{-2\pi i(xl_0+ym_0)}$, giving

$$F(l,m) = K\,F_e(l-l_0,m-m_0) \iint_{-\infty}^{\infty} g(x,y)\, e^{2\pi i[x(l-l_0)+y(m-m_0)]}\,dx\,dy$$

$$= F(l-l_0,m-m_0) \qquad (2)$$

since, in the case of the radioheliograph, the array elements are also pointed to (l_0, m_0). Thus, in this coordinate system pointing the beam is equivalent simply to a change of origin. Furthermore, scanning always gives a square raster in the (l,m) plane. (Beard et al., 1967).

In this coordinate system the observed brightness temperature, T_a, at (l_0, m_0) is given by

$$T_a(l_0, m_0) = K' \iint_{-\infty}^{\infty} T_B(l,m)\, A(l-l_0, m-m_0)\, d\Omega \qquad (3)$$

where $T_B(l,m)$ is the true brightness temperature of the source at (l,m), $A(l,m) = |F(l,m)|^2$ is the power polar diagram of the array, $d\Omega$ is an element of solid angle and K' is a constant of the array which is obtained by calibration.

Since $d\Omega = \dfrac{dl\ dm}{\cos z} = \dfrac{dl\ dm}{n}$, equation 3 becomes

$$T_a(l_0, m_0) = K' \iint_{-\infty}^{\infty} \left\{\frac{T_B(l,m)}{n}\right\} A(l-l_0,\ m-m_0)\ dl\ dm \qquad (4)$$

Since equation 4 is a cross-correlation we have

$$\mathcal{F}(T_a) = K'\ \mathcal{F}\left(\frac{T_B}{n}\right)\ \mathcal{F}(A) \qquad (5)$$

In particular $\mathcal{F}(T_a)_{0,0} = K'\ \mathcal{F}\left(\dfrac{T_B}{n}\right)_{0,0}$ since $\mathcal{F}(A)_{0,0} = 1$.

It follows that

$$\iint_{-\infty}^{\infty} T_a(l,m)\ dl\ dm = K' \iint_{-\infty}^{\infty} \left(\frac{T_B}{n}\right) dl\ dm$$

$$= K' \iint_{-\infty}^{\infty} T_B\ d\Omega \qquad (6)$$

Since sampling in the (1,m) plane is always on a square raster, it can be seen from Bracewell (1956) that the left-hand side of equation 6 is given by the sum of discrete values T_a, sampled by the radioheliograph and that this sum is precisely the flux density of the source.

BIBLIOGRAPHY

Allen, L.R., Anderson, B., Conway, R.G., Palmer, H.P., Reddish, V.C., and Rowson, B., (1962), Mon. Not. R. astr. Soc., 124, 477.

Andrew, B.H., (1967), Astrophys. J., 147, 423.

Arp, H.C., (1964), Astrophys. J., 139, 1378.

Arp, H.C., (1967), Astrophys. J., 1, 1.

Baade, W., and Minkowski, R., (1954), Astrophys. J., 119, 215.

Beard, M., Chandler, G., Hrebeniuk, P. and Willing, M., (1967), Proc. I.R.E.E.A., 28, 334.

Biraud, F., Lequeux, J., and Le Roux, E., (1960), Observatory, 80, 116.

Blesing, R.G., private communication.

Bolton, J.G., Clarke, M.E., Ekers, R.D., Aust. J. Phys., (1965), 18, 627.

Bolton, J.G., Gardner, F.F., and Mackay, M.B., (1964) Aust. J. Phys., 17, 340.

Bolton, J.G., Ekers, J., (1966), Aust. J. Phys., 19, 713.

Bolton, J.G., Ekers, J., (1966a), Aust. J. Phys., 19, 275.

Bracewell, R.N., (1956), Aust. J. Phys., 9, 297.

Bracewell, R.N., and Roberts, J.A., (1954), Aust. J. Phys., 7, 615.

Braude, S.Ya., Lebedeva, O.M., et al., (1969), Mon. Not. R. astr. Soc., 143, 289.

Braude, S.Ya., Lebedeva, O.M. et al., (1969), Astrophys. Letters, 5, 129.

Braude, S.Ya., Zhuk, I.N., et al., (1968), Soviet Phys. Doklady, 13, 512.

Bridle, A.H., and Purton, C.R., (1968), Astron. J., 73, 717.

Broten, N.W., Clarke, R.W., Legg, T.H., Locke, J.L., McLeish, C.W., Richards, R.S., Yen, J.L., Chisholm, R.M., and Galt, J.A., Nature, 216, 44.

Cameron, M.J., (1969), Proc. A.S.A., 1, 229.

Caswell, J.L., Dulk, G.A., Goss, W.M., Radhakrishnan, V., and Green, Anne J., (1971), In preparation.

Caswell, J.L., private communication.

Christiansen, W.N., and Högbom, J.A. (1969), "Radio telescopes", Cambridge Univ. Press, Monograph on Physics.

Clarke, R.W., Broten, N.W., Legg, T.H., Locke, J.L., and Yen, J.L., (1969), Mon. Not. R. astr. Soc., 146, 381.

Cohen, M.H., Moffet, A.T., Shaffer, D., Clark, B.G., Kellermann, K.I., Jauncey, D.L., and Gulkis, S., (1969), Astrophys. J., 158, L83.

Conway, R.G., Kellermann, K.I., and Long, R.J., (1963), Mon. Not. R. astr. Soc., 125, 261.

Cooper, B.F.C., Price, R.M. and Cole, D.J., (1965), Aust. J. Phys., 18, 589.

Day, G.A., Shimmins, A.J., Ekers, R.D., and Cole, D.J., (1966), Aust. J. Phys., 19, 35.

Dent, W.A., and Haddock, F.T., (1966), Astrophys. J., 144, 568.

Donaldson, W., Miley, G.K., Palmer, H.P., and Smith, H., (1969), Mon. Not. R. astr. Soc., 146, 213.

Ekers, R.D., (1969), Aust. J. Phys. Astrophys. Suppl., No. 6.

Ellis, G.R.A., and Hamilton, P.A., (1966), Astrophys. J., 143 (1), 227.

Erickson, W.C., and Cronyn, W.M., (1965), Astrophys. J., 142, 1156.

Fomalont, E.B., (1967)*, Observations of Owens Valley Radio Obs., No. 7.

Fomalont, E.B. (1968)*, Astrophys. J. Suppl. Ser., 15, 203.

Griffin, R.F., (1963), Astron. J., 68, 421.

---

*These references are equivalent.

Harris, D.E., and Roberts, J.A., (1960), P.A.S.P., 72, 237.

Hogg, D.E., Macdonald, G.H., Conway, R.G., and Wade, C.M., (1969), Astron. J., 74, 1206.

Holden, D.J., and Caswell, J.L., (1969), Mon. Not. R. astr. Soc., 143, 407.

Horton, P.W., Conway, R.G., and Daintree, E.J., (1969), Mon. Not. R. astr. Soc., 143, 245.

Kellermann, K.I, (1964a), Astron. J., 69, 205.

Kellermann, K.I., (1964), Astrophys. J., 140, 969.

Kellermann, K.I., (1966), Astrophys. J., 146, 621.

Kellermann, K.I., and Pauliny-Toth, I.I.K., (1968), Astrophys. J., 152, (2Pt1), 639.

Kellermann, K.I., Pauliny-Toth, I.I.K., and Williams, P.J.S., (1969), Astrophys. J., 157, 1.

Kestevan, M.J.L., (1968), Aust. J. Phys., 21, 739.

Komesaroff, M.M., private communication.

Landecker, T.L., private communication.

Lequeux, J., (1962), Ann. d'Astrophys., 25, 221.

Lockhart, I.A., and Sheridan, K.V., (1970), Proc. A.S.A., 1, 344.

Long, R.J., Smith, M.A., Stewart, P., and Williams, P.J.S., (1966), Mon. Not. R. astr. Soc., 134, 371.

Macdonald, G.H., Kenderdine, S., and Neville, A.C., (1968), Mon. Not. R. ast. Soc., 138, 259.

Macdonald, G.H., Neville, A.C., and Ryle, M., (1966), Nature, 211, 1241.

Mackay, C.D., (1969), Mon. Not. R. astr. Soc., 145, 31.

Maltby, P., (1962), Astrophys. J. Suppl., Ser. 67, 124.

Maltby, P., and Moffet, A.T., (1962), Astrophys. J. Suppl. Ser., 67, 141.

Mathews, T.A., Morgan, W.W., and Schmidt, M., (1964), Astrophys. J., 140, 35.

Miley, G.K., Hogg, D.E., and Basart, J., (1970), Astrophys. J., 159, L19.

Mills, B.Y., Slee, O.B., and Hill, E.R., (1958), Aust. J. Phys., 11, 360.

__________, (1960), Aust. J. Phys., 13, 676.

__________, (1961), Aust. J. Phys., 14, 497.

Milne, D.K., (1969), Aust. J. Phys., 22, 613.

Milne, D.K., (1971a), Aust. J. Phys. In press.

Milne, D.K., (1971b), Astrophys. Letters. In press.

Milne, D.K., and Hill, E.R., (1969), Aust. J. Phys., 22, 211.

Moffet, A.T., (1962), Astrophys. J. Suppl. Ser., 67, 93.

Morimoto, M., and Lockhart, I.A., (1968), Proc. A.S.A., 1, 99.

Palmer, H.P., Rowson, B., Anderson, B., Donaldson, W., Miley, G.K., Gent, H., Adgie, R.L., Slee, O.B., and Crowther, J.H., (1967), Nature, 213, 789.

Parker, E.A., (1968), Mon. Not. R. astr. Soc., 138, 407.

Radhakrishnan, V., Goss, W.M., Murray, J.D., Brooks, J.W., (1971), In preparation.

Roger, R.S., Costain, C.H., and Lacey, J.D., (1969), Astron. J., 74, 366.

Ryle, M., and Longair, M.S., (1967), Mon. Not. R. astr. Soc., 136, 123.

Ryle, M., and Windram, M.D., (1968), Mon. Not. R. astr. Soc., 138, 1.

Scheuer, P.A.G., and Williams, P.J.S., (1968), Ann. Rev. Astron. Astrophys., 6, 321.

Schilizzi, R.T., and McAdam, W.B., (1969), Proc. A.S.A., 1, 228.

Schilizzi, R.T., and McAdam, W.B., (1970), Proc. A.S.A., 1, 337.

Searle, L., (1965), Nature, 207, 1282.

Sersic, J.L., (1961), Revta Univ. Nac. Córdoba, 11, No. 3.

Shain, C.A., (1958), Aust. J. Phys., 11, 517.

Shaver, P.A., and Goss, W.M., (1970), Aust. J. Phys. Astrophys. Suppl. No. 14, (Paper II).

Sheridan, K.V., (1958), Aust. J. Phys., 11, 400.

Sheridan, K.V., and Sparks, J.B., (1967), Proc. I.R.E.E.A., 28, 302.

Shimmins, A.J., Clarke, M.E., and Ekers, R.D., (1966), Aust. J. Phys., 19, 649.

Shimmins, A.J., and Day, G.A., (1968), Aust. J. Phys., 21, 377.

Shimmins, A.J., Day, G.A., Ekers, R.D., and Cole, D.J., (1966), Aust. J. Phys., 19, 837.

Shimmins, A.J., Manchester, R.N., Harris, B.J., (1969), Aust. J. Phys. Astrophys. Suppl. No. 8.

Slee, O.B., private communication.

Slish, V.I., (1963), Nature, 199, 692.

Wall, J.V., private communications.

Westerhout, G., (1958), Bull. astr. Inst. Neth., 14, 215.

Westerlund, B.E., and Smith, L.F., (1966), Aust. J. Phys., 19, 181.

Whiteoak, J.B., and Gardner, F.F., private communications.

Wild, J.P., (1965), Proc. Roy. Soc. A., 286, 499.

Wild, J.P., (1967), Proc. I.R.E.E.A., 28, 277.

Wild, J.P., (1967a), Proc. I.R.E.E.A., 28, 279.

Williams, P.J.S., (1963), Nature, 200, 56.

Williams, P.J.S., Collins, R.A., Caswell, J.L., and Holden, D.J., (1968), Mon. Not. R. astr. Soc. 139, 289.

Williams, P.J.S., and Stewart, P., (1967), Mon. Not. R. astr. Soc., 135, 319.

Yates, K.W., (1968), Aust. J. Phys., 21, 167.

Yates, K.W., Wielebinski, R., and Landecker, T.L., (1967), Aust. J. Phys., 20, 595.

Zwicky, F., (1961), paper given at IAU Symposium No. 15, published in "Problems of Extragalactic Research" (1962), Ed. McVittie, G.C. (N.Y. Macmillan), 347.